Developing Methods for incorporating Thermalisation effects into MCTDH

by

Ceridwen Ash

A thesis submitted to

University College London

for the examination of

DOCTOR OF PHILOSOPHY

I, Ceridwen Ash, confirm that the work presented in this thesis is my own. Where information has been derived from other sources, I confirm that this has been indicated in the thesis.

Abstract

The premise of the work that was undertaken in this thesis is the use of mathematical modelling techniques to solve fundamental questions in quantum chemistry. In particular, this project focusses on how thermalisation effects, particularly in the context of proton transfer, can be incorporated into the exact quantum dynamics method MCTDH, which is the multiconfigurational time-dependent Hartree method. This is a computational method set up to solve the time-dependent Schrödinger equation (TDSE) exactly for small systems or molecules.

The question posed in this thesis is what can scientists do when the gas phase zero temperature picture is no longer a useful description for the reactions and processes that we are interested in. For instance, if we look at proton transfer, there is still a lot of uncertainty about the exact mechanism and the role that is played by the environment in this process. In this project ML-ρ-MCTDH is developed and applied in three studies of proton transfer, looking first at a model of symmetric proton transfer, followed by a brief study of salicylaldimine and finally looking at porphycene. Chapter 1 introduces the topic and chapters 2 and 3 cover the theory and methodology underpinning the research focus. In the remaining chapters results are presented and discussed.

Impact Statement

The simulation of molecular systems on a quantum level is an important tool in understanding fundamental reactivity, insight into which is valuable to a wide range of applications in chemistry from drug design to the development of solar panels. Rigorous molecular modelling of this kind is becoming an indispensable counterpart to experimental work, helping to interpret the contribution of quantum effects such as tunnelling and non-adiabatic coupling effects in order to understand chemical properties of technological importance. For modelling reaction rates and mechanisms, MCTDH is a benchmark method in this field, with wide ranging impact on the way that the study of time-resolved molecular dynamics has developed over the years.

Many applications involve the interpretation of time-resolved spectroscopy results obtained experimentally which is particularly useful for the understanding and therefore development of photoactivated molecules. Existing methods for modelling this kind of problem in the gas phase are inadequate due to the important role of the environment, while a classical or semi-classical approach would neglect quantum effects which are known to be correspondingly important.

The development of a multi-layered-density-matrix capability of the Quantics package aims to tackle this choice, by improving the scaling of the existing density matrix scheme in MCTDH in order to allow more realistic systems to be modelled. The work thus underpins a wide range of technological development in which the effect of temperature on quantum dynamics is important. Applications range from dye sensitised solar cells, key to combatting

climate change, to quantum computers, which are key in further information exchange.

"We live in a world where there is more and more information, and less and less meaning."

Jean Baudrillard

Acknowledgements

First of all, I want to thank my supervisor Prof. Graham Worth for his constant support and advice throughout my time at UCL. I'll be forever indebted for his efforts in my education and his patience over the years. I'd also like to thank my second supervisor Dr David Rowley for his support of my overall study and to everyone in the Worth-group past and present; Gareth, Mariana, Angelo, Eryn, Marcus, Alice, Georgia, Thierry and Sandra. I'm grateful to the administrative staff for their support, especially to Jadranka, Liz, Jose, Yael, Louise, Vicky and Stephen. Also thank you to Charles, Dave and Frank for maintaining the cluster and for the entertaining chats. Above all I want to thank my partner Robert and my parents for practical and emotional support which helped me see this though.

Contents

List of Figures

List of Tables

Glossary

ABM Adams-Bashforth-Moulton predictor-corrector integrator

BOA Born-Oppenheimer approximation

CMD Centroid Molecular Dynamics

CMF constant mean field

DFT density functional theory

DFVP Dirac-Frenkel variational principle

DME density matrix evolution

DVR discrete variable representation

EOM equations of motion

ET electron transfer

FKQ-CW Feynman-Kleinert Quasi-Classical Wigner method

GWP Gaussian wavepacket

LE Liouville equation

LvN Liouville-von Neumann

MP2 second order Møller-Plesset theory

PES potential energy surface

PIMC Path integral Monte Carlo method,

PIMD Path integral molecular dynamics

PT proton transfer

QD quantum dynamics

RPMD Ring Polymer Molecular Dynamics

SE Schrödinger equation

SHF single hole function

SIL short iterative Lanczos-Arnoldi integrator

SPDO single particle density operator

SPF single particle function

TDSE time-dependent Schrödinger equation

TISE time-independent Schrödinger equation

TST transition state theory

vMCG variational multi-configurational Gaussian

VMF variable mean field

ZPE zero point energy

Chapter 1

Introduction

1.1 Preface

The dynamics of quantum mechanical systems is important to study in order to understand fundamental reactivity of molecules. While classical mechanics is able to explain the dynamics in simple ground state chemical systems, interpreting phenomena such as tunnelling, the quantisation of nuclear motion seen in many experimental spectra, and various aspects of chemical bonding can only be explained by examining the quantum behaviour of the system.

Tunnelling occurs when a nuclear wavefunction reaches an energy barrier since the wave decays inside the barrier, and if this barrier is narrow enough, the wavefunction does not decay to zero and is still present on the other side of the barrier. The particle can therefore travel to a region that is otherwise forbidden by classical mechanics when it has insufficient activation energy to mount the barrier. The two factors that affect the amount of tunnelling are the size of the particle and the width of the energy barrier, indeed the

probability of tunnelling increases with decreased particle size and decreased barrier width. Tunnelling is potentially important in any reaction involving a proton being transferred between different sites. This is due to its light mass and corresponding highly quantum mechanical nature. The rate determining step in enzyme catalysis, for example, may be controlled by tunnelling [1,2].

Another area of chemistry where nuclear dynamics is especially important is in photochemistry, where the dynamics of the nuclei can have a significant impact on reaction mechanisms due to coupling between electronic and nuclear motion. For instance, the development of dye sensitised solar cells relies on an understanding of photochemistry and therefore of nuclear dynamics [3,4]. In recent years, nuclear dynamics has also become an important topic due to the development of quantum technologies, such as quantum computers.

Realistically, only the smallest quantum dynamical systems can be modelled with full accuracy. This is because the coupling in realistic systems means that the cost of simulating a multidimensional nuclear wavefunction goes up exponentially with the number of degrees of freedom. Therefore the prohibitive computational cost of modelling multidimensional systems imposes limitations on the time scales that can be looked at, and challenges theoreticians to find a representative subset of the problem and to rationally approximate whatever is missing. One common assumption is to treat a system as 'closed', which means that the number of particles and total energy is conserved, as if the system is isolated in a sealed box. In reality there are no closed systems, and any system which is thermalised or interacts in a substantial environment must be treated as 'open'. Similarly, models of large systems often employ classical approximations to the 'bath' (i.e the

less important modes).

The main focus of this project is on the time dependent quantum dynamics method MCTDH (Multi-Configurational Time-Dependent Hartree) which is essentially a computational modelling technique set up to solve the TDSE (time-dependent Schrödinger equation) using numerical integration, as a tool for understanding molecular reactions. Standard MCTDH propagates a nuclear wavepacket and simulates models in the gas phase. In contrast, it is possible to describe quantum dynamics using a density matrix, which is useful in any reaction where thermalisation effects or the environment are important, crucially here in the case of proton transfer (PT). The benefit of the density matrix approach is that it is possible to distinguish the 'system' and 'bath' dynamics and treat them with different levels of approximation within a same framework. This functionality exists in the form of the ρ-MCTDH algorithm, which isn't used often as it is limited due to scaling issues. This motivates the central idea of this project, which is to utilise the multilayer formalism of MCTDH to make the existing ρ-MCTDH package more efficient.

1.2 Existing approaches to thermalisation in dynamics

Adding temperature to a system is straightforward using classical mechanics due to the direct connection between the temperature and the momentum of the particles.

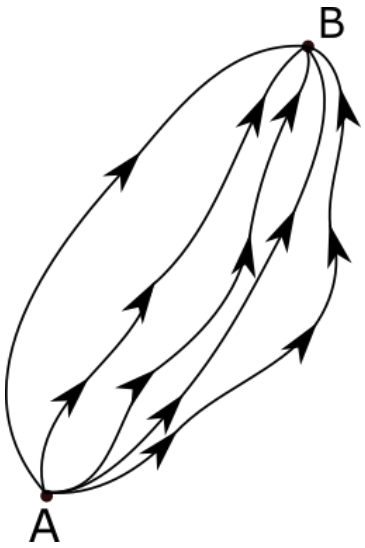

Fig. 1.1: Paths between point A at time t to point B at time $t'(> t)$. Paths which self-intersect or go backwards in time are not allowed.

There are many powerful computational packages to simulate classical molecular dynamics, however this is not the focus of this thesis which deals only with quantum methods. Feynman provided a way to use the ideas of classical mechanics to solve the TDSE.

Path integral molecular dynamics (PIMD) methods were developed to use Feynman path integrals to simulate the molecular dynamics of a quantum system in the condensed phase. In the Feynman path integral formulation of quantum mechanics the functional integral over all quantum mechanically possible paths over configuration space is found, where the value of the integral gives a probability of taking that path (known as the quantum amplitude). This is shown schematically in Figure 1.1

In PIMD methods the nuclei are treated quantum mechanically and each nuclei is mapped into a classical system consisting of set of harmonic potentials

and described by an effective Hamiltonian. This method is non empirical and uses force fields based on the method chosen, and is therefore a classical system with quantum information incorporated.

There are several well established computational techniques which use the PIMD method, including the Centroid Molecular Dynamics (CMD) [5,6] and Ring Polymer Molecular Dynamics (RPMD) methods [7, 8].

Both the RPMD and CMD methods use the quantum Boltzmann operator alongside a modified form of classical mechanics which conserves the quantum mechanical equilibrium distribution. In the CMD method the classical potential energy function is replaced with an imaginary-time centroid potential of mean force [9] whereas in RPMD a classical molecular dynamics simulation is performed in the full phase space of the imaginary-time path integral [7]. For correlation functions involving linear functions of position and/or momentum operators, CMD and RPMD are exact in the limit as time tends to zero, in the limit of a harmonic potential, and in the classical limit. Both methods struggle to simulate correlation functions in the case of strongly nonlinear operators [10–13].

CMD and RPMD have been used simulate quantum mechanical effects in a variety of applications [14–30], they have been shown to capture quantum mechanical effects in many condensed phase molecular dynamics simulations especially in application to molecular liquids. A final computational method using the PIMD approach is the Feynman-Kleinert Quasi-Classical Wigner method (FK-QCW) [31,32], which was developed to use the Feynman-Kleinert approximation of the density operator in order to improve

the Feynman-Kleinert implementation of the classical Wigner approximation for evaluating quantum time correlation functions.

Another approach to modelling molecular dynamics which also makes use of path integrals is the Path integral Monte Carlo method, PIMC. There are various successful implementations of this method dating back to the 1970s [33]. A Monte Carlo method is an algorithm which repeatedly samples possible outcomes until the distribution of results converges. While simulations based on Monte Carlo algorithms are very good at reproducing static properties of a thermalised system, such as enthalpy, the dynamics is non-empirical and therefore approximate. Indeed this is the main limitation of this family of methods, which motivates the adaptation of the MCTDH approach proposed in this thesis. The PIMC method is used to calculate thermodynamic properties, for instance heat capacity, free energy and internal energy. The disadvantage of a statistical sampling approach is that an excessive number of points must be calculated in order to obtain accurate results.

1.3 Thermalisation in open quantum dynamics

To accurately study the dynamics of molecular systems including quantum effects requires solving the TDSE. This, however, is only applicable to pure states of closed systems, i.e. there is no exchange of energy with an environment. As a result thermalisation, which results in a system in an incoherent mixture of states guided by the Boltzmann distribution, cannot take place.

For this, we need to solve instead the Liouville-von Neumann (LvN) equation using a density matrix approach.

Quantum dynamics simulations suffer from an inherent poor scaling, with the computational effort required to solve the TDSE growing exponentially with the number of degrees of freedom included in the system. Traditional methods use time-independent basis sets that form a grid and are typically restricted to 3-4 degrees of freedom. The effort required to solve the LvN equation is even worse as a density matrix effectively squares the number of degrees of freedom to be treated and grid-based methods are restricted to 2 degrees of freedom at most.

For solving the TDSE, MCTDH has enabled accurate solutions for many degrees of freedom to be obtained. This, and the even more powerful multilayer-MCTDH will be described in Chapter 3. MCTDH can also be used to divide a system into "primary" and "secondary" modes, with the secondary modes forming a bath for the primary system and can be treated using classical dynamics to save effort. This partitioning is shown schematically in Figure 1.2. While this allows for some thermalisation effects to be included, the limitation of using a wavefunction is that it is not possible to truly represent the environment surrounding the system, as this would require the open system dynamics to be accounted for. This is the motivation for using a density matrix instead, which can fully account for both open and closed system dynamics.

The MCTDH approach can, however, also be used to propagate density matrices. This alleviates the scaling but the method at present still cannot treat

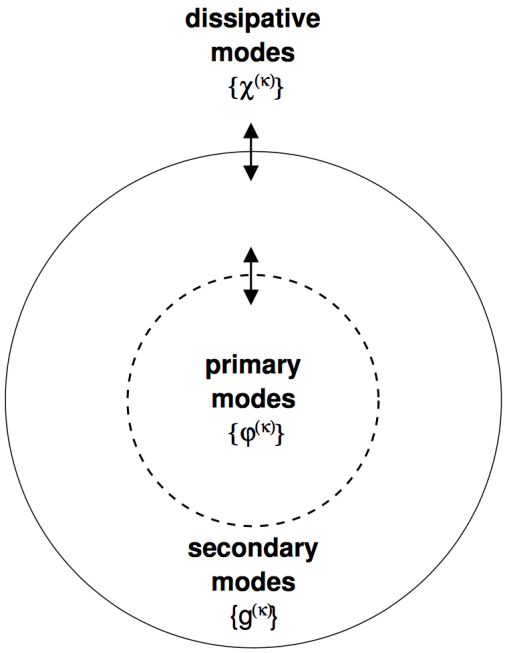

Fig. 1.2: Diagram of system, bath, environment mode correlations [34].

more than a few degrees of freedom. The key to an accurate, general density matrix approach would be to use the ML-MCTDH approach for density matrices. This would bring all of the power of MCTDH to simulations of open systems, including partitioning of degrees of freedom into a primary system, secondary bath and "dissipative" modes that can then be included using dissipation operators (Figure 1.2).

1.4 Introduction to proton transfer

PT is a category of reaction mechanism where an H^+ ion moves from a donor to an acceptor site. It can either occur within a molecule (intramolecular PT) or between molecules (intermolecular). This simple process is important to understand since it is a key part of many reactions in organic chemistry,

playing a role in numerous processes vital to life, from the stability of DNA to enzymatic reactions.

One reason why PT is a notoriously difficult to model is that it can be significantly impacted by nuclear quantum mechanical effects, such as the zero-point energy (ZPE) effect, tunnelling through the reaction barriers, and the coherence of nuclear wave functions. This means that classical models of PT are limited as they do not account for these quantum effects in any reaction where PT plays a role, which motivates why a quantum approach is useful. Another difficulty with predicting the mechanism and timescale of PT is that the environmental conditions of the proton, such as the temperature or presence of a solvent can play a significant role in driving or inhibiting the possible pathways to reaction. Conversely, this second aspect means that studies using purely quantum modelling techniques are also limited, since they are restricted by computational capacity and can usually only fully describe a small number of coupled particles and hence cannot represent these large scale effects.

Similar challenges were encountered by scientists studying electron transfer (ET) processes in the 1950s who also found that classical estimates for reaction rates were often inaccurate, and Marcus theory of ET aimed to address this. Marcus theory corrects the classical model for ET by estimating the Gibbs free energy of activation to includes solvation effects (see Figure 1.3).

Many of the ideas introduced in Marcus theory informs the way that PT is described, which is framed in terms of donor and acceptor states with adiabatic surfaces. PT can be more unpredictable and harder to model than ET,

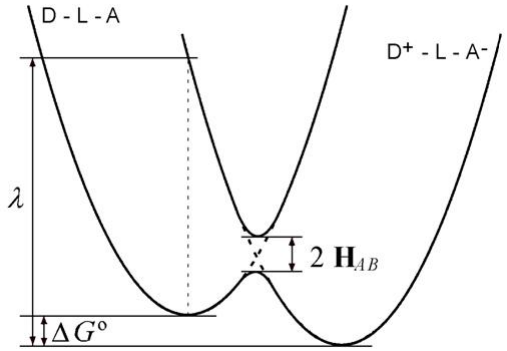

Fig. 1.3: Energy diagram for ET including inner and outer sphere reorganisation and electronic coupling [35]. In this schematic D-L-A stand for the donor, ligand and acceptor components respectively, the horizontal axis represents the reaction coordinate for the PT and the vertical axis is free energy. λ is the reorganization energy, ΔG^o represents the total Gibbs free energy change for the ET, and $\mathbf{H}_{A,B}$ quantifies the electronic coupling between initial and final states.

and often requires a fully quantum dynamical approach. This is partly due to the fact that in ET processes the coupling of the nuclear motion to the electron is minimal and can often be neglected. In contrast, in PT the nuclear motion takes place on a similar timescale which means that the coupling to the nuclear dynamics must be considered. Depending on the PT system, the specific properties of the potential energy surface, such as the barrier height or width will determine whether tunnelling occurs. In contrast, in Marcus theory ET is governed by just one coupling parameter. Another reason that PT is more costly to model than ET is that it occurs over longer timescales, requiring correspondingly long simulations.

The kinetic isotope effect is when the rate of a reaction is observed to be slower when an atom is replaced by its heavier isotope. For example, in a re-

action where a C-H bond is broken, if the hydrogen is replaced by deuterium then the rate of reaction would be expected to slow significantly. This is an example of a primary kinetic isotope effect, whereas it is also possible to see some reduction in reaction rate even when the bond involving the isotope is not broken, which is known as a secondary kinetic isotope effect. The kinetic isotope effect can be used to establish which mechanism in a complex multi step reaction is the rate determining step.

To understand the primary kinetic isotope effect, note first that a molecule containing deuterium swapped for hydrogen has the same potential energy profile as the original molecule containing only hydrogen, since bond distances and strengths depend on atomic charge (which is identical for H and D). However the vibrational frequencies of the C-D bond stretch (reaction coordinate) does differ, since this depends on atomic mass. In particular the zero point energy (ZPE), which is inversely proportional to atomic mass (or more particularly, proportional to the inverse square of the mass), is measurably lower for the C-D bond in comparison to the C-H bond as deuterium is heavier. This means that the activation energy E_a needed to break the bond containing deuterium is larger despite the fact that the barrier height (or potential) is identical to that for hydrogen, since E_a depends on the ZPE.

For this reason the effect with isotopes such as ^{13}C the difference is generally less observable since the difference in mass is relatively insignificant, and for this reason the kinetic isotope effect for ^{13}C is less discernible. Interestingly, experimentally for the substitution of deuterium for hydrogen does not necessarily result in the reaction rate being slower. When deuteration doesn't affect the reaction rate, this is an indication that tunnelling is not a signif-

icant part of the reaction mechanism, which could be due to properties of the PES meaning that tunnelling would be energetically unfavourable, or because the system is already thermalised to an energy level above the barrier height and thus the reaction is apparently barrierless.

In cases where PT is the rate limiting step, a first principles understanding of the mechanism is essential. ET is a fundamentally quantum process due to the small size of electrons. Indeed, electrons are well known to exhibit wave-like characteristics, meaning that a classical description is fundamentally flawed, particularly in ET processes where tunnelling plays a significant role. Although protons are significantly heavier, a classical description is similarly inadequate. This is especially true in the description of PT because of the vital role that coupling to the environment plays in this process. Indeed research suggests that the tunnelling which occurs in many reactions that involve PT far exceeds what would be expected for a particle of its size [1], which is one reason why it is so important to model this effect accurately.

As has been discussed earlier in this chapter, a density matrix description can easily incorporate system-bath coupling effects which makes it an ideal model for ET and PT processes. Systems which are well described by density matrices are those where the quantum character can be adequately represented by a limited number of degrees of freedom which are embedded in an environment system of classical behaviour. An example where density matrix evolution (DME) would not be appropriate is a system where the wavefunction develops into delocalised shapes, for example for a solvated electron, which would require a large number of basis functions.

Wolfseder et al [36] proposed a method for treating ET processes in a non-pertubative approach by using a density matrix description in the framework of Redfield theory. This was applied to a general dissipative ET system and various pump-probe spectra were simulated to femtosecond resolution. The authors also undertook a simulation of coherent photon-echo signals which they resolved in frequency, time and direction of emission with the purpose of understanding the effects of vibrational damping on the process.

To a similar effect, Egorova et al [37] demonstrated the utility of multilevel Redfield theory when applied appropriately to ultrafast photoinduced ET reactions. Dynamics simulations were run on a standard model for ET in the condensed phase, for different temperatures and values of coupling and reorganisation energy and these were compared with results from the self-consistent hybrid method. This model was adapted in a further article by Egorova [38] to investigate the fluorescence spectra in nonadiabatic systems.

The first article on PT considered here is that of double PT in benzoic acid crystals from the perspective of quantum operator theory [39]. To explain the clearly nonclassical tunnelling effects in this system even at high temperatures where the energetic barrier for PT is more accessible, this article applied quantum Kramer's theory, to justify the low activation energy that is observed in kinetic isotope experiments. In particular, the model looked at incorporating the effects of coupling with a condensed phase environment and included symmetric coupling to the intramolecular mode. Calculations were reported for the activation energies of hydrogen and deuterium which agree quantitatively with experiment.

The method of DME was applied to a PT process in a fluctuating double well potential by Berendsen et al, 1993 [40]. This generalised model was constructed to describe a 1-D collision of a classical particle with a quantum oscillator to replicate the process of PT along a hydrogen bond. This system is particularly well represented by DME as nonadiabatic transitions are well characterised in this method and because it is possible to model the system reasonably well using few quantum degrees of freedom. The paper also demonstrated how the classical equations of motion can be ensured to be consistent with the quantum model and conserve total energy.

The same authors proceeded to write a review of the DME procedure [41] and continued developing the model to apply it to PT in aqueous hydrogen malonate [42]. The objective was to calculate the rate of proton tunnelling in the intramolecular double well of this molecule and compare the model results with approximate analytic solutions calculated by Borgis and Hynes 1991 [43] and with the classical rate in the nonadiabatic limit which was also estimated in this paper. The authors considered the use of a biased sampling method to search for configurations with greater tunnelling probability, and found that, after a correction was applied, the resulting rate was equivalent to an unbiased one.

The paper surmises that the differences in the free energy of solvation of the two forms of the molecule (the symmetric and antisymmetric positions of the proton) correspond to the solvent reorganisation energy to ensure no energy splitting between product and reactant states. Despite various limitations of the model the tunnelling rate found using their DME method was similar to the one calculated by Borgis at just 5 times smaller, and their estimate using

classical TST was slightly larger. This study shows the potential of using density matrices to describe PT, which motivates why it is useful to develop this further within the ML-MCTDH formalism. It is hoped that this will be far more efficient than the methods used in these earlier studies, which will allow more complicated and interesting systems to be studied.

1.5 Thesis overview

This thesis looks at the quantum dynamical context leading to the development of density matrices and gives an overview of the derivation and main notational conventions of this construction, also exploring how the density matrix description has been applied to quantum dynamical systems. There is a discussion of the issue of dimensionality with regards to computation, and an exploration of how the MCTDH framework has been constructed to address this.

A full derivation of the equations of motion of the MCTDH algorithm are presented as well as the different versions of the density matrix formulation (ρ-MCTDH). This leads on to the key result of the thesis that the multi-layer formulation of MCTDH can be directly used for the propagation of density matrices. As demonstrated in the results of subsequent chapters, this will allow much larger density matrices to be propagated than presently possible. The problem of modelling the significant quantum effects that can influence the process of ET and PT is discussed, looking at how experimentalists and theoreticians have approached this phenomena. A simple model is implemented to better understand the crucial role the environment

plays in the process of PT, and the three methods (MCTDH, ρ-MCTDH and ML-MCTDH) are compared. The computational effort, timing and error is assessed, as well as the behaviour of each method in a parallel setting and the problem of basis set convergence.

Chapters 2 and 3 cover the theory and methodology underpinning the research focus. In the remaining chapters results are presented and discussed. The question posed in this thesis is what can scientists do when the gas phase zero temperature picture is no longer a useful description for the reactions and processes that we are interested in. For instance, if we look at PT, there is still a lot of uncertainty about the exact mechanism and the role that is played by the environment in this process. The approach which is taken is to use density matrices within the MCTDH framework in a study of PT within salicylaldimine and for a model symmetric PT system. A final study looks at double PT in porphycene. Studies using density matrices with over 10 degrees of freedom are shown to be possible.

Chapter 2

Theory

2.1 Quantum dynamics

Introductions to quantum mechanics begin with the idea that a system may be described by a Hamiltonian operator, $\hat{H}$, and its eigenstates can be found by solving the differential equation

$$\hat{H}|\Psi_n\rangle = E_n|\Psi_n\rangle. \tag{2.1}$$

This is known as the (time independent) Schrödinger equation and the quantities $\{|\Psi_n\rangle\}$ are eigenstates of the system, with associated eigenvalue energies $\{E_n\}$. This is a stationary wavefunction picture of quantum mechanics, and any state of the system can be written as some combination of these eigenstates $\{|\Psi_n\rangle\}$. The premise of quantum mechanics is that if the Schrödinger equation for a system is solved exactly then all physical quantities of the system can be determined, in an equivalent way to Newton's equations in classical mechanics which were for hundreds of years thought to fully explain our physical world. Clearly the complete Hamiltonian describing positions and momenta of all particles in the universe can never be determined, so

in practice a reduced system Hamiltonian is almost always used, thus the system is no longer fully deterministic.

Rather than using the TISE as shown in (2.1), in order to determine dynamical information such as reaction rates and mechanisms we must consider the time-dependant picture. The time dependent case requires more work as evolving wavefunctions are found instead by solving the time dependent Schrödinger equation (TDSE)

$$i\hbar\frac{\partial\Psi(x,t)}{\partial t} = \hat{H}\Psi(x,t) \tag{2.2}$$

This equation shows the 1-dimensional case but the TDSE can be extended to any number of dimensions. Note that $\hbar$ is Planck's constant divided by 2π. Assuming that the wavefunction can be written as a product of distinct position and time parts, as in $\Psi(x,t) = \psi(x)\chi(t)$, and assuming that $\hat{H}$ is time-independent, then this differential can be treated as first order separable which rearranges to give

$$i\hbar\frac{\dot{\chi}(t)}{\chi(t)} = \frac{\hat{H}\psi(x)}{\psi(x)} = E \text{ (constant)}. \tag{2.3}$$

Since the left hand side of this equation is independent of position just as the right hand side is independent of time, then the only way they can be equal is if both sides are equal to a constant, here this constant is denoted E. Then each side may be solved separately, for the particular constant E [44];

$$\hat{H}\psi(x) = \Big\{ -\frac{\hbar^2}{2m}\frac{\partial^2}{\partial x^2} + \hat{V}(x)\Big\}\psi(x) = E\psi(x), \tag{2.4}$$

$$i\hbar\dot{\chi}(t) = E\chi(t) \implies \chi(t) = Ae^{-\frac{i}{\hbar}Et} \text{ (for some constant } A). \tag{2.5}$$

Note that $\hat{V}(x)$ is the potential operator. Then the particular solution of the complete wavefunction can be written $\Psi(x,t) = \psi(x)e^{-\frac{i}{\hbar}Et}$. Note that the potential could also be time-dependent ($V(x,t)$) and multidimensional, and

the importance of this quantity is that for bound potentials the physical solutions will exist for discrete values of the energy, E. For unbound potentials meaningful solutions exist for a continuous range of E. The general solution is therefore a linear sum of these particular energy solutions for the bound potential, and an integral in the unbound case:

$$\Psi(x,t) = \sum_{n=1}^{\infty} a_n(t)\psi_n(x)e^{-\frac{i}{\hbar}E_n t} \text{ (discrete spectrum)} \tag{2.6}$$

$$\Psi(x,t) = \int_0^{\infty} a(E)\psi_E(x)e^{-\frac{i}{\hbar}Et}dE. \text{ (continuous spectrum) [45]} \tag{2.7}$$

These time dependent states of a system are called 'wavepackets'. It is also possible to get a potential which is bound in some regions of configuration space and unbound in other regions. As before, if the TDSE is solved exactly for all time then all physical and dynamical properties can be extracted. However, depending on the complexity of the system potential, the number of terms involved means this calculation can be computationally prohibitive. Therefore in most cases a full solution is only possible for very simple, few particle systems and for short timescales, largely due to the complexity caused by the coupling between different degrees of freedom in the potential. In systems where there is little or no coupling between the degrees of freedom in the potential, the TDSE is easily soluble even for very large systems.

One strategy used to address this issue in atomic and molecular systems is to decouple the electron and nuclear motion by assuming that they are independent of each other. This is called the Born-Oppenheimer approximation [46, 47], which relies on the fact that the difference in mass between an electron and a nucleus causes them to move at different speeds. Therefore the nuclear geometry can be treated as fixed with respect to the electronic motion without too much loss of accuracy. In the Born-Oppenheimer approximation

relativistic effects due to coupling between electronic and nuclear degrees of freedom are therefore neglected, which means that the nuclear and electronic wavepackets can be treated separately which simplifies the problem significantly. The advantage of this is that there are many well established methods (such as DFT, density functional theory or MP2, second order Møller-Plesset theory [48, 49]) designed to provide approximate solutions to the TISE for electrons at a given set of nuclear coordinates. These can be used to build up a relatively accurate picture of the electronic potential energy surface (PES). The PES which is calculated using one of the above methods is the potential energy landscape of the electrons in the configuration space of a molecular system, under the assumption of fixed nuclear coordinates. The TDSE for the nuclear wavefunction can then be solved using this PES. The nuclear problem is significantly more problematic however, as the full configuration interaction must be included in order to establish a quantum dynamical picture which is useful and sufficiently accurate. This is largely due to strong nuclear correlations that must be fully accounted for.

2.2 Density matrices

The use of density matrices to describe quantum systems was introduced by Von Neumann (1927) and has been developed and formalised by researchers such as Wigner [50], Hillery [51] and Fano [52], gaining momentum in recent years due to increased computational capabilities. Density matrices are an alternative to wavepackets in representing quantum dynamical systems, and are superior in some aspects as they are inherently able to describe 'mixed quantum states' and they can easily be constructed to include environmental

effects, as mentioned above. Indeed it is a major drawback that a wavepacket description of quantum dynamics can only describe the pure states (or eigenstates) of a system, since real systems exist in mixed states (non eigenstates) most of the time.

It is well known that pure states are only able to represent wavepackets, which is insufficient for looking at a system which is thermalised, not in equilibrium or open. This is due to the fact that a wavepacket can always be written as a coherent superposition of states $|\Psi_i(t)\rangle$:

$$|\Phi(t)\rangle = \sum_i c_i(t)|\Psi_i(t)\rangle, \tag{2.8}$$

where $|c_i(t)|^2 = p_i$, the probability of observing the system in state $|\Psi_i\rangle$. In contrast the full density operator of a system is defined to be

$$\hat{\rho}(t) = \sum_i |\Psi_i(t)\rangle p_i \langle\Psi_i(t)|. \tag{2.9}$$

Again p_i is the probability of being in state $|\Psi_i(t)\rangle$ and $\sum_i p_i = 1$. Note first that the density operator can represent both pure and mixed states as it is in general an incoherent superposition of pure states $|\Psi_i(t)\rangle\langle\Psi_i(t)|$.

The convention for $|\Psi_i(t)\rangle$ is that they must be normalised, but they do not necessarily need to be orthogonal. It is also worth noting that the states of the system $|\Psi_i(t)\rangle$ do not necessarily need to be energy eigenstates and the p_i form a probability distribution since $\sum_i p_i = 1$ implies that if one $p_j = 1$ then all other p_i must be identically 0. A density matrix is expanded in the basis $\{|n\rangle\}$ with diagonal elements

$$\rho_{nn} = \langle n|\hat{\rho}|n\rangle = \sum_i p_i \langle n|\rho_i|n\rangle = \sum_i p_i \langle n|\Psi_i\rangle\langle\Psi_i|n\rangle = \sum_i p_i |c_n^{(i)}|^2, \tag{2.10}$$

where $\rho_i = |\Psi_i(t)\rangle\langle\Psi_i(t)|$, $c_n^{(i)} = \langle n|\Psi_i\rangle$ and $c_n^{(i)*} = \langle\Psi_i|n\rangle$. The above statement also holds if $|\Psi_i(t)\rangle$ are an orthogonal basis set, but this is not a necessary condition (any normalised basis set will work). Notice that since $|c_n^{(i)}|^2$ is the probability of finding a system described by the normalised eigenstate $|\Phi_i\rangle$ in the state $|n\rangle$, the interpretation of $\sum_i p_i|c_n^{(i)}|^2$ is that it is the probability of finding a system described by the density operator ρ in the state $|n\rangle$. In a thermalised system, p_i are the Boltzmann factors $e^{-E_i/kt}$, where E_i is the energy of state Ψ_i.

For a system described by $\hat{\rho}$, ρ_{mn} represents the quantum coherences between states $|m\rangle$ and $|n\rangle$, for instance tunnelling can be represented by the occupation of these off-diagonal elements of the density matrix. A general off-diagonal element is written:

$$\rho_{mn} = \sum_i p_i \, c_m^{(i)} \, c_n^{(i)*}. \tag{2.11}$$

Since density matrices are to functions as operators are to functions, it is worth demonstrating a few fundamental properties of this formalism.

The equation of motion for density matrices is known as the Liouvillian, $\mathcal{L}(\hat{\rho})$, and is given as follows:

$$\mathcal{L}(\hat{\rho}) = \frac{d\hat{\rho}}{dt} = \frac{-i}{\hbar}[\hat{H}, \hat{\rho}]. \tag{2.12}$$

Similar to the wavefunction equation of motion, the Liouville equation contains full information on a system at a particular time if it is solved exactly. To prove this property holds, firstly consider the direct time derivative of an arbitrary matrix element $\hat{\rho}^{(i)}(t) = |\Psi_i(t)\rangle\langle\Psi_i(t)|$. Then

$$\frac{d}{dt}\hat{\rho}^{(i)}(t) = \Big(\frac{d}{dt}|\Psi_i\rangle\Big)\langle\Psi_i| + |\Psi_i\rangle\Big(\frac{d}{dt}\langle\Psi_i|\Big) \tag{2.13}$$

$$\implies \frac{d}{dt}\hat{\rho}^{(i)} = \frac{1}{i\hbar}(\hat{H}|\Psi_i\rangle\langle\Psi_i| - |\Psi_i\rangle\langle\Psi_i|\hat{H}) = \frac{1}{i\hbar}[\hat{H}, \hat{\rho}^{(i)}]. \tag{2.14}$$

Using the definition that $\hat{\rho} = \sum_i p_i\hat{\rho}^{(i)}$, and noting that p_i is constant with respect to time, then pre-multiplying both sides of the equation with p_i and summing over all degrees of freedom i gives the full expression for the Liouville equation:

$$\frac{d}{dt}\Big(\sum_i p_i\hat{\rho}^{(i)}\Big) = \frac{1}{i\hbar}\Big(\bar{H}\sum_i p_i|\Psi_i\rangle\langle\Psi_i| - \Big(\sum_i p_i|\Psi_i\rangle\langle\Psi_i|\Big)\hat{H}\Big) \tag{2.15}$$

$$\implies \frac{d\hat{\rho}}{dt} = \frac{1}{i\hbar}[\hat{H}, \hat{\rho}]. \text{ [53]} \tag{2.16}$$

Finally, it is useful to consider the proof of the fact that $\mathrm{Tr}(\hat{\rho}) = 1$. As mentioned, the eigenvalues of the density matrix form a probability distribution and since the total of any probability distribution is always 1 we expect $\mathrm{Tr}(\hat{\rho}) = 1$. Let us prove this holds mathematically. Let $\{|n\rangle\}$ be a complete orthonormal basis for our density matrix, then recall that $\sum_n |n\rangle\langle n| = 1$. Now observe

$$\begin{aligned}
\mathrm{Tr}(\hat{\rho}) &= \sum_n \langle n|\sum_i p_i|\Psi_i\rangle\langle\Psi_i|n\rangle \\
&= \sum_i p_i \sum_n \langle\Psi_i|n\rangle\langle n|\Psi_i\rangle \\
&= \sum_i p_i\langle\Psi_i|\Big(\sum_n |n\rangle\langle n|\Big)|\Psi_i\rangle \\
&= \sum_i p_i\langle\Psi_i|\Psi_i\rangle = \sum_i p_i = 1. \text{ [54]}
\end{aligned} \tag{2.17}$$

In fact practical use of the full density operator is limited to very small systems, which motivates the introduction of a 'reduced' density operator.

To understand this better, imagine the complete system Hamiltonian can be partitioned into a core 'system of interest' and a surrounding 'bath', where $\hat{H}_s$, the system, includes the information on the quantum activity of interest and everything else is contained in the bath $\hat{H}_b$. Define $\hat{H} = \hat{H}_s + \hat{H}_b + \hat{H}_{sb}$, where $\hat{H}_{sb}$ describes the interaction between the two other parts. Then the 'reduced density operator' $\hat{\rho}_s$ is defined to be the trace over the degrees of freedom of the bath:

$$\hat{\rho}_s = \mathrm{Tr}_b(\hat{\rho}), \tag{2.18}$$

where $\hat{\rho}$ is the full density operator as defined above. The value of this construction is that ρ_s can be used, under certain conditions of approximation, to describe open systems. One useful assumption which is often made in order to simplify the problem is that the system bath interaction is weak, and that the dynamics of the bath is much faster than that of the system. This is called the Markov approximation, and it is important to note that this must neglect memory effects and implies an assumption of irreversibility. From this point, there are two distinct approaches to deriving an equation of motion which can be used in a similar way to the Liouville equation for the full density operator. The first is the Redfield [55] equation of motion which is derived with a perturbative approach. This gives

$$\frac{\partial \hat{\rho}_s}{\partial t}(t) = \frac{-i}{\hbar}[\hat{H}_s, \hat{\rho}_s] + \hat{R}(t). \tag{2.19}$$

The operator $\hat{R}(t)$ describes the relaxation process of the system due to system-bath coupling. The second is known as the Lindblad [56] [57] equation of motion:

$$\mathcal{L}(\rho) = -i[H, \rho] + \sum_j (V_j \rho V_j^\dagger - \frac{1}{2} V_j^\dagger V_j \rho - \frac{1}{2} \rho V_j^\dagger V_j). \tag{2.20}$$

$\mathcal{L}(\rho)$ is the Liouvillian which was introduced in equation (2.12), which is equivalent to the TDSE in the pure state limit. In this equation the Liouvillian is perturbed to include the Lindblad dissipative terms V_j. It is important to note that the Lindblad equation assumes that the energy can flow from the system to the bath but not from the bath back into the system.

Overall, the properties of density matrices are summarised:

- Density matrices are Hermitian, which means that $\rho_{nm} = \rho^*_{mn}$.
- Diagonal elements of ρ are non-zero: $\rho_{nn} \geq 0$. ρ_{nn} can be seen as the probability of system being found in state $|n\rangle$.
- Expectation value of operator A is $\langle A \rangle = \mathrm{Tr}(A\rho)$.
- $\mathrm{Tr}(\rho) = 1$, if normalised.
- $\mathrm{Tr}(\rho^2) \leq 1$, in general.
- $\mathrm{Tr}(\rho^2) = 1$, for pure states only.

Chapter 3

Methodology

3.1 Preamble

The next challenge is to represent the problem of nuclear dynamics under the Born-Oppenheimer representation efficiently in a computer model. Once the electronic potential energy surface (PES) has been calculated for the configuration space that is considered in the model, the nuclear part must be determined in relation to the PES. Determining the nuclear wavepacket as a function of electronic configurations takes significant computational effort, meaning that it is not feasible to find these quantities for every point on the continuous PES. Therefore points must be chosen on the PES, which are representative of where our system is likely to move in configuration space. The nuclear wavefunction is then represented on these points by 'basis functions' premultiplied by coefficients, and the collective set of points is known as the 'grid'.

A simple evenly spaced grid would be useless at representing the shape of

a complex PES, unless the points are closely spaced which would require a large basis set. This is problematic computationally since the bigger the basis the higher the memory cost. There are a multitude of different basis sets, known as discrete variable representation (DVR), which are used to decide which points on the PES are selected. Conventional methods represent the nuclear wavefunction directly in the time-independent DVR and can only treat 4 or 5 degrees of freedom fully. MCTDH can directly treat up to 20 degrees of freedom of a system accurately, although using mode combination methods more than 20 is possible. Consider the generic form of the MCTDH wavefunction

$$\Psi(\mathcal{Q}_1,\ldots,\mathcal{Q}_f,t)=\sum_{j_1=1}^{n_1}\cdots\sum_{j_f=1}^{n_f}A_{j_1\ldots j_f}(t)\prod_{\kappa=1}^{f}\phi_{j_\kappa}^{(\kappa)}(\mathcal{Q}_\kappa,t). \text{ [58]} \tag{3.1}$$

In this notation, f is the number of degrees of freedom, $\mathcal{Q}_1,\ldots,\mathcal{Q}_f$ are the nuclear coordinates, $A_{j_1\ldots j_f}$ are time-dependent expansion coefficients, and n_κ is the number of basis functions used for representing the κ^{th} degree of freedom. Notice that the basis functions are time dependent, which is important because it ensures that they can evolve in time to optimally represent the wavepacket. The fact that the basis functions are time dependent means that a smaller basis is needed which is one of the reasons that the grid used in MCTDH is more efficient than other methods. The efficiency of the grid method used in MCTDH is one reason why it performs so much better than equivalent procedures.

The variational principle used in MCTDH is the following:

$$\langle\delta\Psi|H-i\frac{\partial}{\partial t}|\Psi\rangle=0. \tag{3.2}$$

This is called the Dirac-Frenkel variational principle [59, 60], and is used to derive the equations of motion which drives the dynamics in MCTDH.

ρ-MCTDH operates in much the same way as MCTDH but instead of a wavefunction, a density operator is propagated with an equation of motion based on one of the Redfield or Lindblad schemes. The general form of these density operators is discussed in the following section which gives a brief outline of the original publication which introduced the development of ρ-MCTDH.

3.2 Examples of ρ-MCTDH

The main papers concerning the development and implementation ρ-MCTDH are by Raab et al [61,62] who developed the extension of the MCTDH package to include the density matrix propagation methodology. Raab outlines the derivation of two main propagator schemes, which are based on different approximate forms of the density operator specifically adapted to be incorporated into the MCTDH formalism. These are known as types I and II respectively.

$$\rho_I(\mathcal{Q}_1,\ldots,\mathcal{Q}_f,\mathcal{Q}_1^{'},\ldots,\mathcal{Q}_f^{'},t)=\sum_{\tau_1=1}^{n_1}\cdots\sum_{\tau_f=1}^{n_f}B_{\tau_1\ldots\tau_f}(t)\times\prod_{\kappa=1}^{f}\sigma_{\tau_\kappa}^{(\kappa)}(\mathcal{Q}_\kappa,\mathcal{Q}_\kappa^{'},t), \tag{3.3}$$

$$\begin{aligned}&\rho_{II}(\mathcal{Q}_1,\ldots,\mathcal{Q}_f,\mathcal{Q}_1^{'},\ldots,\mathcal{Q}_f^{'},t)\\&=\sum_{j_1,l_1=1}^{n_1}\cdots\sum_{j_f,l_f=1}^{n_f}B_{j_1\ldots j_f,l_1\ldots l_f}(t)\prod_{\kappa=1}^{f}\left|\phi_{j_k}^{(\kappa)}(\mathcal{Q}_\kappa,t)\right\rangle\left\langle\phi_{l_k}^{(\kappa)}(\mathcal{Q}_\kappa^{'},t)\right|.\end{aligned} \tag{3.4}$$

Thus in type I ρ is described by single particle density operators (or SPDOs $\sigma_{\tau_\kappa}^{(\kappa)}(\mathcal{Q}_\kappa,\mathcal{Q}_\kappa^{'},t)$) whereas the basis for type II are single particle functions

(SPFs) like in standard MCTDH.

One of these papers by Raab focused on the type II density operator applied to a model pyrazine system, which is particularly useful for benchmarking purposes since the full 24-mode model has already been investigated using MCTDH [63], and experimental results are also well established. Raab demonstrated the capability his package has to propagate over a range of temperatures, with results for the state populations, linear absorption spectrum and Fourier transform of autocorrelation function taken at 0K, 300K and 500K with clearly explicable trends. Consideration was taken to determine which integration method (CMF - constant mean field, VMF - variable mean field) and propagation scheme was the most efficient in terms of time and CPU and overall accuracy in a series of tests at different temperatures and with differing numbers of basis functions. The conclusion was that DFVP (based on the Dirac-Frenkel/MacLachlan variational principle) along with the CMF integrator yielded the most accurate results in combination with efficiency and CPU time.

In a second article by Raab [62] a modified Henon-Heiles system was used, along with an application to pyrazine, to focus in detail on the effect that the number of basis sets and grid points has on the efficiency of the calculations. Both density types I and II were tested equally in this paper, in the context of open, closed and varyingly thermalised systems for timescales up to 1000fs. A measures of the error incurred during propagation was measured in each example, in different ways depending on the propagation method; type I or II. For density II the trace was conserved by construction, as it should be if a closed system was perfectly modelled. For type I, the trace begins at

value 1 and any decrease gives an indication of error. Similarly, the loss of energy of closed systems, $\Delta E/E_0$ was noted. Both of these errors arise due to the construction of the equations of motion, as will be shown below, and will become negligible on convergence.

3.3 Multilayer MCTDH

Multilayer MCTDH is a more immediate extension of the MCTDH code, in comparison with the use of a density operator. Indeed, in order to tackle larger problems using MCTDH, it is often necessary to combine several modes in the input file in order to reduce the configuration space and therefore the computation time. The extension to this idea was pioneered by Wang and Thoss [64] and extended further by Manthe [65] to deal with larger problems more efficiently by specifying exactly how the wavefunction of each mode is decomposed into lower dimensional SPFs, as distinct from ordinary MCTDH where they are simply represented by a base-layer (or grid).

Examples of the precise specification for the 'multilayered' basis set is discussed below, but it is worth beginning by defining the generalised form of the ML-MCTDH wavefunction:

$$|\phi_n^k(t)\rangle = \sum_I B_I^{k,n}(t)|u_I^k(t)\rangle \equiv \sum_{i_1}\sum_{i_2}\cdots\sum_{i_{\mathcal{Q}(k)}} B_{i_1 i_2 \ldots i_{\mathcal{Q}(k)}}^{k,n}(t)\prod_{q=1}^{\mathcal{Q}(k)}|v_{i_q}^{k,q}(t)\rangle. \tag{3.5}$$

The constituents of this equation are defined analogously to the ordinary MCTDH wavefunction outlined in Section 3.4, but the main idea is that the lowest dimensional SPFs are contained in a sequence of higher dimensional

layers of SPFs. The propagation and expansion coefficients are calculated at each 'layer' and the basis can be set up to accommodate as many or as few layers of SPFs as are required by the problem. Clearly some problems are naturally better suited to this method, because any effort that is saved by propagating lower dimensional SPFs will be offset by the cost of minimising the additional layers of coefficients and by the extra propagation steps.

In a system which is mostly weakly coupled, combining some of the slightly more correlated modes is an effective strategy. However, if a model has a more intricate system of coupling then this strategy of mode combination will not simplify the calculation. While ML-MCTDH is an entirely general method which can in theory be applied to any chemical model of interest, it has mostly been used to investigate weakly coupled symmetric system-bath type models where the majority of modes belong to a simple harmonic oscillator type bath. The focus on these somewhat simplified models is dually a consequence of the research interests of the academics who have thus far used this method, and to the inherent challenge of specifying an efficient multilayer basis decomposition for systems with more complex coupling schemes. The dimensionality issues inherent in a problem which is asymmetric or strongly coupled are not fatal to this method but will have greater computational effort unless an optimal basis can be found. While ordinary MCTDH is only viable up to 25 to 30 degrees of freedom, the power of ML-MCTDH is its ability to propagate systems with many hundreds of modes to numerical accuracy. Indeed this method has proved powerful in applications to a range of problems [66–71].

One application which is particularly pertinent uses ML-MCTDH to inves-

tigate two PT reactions in a condensed phase environment [67]. The article varies the temperature and system-bath coupling strength to understand the relationship these factors have with the thermal rate constant and quantum flux correlation function of each system. In this paper an approximation is made for estimating the thermal energy, based on sampling from the Boltzmann distribution. This is discussed further in Chapter 5. Similar to previous examples discussed, the models in this paper are constructed with a double-well potential coupled to a bath of harmonic oscillators. It is easy to see how this system would be well represented by a density matrix approach, due to the fact that it is described by a small number of modes and because of the important role of the environment.

To explain how the basis is set up, consider Figure 3.1, which corresponds to distinct multilayer basis specifications. The top node of the figure indicates the full MCTDH-wavefunction which is n-dimensional for an n-mode system. Each subsequent layer reduces the dimension by one. The 'zeroth layer' in the ML-basis-section specifies how many 'groups' of layers the wavefunction is represented and the number of SPFs in each group. In the first example, the basis splits into five groups, the first of which consists of three SPFs and the others contain just two. Regardless of how many layers are used, the base layer is the generic MCTDH grid, as with ordinary MCTDH, and therefore does not need to be specified in the input file, but is indicated in the diagram with the square boxes.

The second example (lower diagram) splits into five groups of SPFs. Following along the furthest right branch of the second tree, this section of the basis contains the modes x14 - x17. The top layer of this branch consists

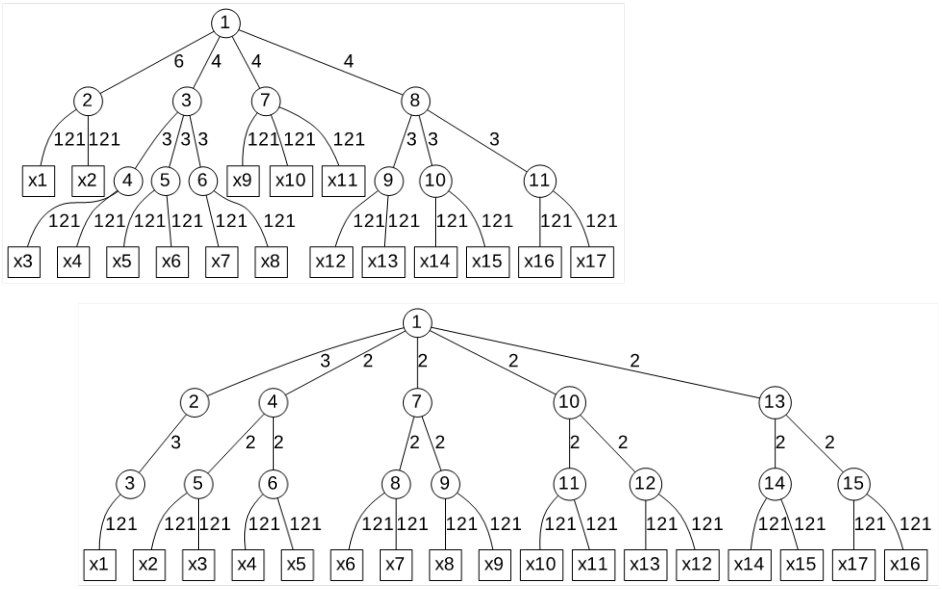

Fig. 3.1: ML-MCTDH tree representing two different basis set contractions for a 17-mode PT model.

of four SPFs which splits into two groups of two SPFs. Both of these 17-mode calculations were applied to the spin boson model proposed by Craig et al [67]. More information on these calculations and the relevant inputs is discussed later, but it is worth noting here that the latter basis gave a better converged result while the former was significantly faster.

3.4 Introduction to MCTDH

Once the electronic potential energy surface has been determined using a chosen electronic structure method such as DFT, Hartree Fock etc. (or parametrised by a model), the nuclear dynamics of a system can be explicitly calculated using MCTDH. This method works within the BOA and provides a numerically exact solution to the TDSE. Whereas the PES is calculated from the time independent electronic SE, the TDSE allows us to capture the kind of non equilibrium information about a molecules behaviour which is

required in order to understand reaction pathways and the role that is played by quantum effects. While much information can be gained from simply considering the time independent electronic structure, accurate information on quantum effects or non equilibrium behaviour for instance in a reaction is simply lost in this kind of single point calculation due to the fact that a molecule is rarely completely stationary.

The standard method, which exactly propagates a nuclear wavefunction using time dependent coefficients, has existed since the 1960's [72]. Building on this, the MCTDH method which was developed in the 1990's [58, 73–77] uses a smaller number of optimal time dependent coefficients and SPFs. In Chapter 4 we will revisit the exact method in order to demonstrate how a new Chebyshev integrator has been implemented to contract the time evolution into a single timestep.

Start by recalling the TDSE, here in atomic units:

$$i\dot{\Psi} = \hat{H}\Psi. \tag{3.6}$$

In order to solve this computationally we need to represent the full multidimensional wavefunction as a product of some basis. In the standard method this is

$$\Psi(Q_1, \ldots, Q_f, t) = \sum_{j_1=1}^{N_1} \cdots \sum_{j_f=1}^{N_f} C_{j_1 \ldots j_f}(t) \prod_{\kappa=1}^{f} \chi_{j_\kappa}^{(\kappa)}(Q_\kappa). \tag{3.7}$$

The DFVP [60] is used to derive equations of motion for each of the time dependent expansion coefficients:

$$\langle \delta\Psi | \hat{H} - i\frac{\partial}{\partial t} | \Psi \rangle = 0 \tag{3.8}$$

which gives coefficients

$$i\dot{C}_J = \sum_L \hat{H}_{JL} C_L \tag{3.9}$$

where the notation J and L has been introduced to simplify it to $J = j_1 \dots j_f$,

$$\hat{H}_{JL} = \langle \chi_{j_f}^{(1)} \dots \chi_{j_f}^{(f)} | \hat{H} | \chi_{j_f}^{(1)} \dots \chi_{j_f}^{(f)} \rangle. \tag{3.10}$$

In this formalism the wavepacket is represented in the full product primitive basis. In contrast, in MCTDH this is simplified by introducing a smaller set of optimal time dependent basis functions, which means that the wavepacket is expanded much more compactly as:

$$\begin{aligned} \Psi(Q_1, \dots, Q_f, t) &= \sum_{j_1=1}^{n_1} \cdots \sum_{j_f=1}^{n_f} A_{j_1 \dots j_f}(t) \prod_{\kappa=1}^{f} \phi_{j_\kappa}^{(\kappa)}(Q_\kappa, t) \\ &= \sum_J A_J \Phi_J, \end{aligned} \tag{3.11}$$

where each degree of freedom is represented by a small set of optimal time dependent SPFs, and each SPF is comprised of a linear combination of the primitive basis functions which is a time independent grid called the DVR [78–81] (discrete variable representation):

$$\phi_{j_\kappa}^{(\kappa)}(Q_\kappa, t) = \sum_{i_\kappa=1}^{N_\kappa} c_{i_\kappa j_\kappa}^{(\kappa)}(t) \chi_{i_\kappa}^{(\kappa)}(Q_\kappa). \tag{3.12}$$

The DVR has been derived for sine, exponential, Legendre polynomial and harmonic oscillator functions [58, 82]. Ideally the basis functions should be orthonormal in order to reduce the effort of computation, so the following constraint has been applied without loss of generality:

$$\langle \phi_j^{(\kappa)}(0) | \phi_\ell^{(\kappa)}(0) \rangle = \delta_{j\ell}, \tag{3.13}$$

$$\langle \phi_j^{(\kappa)}(t) | \dot{\phi}_\ell^{(\kappa)}(t) \rangle = -i \langle \phi_j^{(\kappa)}(t) | g^{(\kappa)} | \phi_\ell^{(\kappa)}(t) \rangle. \tag{3.14}$$

This is the same as just applying the more general constraint $g^{(\kappa)} = 0$.

Now we apply the DFVP which results in the following equations of motion for the time-dependent MCTDH coefficients and SPFs:

$$i\dot{A}_J = \sum_L \langle \Phi_J | \hat{H} | \Phi_L \rangle A_L, \tag{3.15}$$

$$i\dot{\boldsymbol{\phi}}^{(\kappa)} = (1 - P^{(\kappa)})(\boldsymbol{\rho}^{(\kappa)})^{-1} \langle \mathbf{H} \rangle^{(\kappa)} \boldsymbol{\phi}^{(\kappa)}. \tag{3.16}$$

The derivation of these equations of motion are detailed later in this chapter. This section has outlined how MCTDH operates for single state problems, however the adaptation for multistate problems is seen in [82, 83]. If some SPFs are of GWP type the method is called G-MCTDH.

$$\Psi(Q_1, \ldots, Q_f, t) = \sum_{j_1=1} \cdots \sum_{j_f=1} A_{j_1 \ldots j_f}(t) \prod_{\kappa=1}^{d} \phi_{j_\kappa}^{(\kappa)}(Q_\kappa, t) \prod_{\kappa=(d+1)}^{f} g_{j_\kappa}^{(\kappa)}(Q_\kappa, t). \tag{3.17}$$

In the case where the DVR is replaced by a basis of multidimensional time dependent GWPs this is called the vMCG method (variational multiconfigurational Gaussian) [34, 84–86]. The flexibility of vMCG basis in comparison to a grid based method means that the dynamics can be calculated without pre-calculating the PES, in what is known as the direct dynamics approach [87–90].

3.5 Derivation of MCTDH equations of motion

First define the following notation $J = (j_1, j_2, \ldots, j_f)$ is an ordered list of indices, $A_J = A_{j_1 \ldots j_f}$, $\Phi_J = \Pi_{\kappa=1}^{J} \psi_{j_\kappa}^{\kappa}$ and a trick which is used later to simplify the derivation is what is called a 'single-hole' function, where the Hartree

product includes everything except one degree of freedom. For simplification the time dependence of all SPFs (likewise coefficients) is not explicitly indicated but can be assumed, i.e. $A_J = A_{j_1 \dots j_f(t)}$, $\Phi_J = \Pi_{\kappa=1}^{J} \phi_{j_\kappa}^{\kappa}(t)$. For some integer p, the single hole function where the p-th degree of freedom is missing:

$$\begin{aligned}\Psi_\ell^{(p)} &= \sum_{j_1=1}^{n_1} \cdots \sum_{j_{p-1}=1}^{n_{p-1}} \sum_{j_{p+1}=1}^{n_{p+1}} \cdots \sum_{j_f=1}^{n_f} A_{j_1 \dots j_{p-1} \ell j_{p+1} \dots j_f} \psi_{j_1}^{(1)} \dots \psi_{j_{p-1}}^{(p-1)} \psi_{j_{p+1}}^{(p+1)} \dots \psi_{j_f}^{(f)} \\ &= \sum_{J^\kappa} A_{J_\ell^\kappa} \Phi_{J^\kappa}, \end{aligned} \tag{3.18}$$

where $J^\kappa = (j_1, \dots, j_{\kappa-1}, j_{\kappa+1}, \dots, j_f)$ and $J_\ell^\kappa = (j_1, \dots, j_{\kappa-1}, \ell, j_{\kappa+1}, \dots, j_f)$, $\Phi_{J^\kappa} = \sum_{\nu \neq \kappa}^{f} \psi_{j_\nu}^{(\kappa)}$ and the index ℓ is an integer which depends on the derivative, as seen in (3.22). We see in the next section how this is useful. Using this, the multi-configurational wavefunction can be simplified with this notation to:

$$\Psi = \sum_{j_1}^{n_1} \sum_{j_2}^{n_2} \cdots \sum_{j_f}^{n_f} A_{j_1, \dots, j_f} \psi_{j_1}^{(1)} \psi_{j_2}^{(2)} \dots \psi_{j_f}^{(f)} = \sum_J A_J \Psi_J = \Psi = \sum_{\ell=1}^{n_\kappa} \psi_\ell^{(\kappa)} \Psi_\ell^{(\kappa)}. \tag{3.19}$$

Consider the partial derivative of the wavefunction with respect to an arbitrary choice of coefficient, A_J. The only term that survives is the one that has A_J as a prefactor:

$$\frac{\partial \Psi}{\partial A_J} = \Phi_J. \tag{3.20}$$

Similarly consider the partial derivative with respect to some arbitrary $\psi_j^{(\kappa)}$:

$$\frac{\partial \Psi}{\partial \psi_j^{(\kappa)}} = \Psi_j^{(\kappa)}. \tag{3.21}$$

Since the coefficients SPFs are each time dependent the time derivative gives;

$$\dot{\Psi} = \sum_J \dot{A}_J \Phi_J + \sum_{\kappa=1}^{f} \sum_{j=1}^{n_\kappa} \dot{\psi}_j^{(\kappa)} \Psi_j^{(\kappa)}. \tag{3.22}$$

To derive the equation of motion for the coefficients, apply the DFVP to the following:

$$\begin{aligned}
\langle\frac{\partial\Psi}{\partial A_J}|\hat{H}|\Psi\rangle = \langle\Phi_J|H|\Psi\rangle &= \sum_L\langle\Phi_J|H|\Psi_L\rangle A_L \\
&= i\langle\frac{\partial\Psi}{\partial A_J}|\dot{\Psi}\rangle \\
&= i\langle\Phi_J|\dot{\Psi}\rangle \\
&= i\sum_L\langle\Phi_J|\dot{A}_L\Phi_L\rangle + i\sum_{\kappa=1}^{f}\sum_{\ell=1}^{n_\kappa}\langle\Phi_J|\dot{\psi}_\ell^{(\kappa)}\Psi_\ell^{(\kappa)}\rangle \\
&= i\dot{A}_J + i\sum_{\kappa=1}^{f}\sum_{\ell=1}^{n_\kappa}\langle\psi_{j_\kappa}^{(\kappa)}|\dot{\psi}_\ell^{(\kappa)}\rangle\langle\Phi_{J^\kappa}|\Psi_\ell^{(\kappa)}\rangle \\
&= i\dot{A}_J + i\sum_\kappa\sum_\ell(-ig_{j_\kappa\ell}^{(\kappa)})A_{J_\ell^\kappa}, \qquad (3.23)
\end{aligned}$$

where we have defined $g_{j_\kappa\ell}^{(\kappa)}$ and $A_{J_\ell^\kappa}$ in the following way:

$$g_{j_\kappa\ell}^{(\kappa)} = i\langle\psi_{j_\kappa}^{(\kappa)}|\dot{\psi}_\ell^{(\kappa)}\rangle = \langle\psi_{j_\kappa}^{(\kappa)}|\hat{g}_{(\kappa)}|\psi_\ell^{(\kappa)}\rangle \qquad (3.24)$$

$$A_{J_\ell}^\kappa = \langle\Phi_{J^\kappa}|\Psi_\ell^{(\kappa)}\rangle. \qquad (3.25)$$

Rearranging for $\dot{A}_J$ gives us that

$$i\dot{A}_J = \sum_L\langle\Phi_J|H|\Phi_J\rangle A_L - i\sum_{\kappa=1}^{f}\sum_{\ell=1}^{n_\kappa}g_{j_\kappa\ell}^{(\kappa)}A_{J_\ell^\kappa}. \qquad (3.26)$$

Now consider the partial derivative of the wavefunction with respect to one of the SPFs:

$$\begin{aligned}\langle\frac{\partial\Psi}{\partial\psi_j^{(\kappa)}}|\hat{H}|\Psi\rangle &= \langle\Psi_j^{(\kappa)}|H|\Psi\rangle \\ &= \langle\Psi_j^{(\kappa)}|H|\sum_\ell \Psi_\ell^{(\kappa)}\psi_\ell^{(\kappa)}\rangle = \sum_{\ell=1}^{n_\kappa}\langle H\rangle_{j\ell}^{(\kappa)} \\ &= i\langle\frac{\partial\Psi}{\partial\psi_j^{(\kappa)}}|\dot{\Psi}\rangle \\ &= \underbrace{i\sum_L\langle\Psi_j^{(\kappa)}|\Phi_L\rangle\dot{A}_L}+\underbrace{i\langle\Psi_j^{(\kappa)}|\sum_{\nu=1}^{f}\sum_{\ell=1}^{n_\nu}\dot{\psi}_\ell^{(\nu)}\Psi_\ell^{(\nu)}\rangle}\,. \end{aligned} \tag{3.27}$$

The first part simplifies in the case where $\hat{g}^{(\kappa)}=0$ to

$$i\sum_L\langle\Psi_j^{(\kappa)}|\Phi_L\rangle\dot{A}_L=\sum_L\langle\Psi_j^{(\kappa)}|\Phi_L\rangle\langle\Phi_L|H|\Psi\rangle, \tag{3.28}$$

since $i\dot{A}_L$ reduces to simply $\langle\Phi_L|H|\Psi\rangle$ when $\hat{g}^{(\kappa)}=0$. Recall that

$$\Phi_L=\Phi_{L^\kappa}\psi_{\ell_\kappa}^{(\kappa)},\Psi_j^{(\kappa)}=\sum_{J^\kappa}A_{J^\kappa}\Phi_{J^\kappa}. \tag{3.29}$$

So the first part of (3.27) simplifies to

$$\sum_{L^\kappa,\ell_\kappa}A_{L_j^\kappa}^*|\psi_{\ell_\kappa}^{(\kappa)}\rangle\langle\psi_{\ell_\kappa}^{(\kappa)}\Phi_{L^\kappa}|H|\Psi\rangle=P^{(\kappa)}\langle\Psi_j^{(\kappa)}|H|\Psi\rangle=P^{(\kappa)}\sum_{\ell=1}^{n_\kappa}\langle H\rangle_{j\ell}^{(\kappa)}\psi_\ell^{(\kappa)}, \tag{3.30}$$

where $P^{(\kappa)}$ is the 'projector' onto a single particle function with degree of freedom κ:

$$P^{(\kappa)}=\sum_{j=1}^{n_\kappa}|\psi_{\ell_\kappa}^{(\kappa)}\rangle\langle\psi_{\ell_\kappa}^{(\kappa)}|. \tag{3.31}$$

Now consider the second part of (3.27)

$$i\langle\Psi_j^{(\kappa)}|\sum_{\nu=1}^{f}\sum_{\ell=1}^{n_\nu}\dot{\psi}_\ell^{(\nu)}\Psi_\ell^{(\nu)}\rangle=i\langle\Psi_j^{(\kappa)}|\sum_{\ell=1}^{n_\kappa}\dot{\psi}_\ell^{(\kappa)}\Psi_j^{(\kappa)}\rangle=i\sum_{\ell=1}^{n_\kappa}\rho_{j\ell}^{(\kappa)}\dot{\psi}_\ell^{(\kappa)}. \tag{3.32}$$

Because the constraint means that out of the sum over the f degrees of freedom the only survivor is when $\nu=\kappa$ since $\langle\psi_j^\kappa|\psi_\ell^\nu\rangle=0$. Then overall the equations of motion for coefficients and SPFs are as summarised in (3.15) and (3.16).

3.6 Derivation of ρ-MCTDH EOM for type II density operators

Consider the multiconfigurational expansion for the density operator for a system with f degrees of freedom, $\underline{Q} = (Q_1, \ldots, Q_f)$:

$$\rho(Q_1, \ldots, Q_f, Q'_1, \ldots, Q'_f, t) = \sum_{\tau_1=1}^{n_1} \cdots \sum_{\tau'_f=1}^{n_f} B_{\tau_1,\ldots,\tau_f,\tau'_1,\ldots,\tau'_f}(t) \prod_{\kappa=1}^{f} \sigma^{(\kappa)}_{\tau_\kappa}(Q_\kappa, Q'_\kappa, t)$$
$$= \sum_{T} B_T \Omega_T = \sum_{\nu=1}^{n_\kappa} \sigma^{(\kappa)}_\nu \Pi^{(\kappa)}_\nu, \tag{3.33}$$

where $\sigma^{(\kappa)}_{\tau_\kappa} = |\varphi^{(\kappa)}_i(Q_\kappa)\rangle\langle\varphi^{(\kappa)}_j(Q'_\kappa)|$ for $\tau_\kappa = (i,j)$; $\{\varphi_i\}$ are SPFs. $T = (\tau_1, \ldots, \tau_f, \tau'_1, \ldots, \tau'_f)$ are the indices we sum over for type II coefficients. B_T are the coefficients and are Hermitian:

$$\Omega_T = \sum_{\kappa=1}^{f} \sigma^{(\kappa)}_{\tau_\kappa}; \tag{3.34}$$

$$(\tau_\kappa, \ell) = (\tau_1, \ldots, \tau_{\kappa-1}, \ell, \tau_{\kappa+1}, \ldots, \tau_f); \tag{3.35}$$

$$\Omega_{\tau_\kappa} = \sigma^{(1)}_{\tau_1} \cdots \sigma^{(\kappa-1)}_{\tau_{\kappa-1}} \sigma^{(\kappa+1)}_{\tau_{\kappa+1}} \cdots \sigma^{(f)}_{\tau_f}. \tag{3.36}$$

The 'single-hole density operators' are

$$\Pi^{(\kappa)}_\nu = \sum_{\tau_\kappa} B_{\tau_{\kappa,\nu}} \Omega_{\tau_\kappa}. \tag{3.37}$$

To set up the problem we first note that the evolution of our quantum system within this context is described by $\dot{\rho} = \mathcal{L}(\rho)$ instead of the TDSE. Our variational principle (Dirac-Frenkel/MacLachlan) says that

$$\langle\langle \delta\rho | \dot{\rho} - \mathcal{L}(\rho) \rangle\rangle = 0 \iff \langle\langle \delta\rho | \mathcal{L}(\rho) \rangle\rangle = \langle\langle \delta\rho | \dot{\rho} \rangle\rangle. \tag{3.38}$$

The constraints are $\langle\langle \sigma^{(\kappa)}_\mu(0) | \sigma^{(\kappa)}_\nu(0) \rangle\rangle = \delta_{\mu\nu}$ and $\langle\langle \sigma^{(\kappa)}_\mu | \dot{\sigma}^{(\kappa)}_\nu \rangle\rangle = -i\langle\langle \sigma^{(\kappa)}_\mu | \mathcal{G}^{(\kappa)} \sigma^{(\kappa)}_\nu \rangle\rangle$ for all t. We also have that $\mathcal{G} = \sum_{\kappa=1}^{f} \mathcal{G}^{(\kappa)}$ is the constraint superoperator

analogous to the constraint operator in MCTDH, where $\mathcal{G}^{(\kappa)}$ acts on degree of freedom (κ). It is defined as having the property that $\langle\langle\sigma_\mu^{(\kappa)}|\dot{\sigma}_\nu^{(\kappa)}\rangle\rangle = -i\langle\langle\sigma_\mu^{(\kappa)}|\mathcal{G}^{(\kappa)}\sigma_\nu^{(\kappa)}\rangle\rangle$. The norm is $\langle\langle A|B\rangle\rangle = \mathrm{Tr}\{A^\dagger B\}$.

Step 1: derive $\dot{B}_T$.

Take an arbitrary coefficient

$$B_A \in \{B_T | T = (\tau_1, \ldots, \tau_f, \tau_1', \ldots, \tau_f'), \{\tau_i\} \in \mathbb{N}, \tau_i \leq n_i\}. \tag{3.39}$$

Now observe that

$$\frac{\partial\rho}{\partial B_A} = 0 + \cdots + \frac{\partial B_A}{\partial B_A} \cdot \sum_{\kappa=1}^{f} \sigma_{\tau_\kappa}^{(\kappa)} + 0 + \cdots + 0 = 1 \cdot \Omega_A = \Omega_A. \tag{3.40}$$

Note that Ω_A is defined in (3.34) where the multi indices A corresponds to the arbitrary coefficient B_A as chosen above.

Similarly fix $\sigma_{\tau_q}^{(q)} \in \{\sigma_{\tau_\kappa}^{(\kappa)} | \kappa \in \mathbb{N}, \kappa \leq f\}$, one single particle density operator with degree of freedom (q), and observe that the partial derivative with respect to this is:

$$\begin{aligned}\frac{\partial\rho}{\partial\sigma_{\tau_q}^{(q)}} &= 0 + 0 + \cdots + B_{\{\tau_q\}}\sigma_{\tau_1}^{(1)} \cdots \frac{\partial\sigma_{\tau_q}^{(q)}}{\partial\sigma_{\tau_q}^{(q)}}\sigma_{\tau_{q+1}}^{(q+1)} \cdots \sigma_{\tau_f}^{(f)} + 0 + \cdots \\ &= \Pi_\nu^{(q)}.\end{aligned} \tag{3.41}$$

where $\Pi_\nu^{(q)}$ is defined in (3.37) and fixed for degree of freedom (q).

Now find $\dot{\rho}$, analogously to the derivation for the MCTDH wavefunction (consider $\{B_T\}$ constant with respect to t):

$$\begin{aligned}\frac{\partial\rho}{\partial t} &= \frac{\partial}{\partial t}\left(\sum_T B_T\Omega_T\right) = \sum_T \frac{\partial B_T}{\partial f}\Omega_T + \frac{\partial}{\partial t}\left(\sum_{\nu=1}^{n_\kappa}\Pi_\nu^{(\kappa)}\sigma_\nu^{(\kappa)}\right) \\ &= \sum_T \dot{B}_T\Omega_T + \sum_{\nu=1}^{n_1}\Pi_\nu^{(1)}\dot{\sigma}_\nu^{(1)} + \cdots + \sum_{\nu=1}^{n_f}\Pi_\nu^{(f)}\dot{\sigma}_\nu^{(f)} \quad (\kappa\text{-th term missing due to } \Pi_\nu^{\kappa}) \\ &= \sum_T \dot{B}_T\Omega_T + \sum_{\kappa=1}^{f}\sum_{\nu=1}^{n_\kappa}\Pi_\nu^{(\kappa)}\dot{\sigma}_\nu^{(\kappa)} = \dot{\rho}.\end{aligned} \tag{3.42}$$

We now substitute these results into the variational principle; i.e. put $\frac{\partial\rho}{\partial B_A} = \Omega_A$, $\frac{\partial\rho}{\partial\sigma^{(q)}_{\tau_q}} = \Pi^{(q)}_\nu$ and $\dot\rho = \sum_T \dot B_T\Omega_T + \sum_{\kappa=1}^{f}\sum_{\nu=1}^{n_\kappa}\Pi^{(\kappa)}_\nu\dot\sigma^{(\kappa)}_\nu$ into $\langle\langle\delta\rho|\mathcal{L}(\rho)\rangle\rangle = \langle\langle\delta\rho|\dot\rho\rangle\rangle$:

$$\begin{aligned}
\langle\langle\delta\rho|\mathcal{L}(\rho)\rangle\rangle &= \langle\langle\frac{\partial\rho}{\partial B_A}|\dot\rho\rangle\rangle \\
&= \langle\langle\Omega_A|\left(\sum_T \dot B_T\Omega_T + \sum_{\kappa=1}^{f}\sum_{\nu=1}^{n_\kappa}\Pi^{(\kappa)}_\nu\dot\sigma^{(\kappa)}_\nu\right)\rangle\rangle \\
&= \langle\langle\Omega_A|\sum_T \dot B_T\Omega_T\rangle\rangle + \langle\langle\Omega_A|\sum_{\kappa=1}^{f}\sum_{\nu=1}^{n_\kappa}\Pi^{(\kappa)}_\nu\dot\sigma^{(\kappa)}_\nu\rangle\rangle \\
&= \sum_T\langle\langle\Omega_A|\dot B_T\Omega_T\rangle\rangle + \sum_{\kappa=1}^{f}\sum_{\nu=1}^{n_\kappa}\langle\langle\Omega_A|\Pi^{(\kappa)}_\nu\dot\sigma^{(\kappa)}_\nu\rangle\rangle, \qquad (3.43)
\end{aligned}$$

where we have used the fact that $\mathrm{Tr}\{A+B\} = \mathrm{Tr}\{A\} + \mathrm{Tr}\{B\}$. Next we use that $\dot B_T$ is just a coefficient to continue the calculation from (3.43):

$$\langle\langle\delta\rho|\mathcal{L}(\rho)\rangle\rangle = \sum_T \dot B_T\langle\langle\Omega_A|\Omega_T\rangle\rangle + \sum_{\kappa=1}^{f}\sum_{\nu=1}^{n_\kappa}\mathrm{Tr}\{\Omega^\dagger_A\Pi^{(\kappa)}_\nu\dot\sigma^{(\kappa)}_\nu\}. \qquad (3.44)$$

Take any two distinct arbitrary multi indices A and T, and recall the definition of Ω_T in (3.34) then using general properties of traces over operators $\mathrm{Tr}\{\Omega^\dagger_A\Omega_T\} = 0$ for all $A \neq T$ as $\langle\langle\sigma^{(\kappa)}_\mu|\sigma^{(\kappa)}_\nu\rangle\rangle = \delta_{\mu\nu}$ and further $\mathrm{Tr}\{\ \Omega^\dagger_A\Omega_A\} = \mathrm{Tr}\{1\} = 1$. Hence we obtain

$$\begin{aligned}
\langle\langle\delta\rho|\mathcal{L}(\rho)\rangle\rangle &= \dot B_A\langle\langle\Omega_A|\Omega_A\rangle\rangle \\
&\quad + \sum_{\kappa=1}^{f}\sum_{\nu=1}^{n_\kappa}\mathrm{Tr}\{(\sigma^{(1)}_{\tau_1}\cdots\sigma^{(f)}_{\tau_f})^\dagger\sigma^{(1)}_{\tau_1}\cdots\sigma^{(\kappa-1)}_{\tau_{\kappa-1}}\sigma^{(\kappa+1)}_{\tau_{\kappa+1}}\cdots\sigma^{(f)}_{\tau_f}\dot\sigma^{(\kappa)}_\nu B_{\tau_\nu,\ell}\} \\
&= \dot B_A + \sum_{\kappa=1}^{f}\sum_{\nu=1}^{n_\kappa}\mathrm{Tr}\{B_{\tau_\nu,\ell}\sigma^{(\kappa)\dagger}_{\tau_\kappa}\dot\sigma^{(\kappa)}_\nu\} \\
&= \dot B_A + \sum_{\kappa=1}^{f}\sum_{\nu=1}^{n_\kappa}B_{\tau_\nu,\ell}\langle\langle\sigma^{(\kappa)}_{\tau_\kappa}|\dot\sigma^{(\kappa)}_\nu\rangle\rangle. \qquad (3.45)
\end{aligned}$$

Note that the second equality in (3.45) comes from the fact that $\sigma^{(\kappa)}_{\tau_\kappa}$ is missing from the expression so all terms cancel except for $\sigma^{(\kappa)\dagger}_{\tau_\kappa}$. Next we

continue the calculation by using the definition of the constraint operator

$$\langle\langle\sigma_\mu^{(\kappa)}|\dot{\sigma}_\nu^{(\kappa)}\rangle\rangle = -i\langle\langle\sigma_\mu^{(\kappa)}|\mathcal{G}^{(\kappa)}\sigma_\nu^{(\kappa)}\rangle\rangle \tag{3.46}$$

to obtain:

$$\begin{aligned}\langle\langle\delta\rho|\mathcal{L}(\rho)\rangle\rangle &= \dot{B}_A - i\sum_{\kappa=1}^{f}\sum_{\nu=1}^{n_\kappa} B_{\tau_\nu,\ell}\langle\langle\sigma_{\tau_\kappa}^{(\kappa)}|\mathcal{G}^{(\kappa)}\sigma_\nu^{(\kappa)}\rangle\rangle \\ &= \dot{B}_A - i\sum_{\kappa=1}^{f}\sum_{\nu=1}^{n_\kappa} B_{\tau_\nu,\ell}\,\mathrm{Tr}\{\Pi_\nu^{(\kappa)}\Omega_A^\dagger\mathcal{G}^{(\kappa)}\sigma_\nu^{(\kappa)}\}. \end{aligned}\tag{3.47}$$

Next we use $\mathrm{Tr}\{ABCD\} = \mathrm{Tr}\{BCDA\}$ to continue the calculation:

$$\begin{aligned}\langle\langle\delta\rho|\mathcal{L}(\rho)\rangle\rangle &= \dot{B}_A - i\sum_{\kappa=1}^{f}\sum_{\nu=1}^{n_\kappa} B_{\tau_\nu,\ell}\,\mathrm{Tr}\{\Omega_A^\dagger\mathcal{G}^{(\kappa)}\sigma_\nu^{(\kappa)}\Pi_\nu^{(\kappa)}\} \\ &= \dot{B}_A - i\sum_{\nu=1}^{n_\kappa}\langle\langle\Omega_A|\sum_{\kappa=1}^{f}\mathcal{G}^{(\kappa)}\sigma_\nu^{(\kappa)}\Pi_\nu^{(\kappa)}\rangle\rangle \\ &= \dot{B}_A + \langle\langle\Omega_A|\mathcal{G}\sum_{\nu=1}^{n_\kappa}\sigma_\nu^{(\kappa)}\Pi_\nu^{(\kappa)}\rangle\rangle = \dot{B}_A - i\langle\langle\Omega_A|\mathcal{G}(\rho)\rangle\rangle. \end{aligned}\tag{3.48}$$

We now have that (3.48) implies that

$$\begin{aligned}\dot{B}_A &= \langle\langle\Omega_A|\mathcal{L}(\rho)\rangle\rangle + i\langle\langle\Omega_A|\mathcal{G}(\rho)\rangle\rangle \\ &= \langle\langle\Omega_A|(\mathcal{L}+i\mathcal{G})(\rho)\rangle\rangle, \end{aligned}\tag{3.49}$$

where A is arbitrary.

Step 2: derive $\dot{\varphi}^{(\kappa)}$. First substitute $\dot{B}_T$ into $\dot{\rho}$:

$$\dot{\rho} = \sum_{j=1}^{f}\sum_{\nu=1}^{n_\kappa}\Pi_\nu^{(j)}\dot{\sigma}_\nu^{(j)} + \sum_T \Omega_T\langle\langle\Omega_A|(\mathcal{L}+i\mathcal{G})(\rho)\rangle\rangle. \tag{3.50}$$

Fix the degree of freedom κ and consider $\delta\sigma_\nu^{(\kappa)}$. The variation, $\delta\rho = \sum_\mu \Pi_\nu^{(\kappa)}\delta\sigma_\mu^{(\kappa)}$:

$$\begin{aligned}
\langle\langle\delta\rho|\mathcal{L}\rho\rangle\rangle &= \sum_\mu \langle\langle \Pi_\mu^{(\kappa)}\delta\sigma_\mu^{(\kappa)}|\dot\rho\rangle\rangle \\
&= \sum_\mu \langle\langle \Pi_\mu^{(\kappa)}\delta\sigma_\mu^{(\kappa)}| \left[\sum_{j=1}^{f}\sum_{\nu=1}^{n_\kappa}\Pi_\nu^{(j)}\dot\sigma_\nu^{(j)} + \sum_T \Omega_T\langle\langle\Omega_T|(\mathcal{L}+i\mathcal{G})\rho\rangle\rangle\right]\rangle\rangle \\
&= \sum_\mu \langle\langle \Pi_\mu^{(\kappa)}\delta\sigma_\mu^{(\kappa)}| \sum_{j=1}^{f}\sum_{\nu=1}^{n_\kappa}\Pi_\nu^{(j)}\dot\sigma_\nu^{(j)}\rangle\rangle \\
&+ \sum_\mu\sum_T \langle\langle \Pi_\mu^{(\kappa)}\delta\sigma_\mu^{(\kappa)}|\Omega_T\rangle\rangle\langle\langle\Omega_T|(\mathcal{L}+i\mathcal{G})\rho\rangle\rangle, \qquad (3.51)
\end{aligned}$$

In the final step of (3.51) the first term has been simplified by applying the additivity property of traces: $\mathrm{Tr}\{A+B\} = \mathrm{Tr}\{A\} + \mathrm{Tr}\{B\}$. Similarly, the second term has been simplified using the property that $\mathrm{Tr}\{A\cdot\mathrm{Tr}\{B\}\} = \mathrm{Tr}\{A\}\,\mathrm{Tr}\{B\}$. In the next step the following property is used to simplify the expression further: $\mathrm{Tr}\{\delta\sigma_\mu^{(\kappa)t}\Pi_\mu^{(\kappa)t}\Pi_\nu^{(j)}\dot\sigma_\nu^{(j)}\} = 0$ unless $j=\kappa$ so the sum $\sum_{j=1}^{f}$ disappears due to $\langle\langle\sigma^{(\kappa)}|\sigma^{(j)}\rangle\rangle = \delta_{ij}$, and therefore we obtain

$$\begin{aligned}
\langle\langle\delta\rho|\mathcal{L}\rho\rangle\rangle &= \sum_\mu\sum_\nu \langle\langle \Pi_\mu^{(\kappa)}\delta\sigma_\mu^{(\kappa)}|\Pi_\nu^{(\kappa)}\dot\sigma_\nu^{(\kappa)}\rangle\rangle \\
&+ \sum_\mu\sum_T \langle\langle \Pi_\mu^{(\kappa)}\delta\sigma_\mu^{(\kappa)}|\Omega_T\rangle\rangle\langle\langle\Omega_T|(\mathcal{L}+i\mathcal{G})\rho\rangle\rangle. \qquad (3.52)
\end{aligned}$$

It follows that

$$\begin{aligned}
\sum_{\mu\nu}\langle\langle \Pi_\mu^{(\kappa)}\delta\sigma_\mu^{(\kappa)}|\Pi_\nu^{(\kappa)}\dot\sigma_\nu^{(\kappa)}\rangle\rangle &= \sum_\mu \langle\langle \Pi_\mu^{(\kappa)}\delta\sigma_\mu^{(\kappa)}|\mathcal{L}\rho\rangle\rangle \\
&- \sum_\mu\sum_T \langle\langle \Pi_\mu^{(\kappa)}\delta\sigma_\mu^{(\kappa)}|\Omega_T\rangle\rangle\langle\langle\Omega_T|(\mathcal{L}+i\mathcal{G})\rho\rangle\rangle. \qquad (3.53)
\end{aligned}$$

We wish to write (3.53) more simply. First we use the following:

$$D^{(\kappa)}_{\mu\nu} = \langle\langle \Pi^{(\kappa)}_{\mu} | \Pi^{(\kappa)}_{\nu} \rangle\rangle, \tag{3.54}$$

$$\rho^{(\kappa)} = \sum_{\nu=1}^{n_\kappa} |\sigma^{(\kappa)}_{\nu}\rangle\rangle\langle\langle \sigma^{(\kappa)}_{\nu}|, \tag{3.55}$$

$$\langle \mathcal{L} + i\mathcal{G} \rangle^{(\kappa)}_{\mu\nu} = \langle\langle \Pi^{(\kappa)}_{\mu} | (\mathcal{L} + i\mathcal{G}) \Pi^{(\kappa)}_{\nu} \rangle\rangle. \tag{3.56}$$

Use also the facts that $\sum_T \Omega_T = \sum_{\tau_\kappa=1}^{n_\kappa} \sum_{T_\kappa} \Omega_{T_\kappa} \sigma^{(\kappa)}_{\tau_\kappa}$ and $\Pi^{(\kappa)}_{\nu} = \sum_{L_\kappa} B_{L_\kappa,\nu} \Omega_{L_\kappa}$. Now note that

$$\begin{aligned}
\Pi^{(\kappa)\dagger}_{\mu} \Pi^{(\kappa)}_{\nu} &= \sum_{T_\kappa} \sum_{L_\kappa} B^*_{T_\kappa,\mu} B_{T_L,\nu} \Omega^\dagger_{T_\kappa} \Omega_{T_L} \\
&= \sum_{T_\kappa, L_\kappa} B^*_{T_\kappa,\mu} B_{T_L,\nu} \sigma^{(f)\dagger}_{\tau_f} \cdots \sigma^{(\kappa+1)\dagger}_{\tau_{\kappa+1}} \sigma^{(\kappa-1)\dagger}_{\tau_{\kappa-1}} \cdots \sigma^{(1)\dagger}_{\tau_1} \sigma^{(1)}_{\tau_1} \cdots \sigma^{(\kappa-1)}_{\tau_{\kappa-1}} \sigma^{(\kappa+1)}_{\tau_{\kappa+1}} \sigma^{(f)}_{\tau_f} \\
&= \sum_{T_\kappa, L_\kappa} B^*_{T_\kappa,\mu} B_{T_L,\nu},
\end{aligned} \tag{3.57}$$

which is just a constant (with respect to coordinate). Therefore the first component of the expression (3.53) which we are trying to rewrite is:

$$\begin{aligned}
\sum_{\mu\nu} \langle\langle \Pi^{(\kappa)}_{\mu} \delta\sigma^{(\kappa)}_{\mu} | \Pi^{(\kappa)}_{\nu} \dot{\sigma}^{(\kappa)}_{\nu} \rangle\rangle &= \sum_{\mu\nu} \mathrm{Tr}\{ \delta\sigma^{(\kappa)\dagger}_{\mu} \Pi^{(\kappa)\dagger}_{\mu} \Pi^{(\kappa)}_{\nu} \dot{\sigma}^{(\kappa)}_{\nu} \} \\
&= \langle\langle \Pi^{(\kappa)}_{\mu} | \Pi^{(\kappa)}_{\nu} \rangle\rangle \langle\langle \delta\sigma^{(\kappa)}_{\mu} | \dot{\sigma}^{(\kappa)}_{\nu} \rangle\rangle \\
&= \sum_{\mu\nu} D^{(\kappa)}_{\mu\nu} \langle\langle \delta\sigma^{(\kappa)}_{\mu} | \dot{\sigma}^{(\kappa)}_{\nu} \rangle\rangle \\
&= -i \sum_{\mu\nu} D^{(\kappa)}_{\mu\nu} \langle\langle \delta\sigma^{(\kappa)}_{\mu} | \mathcal{G} \sigma^{(\kappa)}_{\nu} \rangle\rangle.
\end{aligned} \tag{3.58}$$

Now we simplify the second term in our derived expression:

$$
\begin{aligned}
&\sum_{\mu}\sum_{T}\langle\langle\Pi_{\mu}^{(\kappa)}\delta\sigma_{\mu}^{(\kappa)}|\Omega_{T}\rangle\rangle\langle\langle\Omega_{T}(\mathcal{L}+i\mathcal{G})\rho\rangle\rangle\\
=&\sum_{\mu}\sum_{T_\kappa}\sum_{L_\kappa}\sum_{\tau_\kappa=1}^{n_\kappa}B_{L_\kappa}^{*}\langle\langle\Omega_{L_\kappa}\delta\sigma_{\mu}^{(\kappa)}|\sigma_{\tau_\kappa}\Omega_{\tau_\kappa}\rangle\rangle\langle\langle\sigma_{\tau_\kappa}\Omega_{T_\kappa}(\mathcal{L}+i\mathcal{G})\rho\rangle\rangle\\
=&\sum_{\mu}\sum_{T_\kappa}\sum_{L_\kappa}\sum_{\tau_\kappa=1}^{n_\kappa}\mathrm{Tr}\{\sigma_{\tau_\kappa}\Omega_{T_\kappa}\Omega_{L_\kappa}^{\dagger}\delta\sigma_{\mu}^{(\kappa)\dagger}\}\langle\langle\sigma_{\tau_\kappa}\Omega_{T_\kappa}B_{L_\kappa}(\mathcal{L}+i\mathcal{G})(\sum_{\tau_j}^{n_j}\Pi_{\tau_j}^{(j)}\sigma_{\tau_j}^{(j)}\rangle\rangle\\
=&\sum_{\mu}\sum_{\tau_j=1}^{n_j}\mathrm{Tr}\{\delta\sigma_{\mu}^{(\kappa)\dagger}\sigma_{\tau_\kappa}\}\langle\langle\sigma_{\tau_\kappa}\sum_{T_\kappa}B_{T_\kappa}\Omega_{T_\kappa}(\mathcal{L}+i\mathcal{G})\Pi_{\tau_j}^{(j)}\sigma_{\tau_j}^{(j)}\rangle\rangle\\
=&\sum_{\mu}\sum_{\nu}\langle\langle\delta\sigma_{\mu}^{(\kappa)}|\sigma_{\tau_\kappa}\rangle\rangle\langle\langle\sigma_{\tau_\kappa}\Pi_{\mu}^{(\kappa)}|(\mathcal{L}+i\mathcal{G})\Pi_{\nu}^{(\kappa)}\sigma_{\nu}^{(\kappa)}\rangle\rangle\\
=&\sum_{\mu\nu}\langle\langle\delta\sigma_{\mu}^{(\kappa)}|\rho^{(\kappa)}\langle\mathcal{L}+i\mathcal{G}\rangle_{\mu\nu}^{(\kappa)}\sigma_{\nu}^{(\kappa)}\rangle\rangle. \qquad (3.59)
\end{aligned}
$$

Notice that $\sum_{\mu\nu}D_{\mu\nu}\langle\langle\delta\sigma_{\mu}^{(\kappa)}|\dot{\sigma}_{\nu}^{(\kappa)}\rangle\rangle=\sum_{\mu\nu}D_{\mu\nu}(-i\langle\langle\delta\sigma_{\mu}^{(\kappa)}|\mathcal{G}\sigma_{\nu}^{(\kappa)}\rangle\rangle)$. Then

$$
\begin{aligned}
&\sum_{\mu\nu}D_{\mu\nu}\langle\langle\delta\sigma_{\mu}^{(\kappa)}|\dot{\sigma}_{\nu}^{(\kappa)}\rangle\rangle\\
=&\sum_{\mu\nu}D_{\mu\nu}\langle\langle\delta\sigma_{\mu}^{(\kappa)}|\dot{\sigma}_{\nu}^{(\kappa)}\rangle\rangle-i\sum_{\mu\nu}D_{\mu\nu}\langle\langle\delta\sigma_{\mu}^{(\kappa)}|\mathcal{G}\sigma_{\nu}^{(\kappa)}\rangle\rangle+i\sum_{\mu\nu}D_{\mu\nu}\langle\langle\delta\sigma_{\mu}^{(\kappa)}|\mathcal{G}\sigma_{\nu}^{(\kappa)}\rangle\rangle\\
=&\sum_{\mu\nu}D_{\mu\nu}\langle\langle\delta\sigma_{\mu}^{(\kappa)}|\dot{\sigma}_{\nu}^{(\kappa)}+i\mathcal{G}^{(\kappa)}\sigma_{\nu}^{(\kappa)}\rangle\rangle-i\sum_{\mu\nu}D_{\mu\nu}\langle\langle\delta\sigma_{\mu}^{(\kappa)}|\mathcal{G}\sigma_{\nu}^{(\kappa)}\rangle\rangle. \qquad (3.60)
\end{aligned}
$$

Finally consider

$$
\begin{aligned}
\sum_{\mu}\langle\langle\Pi_{\mu}^{(\kappa)}\delta\sigma_{\mu}^{(\kappa)}|\mathcal{L}\rho\rangle\rangle&=\sum_{\mu}\langle\langle\Pi_{\mu}^{(\kappa)}\delta\sigma_{\mu}^{(\kappa)}|\mathcal{L}\sum_{\nu}\Pi_{\nu}^{(\kappa)}\sigma_{\nu}^{(\kappa)}\rangle\rangle\\
&=\sum_{\mu\nu}\langle\langle\Pi_{\mu}^{(\kappa)}\delta\sigma_{\mu}^{(\kappa)}|\Pi_{\nu}^{(\kappa)}\sigma_{\nu}^{(\kappa)}\rangle\rangle \qquad (3.61)
\end{aligned}
$$

and

$$\begin{aligned}
&\sum_{\mu}\langle\langle\Pi_{\mu}^{(\kappa)}\delta\sigma_{\mu}^{(\kappa)}|\mathcal{L}\rho\rangle\rangle + i\sum_{\mu\nu}\Pi_{\mu}^{(\kappa)}|\Pi_{\nu}^{(\kappa)}\rangle\rangle\langle\langle\delta\sigma_{\mu}^{(\kappa)}|\mathcal{G}\sigma_{\nu}^{(\kappa)}\rangle\rangle \\
=&\sum_{\mu\nu}\langle\langle\Pi_{\mu}^{(\kappa)}\delta\sigma_{\mu}^{(\kappa)}|(\mathcal{L}+i\mathcal{G})\Pi_{\mu}^{(\kappa)}\sigma_{\nu}^{(\kappa)}\rangle\rangle \\
=&\sum_{\mu\nu}\delta\sigma_{\mu}^{(\kappa)}|\langle\mathcal{L}+i\mathcal{G}\rangle_{\mu\nu}^{(\kappa)}\sigma_{\nu}^{(\kappa)}\rangle\rangle. \qquad (3.62)
\end{aligned}$$

Then we can put all these parts together to rewrite (3.53);

$$\begin{aligned}
&\sum_{\mu\nu}\langle\langle\Pi_{\mu}^{(\kappa)}\delta\sigma_{\mu}^{(\kappa)}|\Pi_{\nu}^{(\kappa)}\dot{\sigma}_{\nu}^{(\kappa)}\rangle\rangle \\
=&\sum_{\mu}\langle\langle\Pi_{\mu}^{(\kappa)}\delta\sigma_{\mu}^{(\kappa)}|\mathcal{L}\rho\rangle\rangle - \sum_{\mu}\sum_{T}\langle\langle\Pi_{\mu}^{(\kappa)}\sigma_{\mu}^{(\kappa)}|\Omega_T\rangle\rangle\langle\langle\Omega_T|(\mathcal{L}+i\mathcal{G})\rho\rangle\rangle, \qquad (3.63)
\end{aligned}$$

which becomes

$$\begin{aligned}
&\sum_{\mu\nu}D_{\mu\nu}\langle\langle\delta\sigma_{\mu}^{(\kappa)}|\dot{\sigma}_{\nu}^{(\kappa)}+i\mathcal{G}^{(\kappa)}\sigma_{\nu}^{(\kappa)}\rangle\rangle - i\sum_{\mu\nu}D_{\mu\nu}\langle\langle\delta\sigma_{\mu}^{(\kappa)}|\mathcal{G}\sigma_{\nu}^{(\kappa)} \\
=&\sum_{\mu}\langle\langle\Pi_{\mu}^{(\kappa)}\delta\sigma_{\mu}^{(\kappa)}|\mathcal{L}\rho\rangle\rangle - \sum_{\mu\nu}\delta\sigma_{\mu}^{(\kappa)}|\langle\mathcal{L}+i\mathcal{G}\rangle_{\mu\nu}^{(\kappa)}\sigma_{\nu}^{(\kappa)}\rangle\rangle. \qquad (3.64)
\end{aligned}$$

This implies the following:

$$\begin{aligned}
&\sum_{\mu\nu}D_{\mu\nu}\langle\langle\delta\sigma_{\mu}^{(\kappa)}|\dot{\sigma}_{\nu}^{(\kappa)}+i\mathcal{G}^{(\kappa)}\sigma_{\nu}^{(\kappa)}\rangle\rangle \\
=&\sum_{\mu\nu}\langle\langle\delta\sigma_{\mu}^{(\kappa)}|\langle\mathcal{L}+i\mathcal{G}\rangle_{\mu\nu}^{(\kappa)}\sigma_{\nu}^{(\kappa)}\rangle\rangle - \sum_{\mu\nu}\langle\langle\delta\sigma_{\mu}^{(\kappa)}|\rho^{(\kappa)}\langle\mathcal{L}+i\mathcal{G}\rangle_{\mu\nu}^{(\kappa)}\sigma_{\nu}^{(\kappa)}\rangle\rangle \\
=&\sum_{\mu\nu}\langle\langle\delta\sigma_{\mu}^{(\kappa)}|(1-\rho^{(\kappa)})\langle\mathcal{L}+i\mathcal{G}\rangle_{\mu\nu}^{(\kappa)}\sigma_{\nu}^{(\kappa)}\rangle\rangle. \qquad (3.65)
\end{aligned}$$

Now we expand the following:

$$\begin{aligned}\sum_{\nu}\langle\mathcal{L}+i\mathcal{G}\rangle_{\mu\nu}^{(\kappa)}\sigma_{\nu}^{(\kappa)} &= \sum_{\nu}\langle\langle\Pi_{\mu}^{(\kappa)}|(\mathcal{L}+i\mathcal{G})\Pi_{\nu}^{(\kappa)}\rangle\rangle\sigma_{\nu}^{(\kappa)}\\ &= \sum_{\nu}\mathrm{Tr}\{\Pi_{\mu}^{(\kappa)\dagger}(\mathcal{L}+i\mathcal{G})\Pi_{\nu}^{(\kappa)}\}\sigma_{\nu}^{(\kappa)}\\ &= \sum_{\nu}\mathrm{Tr}\{\Pi_{\mu}^{(\kappa)\dagger}(\mathcal{L}+i\mathcal{G})\Pi_{\nu}^{(\kappa)}\}_{\kappa}\sigma_{\nu}^{(\kappa)}\\ &= \sum_{\nu}\mathrm{Tr}\{\Pi_{\mu}^{(\kappa)\dagger}(\mathcal{L}+i\mathcal{G})\Pi_{\nu}^{(\kappa)}\sigma_{\nu}^{(\kappa)}\}_{\kappa}\\ &= \sum_{\nu}\mathrm{Tr}\{\Pi_{\mu}^{(\kappa)\dagger}(\mathcal{L}+i\mathcal{G})\rho\}_{\kappa}. \end{aligned} \tag{3.66}$$

Using this, rewrite

$$\begin{aligned}&\sum_{\mu\nu}\langle\langle\delta\sigma_{\mu}^{(\kappa)}|(1-\rho^{(\kappa)})\mathcal{L}+i\mathcal{G}\rangle_{\mu\nu}^{(\kappa)}\sigma_{\nu}^{(\kappa)}\rangle\rangle\\ =&\sum_{\mu}\langle\langle\delta\sigma_{\mu}^{(\kappa)}|(1-\rho^{(\kappa)})\,\mathrm{Tr}\{\Pi_{\mu}^{(\kappa)\dagger}(\mathcal{L}+i\mathcal{G})\rho\}_{\kappa}. \end{aligned} \tag{3.67}$$

Therefore in summary the equations of motion for coefficients and density operators are:

$$\dot{B}_{J,L} = \langle\Phi_J|(\mathcal{L}+i\mathcal{G})(\rho)|\Phi_L\rangle = B_{L,J}^{*} \tag{3.68}$$

$$\dot{\varphi}^{(\kappa)} = -ig^{(\kappa)}\varphi^{(\kappa)} + (1-\rho^{(\kappa)})\,\mathrm{Tr}\{(\mathcal{L}+i\mathcal{G})(\rho)\}_{\kappa}[\mathcal{D}^{(1),(\kappa)}]^{-1}\varphi^{(\kappa)}. \tag{3.69}$$

3.7 Derivation of ρ-MCTDH EOM for type I density operators

Recall that the MCTDH form of the density matrix can be written as follows, and rewritten in the 'single hole' form;

$$\rho = \sum_{T} B_T\Omega_T = \sum_{\kappa=1}^{f}\sum_{\nu=1}^{n_\kappa}\Pi_{\nu}^{(\kappa)}\sigma_{\nu}^{(\kappa)}. \tag{3.70}$$

Start by taking the partial derivative with respect to the coefficients B_T:

$$\frac{\partial \rho}{\partial \beta_T} = \Omega_T = \prod_{k=1}^{f} \sigma_{\tau_k}^{(k)}(Q_k, Q_k', t). \tag{3.71}$$

Similarly

$$\frac{\partial \rho}{\partial \sigma_\mu^{(\kappa)}} = \Pi_\nu^{(\kappa)} = \sum_{\tau_\kappa} B_{\tau_{\kappa,\nu}} \Omega_{\tau,k}. \tag{3.72}$$

The DFVP implies that $\langle\langle \delta\rho | \mathcal{L}(\rho)\rangle\rangle = \langle\langle \delta\rho | \dot{\rho}\rangle\rangle$. We are interested in variations on δB_T:

$$\begin{aligned}
\langle\langle \frac{\partial \rho}{\partial \beta_T} | \mathcal{L}(\rho)\rangle\rangle &= \langle\langle \Omega_T | \mathcal{L}(\rho)\rangle\rangle \\
&= \langle\langle \partial\rho | \dot{\rho}\rangle\rangle \\
&= \langle\langle \Omega_T | \{ \sum_{T_1} \dot{B}_{T_1} \Omega_{T_1} + \sum_{\kappa=1}^{f} \sum_{\nu=1}^{n_\kappa} \Pi_\nu^{(\kappa)} \dot{\sigma}_\nu^{(\kappa)} \} \rangle\rangle \\
&= \langle\langle \Omega_T | \sum_{T_1} \dot{B}_{T_1} \Omega_{T_1} \rangle\rangle + \sum_{\kappa=1}^{f} \sum_{\nu=1}^{n_\kappa} \langle\langle \Omega_T | \Pi_\nu^{(\kappa)} \dot{\sigma}_\nu^{(\kappa)} \rangle\rangle \\
&= \sum_{T_1} \dot{B}_{T_1} \langle\langle \Omega_T | \Omega_{T_1} \rangle\rangle + \sum_{\kappa=1}^{f} \sum_{\nu=1}^{n_\kappa} \sum_{\tau_\kappa} \langle\langle \Omega_T | B_{\tau_{\kappa,\nu}} \Omega_\nu^{(\kappa)} \dot{\sigma}_\nu^{(\kappa)} \rangle\rangle \\
&= \dot{B}_T + \sum_{\kappa=1}^{f} \sum_{\nu=1}^{n_\kappa} \sum_{\tau_\kappa} \mathrm{Tr}\{ \sigma_{\tau_f}^{(\kappa)\dagger} \sigma_{\tau_{f-1}}^{(\kappa)\dagger} \dots \sigma_{\tau_1}^{(\kappa)\dagger} B_{\tau_{\kappa,\nu}} \sigma_{\tau_1}^{(\kappa)} \dots \sigma_{\nu-1}^{(\kappa)} \sigma_{\nu+1}^{(\kappa)} \dots \sigma_{\tau_f}^{(\kappa)} \dot{\sigma}_\nu^{(\kappa)} \} \\
&= \dot{B}_T + \sum_{\kappa=1}^{f} \sum_{\nu=1}^{n_\kappa} \sum_{\tau_\kappa} B_{\tau_{\kappa,\nu}} \langle\langle \sigma_\nu^{(\kappa)} | \dot{\sigma}_\nu^{(\kappa)} \rangle\rangle \\
&= \dot{B}_T - i \sum_{\kappa=1}^{f} \left(\sum_{\nu=1}^{n_\kappa} \sum_{\tau_\kappa} B_{\tau_{\kappa,\nu}} \langle\langle \sigma_\nu^{(\kappa)} | \mathcal{G}^{(\kappa)} \sigma_\nu^{(\kappa)} \rangle\rangle \right) \\
&= \dot{B}_T - i \sum_{T} B_T \langle\langle \Omega_T | \mathcal{G} \Omega_T \rangle\rangle \\
&= \dot{B}_T - \langle\langle \Omega_T | i\mathcal{G} \{ \sum_{T} B_T \Omega_T \} \rangle\rangle \\
&= \dot{B}_T - \langle\langle \Omega_T | i\mathcal{G}(\rho) \rangle\rangle.
\end{aligned} \tag{3.73}$$

Overall this implies that

$$\Omega_T | \mathcal{L}(\rho)\rangle\rangle = \dot{B}_T - \langle\langle \Omega_T | i\mathcal{G}(\rho)\rangle\rangle, \tag{3.74}$$

which in turn implies

$$\dot{B}_T = \langle\langle \Omega_T | \mathcal{L}(\rho) \rangle\rangle + \langle\langle \Omega_T | i\mathcal{G}(\rho) \rangle\rangle = \langle\langle \Omega_T | (\mathcal{L} + i\mathcal{G})(\rho) \rangle\rangle. \tag{3.75}$$

Now consider the variations in $\delta\sigma_\mu^{(\kappa)}$. We do this differently. First substitute in $\dot{B}_T$ in $\dot{\rho}$:

$$\begin{aligned}\dot{\rho} &= \sum_T \dot{B}_T \Omega_T + \sum_{\kappa=1}^{f} \sum_{\nu=1}^{n_\kappa} \Pi_\nu^{(\kappa)} \dot{\sigma}_\nu^\kappa \\ &= \sum_T \Omega_T \langle\langle \Omega_T | (\mathcal{L} + i\mathcal{G})(\rho) \rangle\rangle + \sum_{\kappa=1}^{f} \sum_{\nu=1}^{n_\kappa} \Pi_\nu^{(\kappa)} \dot{\sigma}_\nu^\kappa. \end{aligned} \tag{3.76}$$

Recall the DFVP $\langle\langle \delta\rho | \mathcal{L}\rho \rangle\rangle = \langle\langle \delta\rho | \dot{\rho} \rangle\rangle$ and $\langle\langle \delta\rho = \sum_\mu \langle\langle \Pi_\mu^{(\kappa)} \delta\sigma_\mu^{(\kappa)} |$. Then

$$\begin{aligned}\langle\langle \delta\rho | \dot{\rho} \rangle\rangle &= \sum_\mu \langle\langle \Pi_\mu^{(\kappa)} \delta\sigma_\mu^{(\kappa)} | \{ \sum_T \Omega_T \langle\langle \Omega_T | (\mathcal{L} + i\mathcal{G})(\rho) \rangle\rangle + \sum_{\kappa=1}^{f} \sum_{\nu=1}^{n_\kappa} \Pi_\nu^{(\kappa)} \dot{\sigma}_\nu^\kappa \} \rangle\rangle \\ &= \sum_\mu \langle\langle \Pi_\mu^{(\kappa)} \delta\sigma_\mu^{(\kappa)} | \sum_{\kappa=1}^{f} \sum_{\nu=1}^{n_\kappa} \Pi_\nu^{(\kappa)} \dot{\sigma}_\nu^\kappa \rangle\rangle + \sum_\mu \langle\langle \Pi_\mu^{(\kappa)} \delta\sigma_\mu^{(\kappa)} | \{ \sum_T \Omega_T \langle\langle \Omega_T | (\mathcal{L} + i\mathcal{G})\rho \rangle\rangle \} \rangle\rangle \\ &= \sum_\mu \sum_{\kappa=1}^{f} \sum_{\nu=1}^{n_\kappa} \langle\langle \Pi_\mu^{(\kappa)} \delta\sigma_\mu^{(\kappa)} | \Pi_\nu^{(\kappa)} \dot{\sigma}_\nu^\kappa \rangle\rangle + \sum_\mu \sum_T \langle\langle \Pi_\mu^{(\kappa)} \delta\sigma_\mu^{(\kappa)} | \Omega_T \rangle\rangle \langle\langle \Omega_T | (\mathcal{L} + i\mathcal{G})\rho \rangle\rangle \\ &= \langle\langle \delta\rho | \mathcal{L}(\rho) \rangle\rangle \\ &= \sum_\mu \langle\langle \Pi_\mu^{(\kappa)} \delta\sigma_\mu^{(\kappa)} | \mathcal{L}(\rho) \rangle\rangle. \end{aligned} \tag{3.77}$$

Then altogether

$$\begin{aligned}&\sum_{\mu\nu} \langle\langle \Pi_\mu^{(\kappa)} \delta\sigma_\mu^{(\kappa)} | \Pi_\mu^{(\kappa)} \dot{\sigma}_\mu^{(\kappa)} \\ =& \sum_\mu \langle\langle \Pi_\mu^{(\kappa)} \delta\sigma_\mu^{(\kappa)} | \mathcal{L}(\rho) \rangle\rangle - \sum_\mu \sum_T \langle\langle \Pi_\mu^{(\kappa)} \delta\sigma_\mu^{(\kappa)} | \Omega_T \rangle\rangle \langle\langle \Omega_T | (\mathcal{L} + i\mathcal{G})\rho \rangle\rangle. \end{aligned} \tag{3.78}$$

The next step is to add $i\mathcal{G}$ to each side of (3.78). The left hand side of (3.78)

can therefore be simplified as follows:

$$\begin{aligned}
&\sum_{\mu\nu}\langle\langle\Pi_\mu^{(\kappa)}\delta\sigma_\mu^{(\kappa)}|\Pi_\mu^{(\kappa)}\dot{\sigma}_\mu^{(\kappa)} + i\sum_{\mu\nu}\langle\langle\Pi_\mu^{(\kappa)}\delta\sigma_\mu^{(\kappa)}|\mathcal{G}\rho\rangle\rangle \\
=&\sum_{\mu\nu}\langle\langle\Pi_\mu^{(\kappa)}\delta\sigma_\mu^{(\kappa)}|\{\Pi_\mu^{(\kappa)}\dot{\sigma}_\mu^{(\kappa)} + \mathcal{G}\rho\}\rangle\rangle \\
=&\sum_{\mu\nu}\langle\langle\Pi_\mu^{(\kappa)}\delta\sigma_\mu^{(\kappa)}|\{\Pi_\mu^{(\kappa)}\dot{\sigma}_\mu^{(\kappa)} + \mathcal{G}(\Pi_\mu^{(\kappa)}\sigma_\mu^{(\kappa)})\}\rangle\rangle \\
=&\sum_{\mu\nu}\langle\langle\Pi_\mu^{(\kappa)}|\Pi_\nu^{(\kappa)}\rangle\rangle\langle\langle\delta\sigma_\mu^{(\kappa)}|\dot{\sigma}_\nu^{(\kappa)} + i\mathcal{G}^{(\kappa)}\sigma_\nu^{(\kappa)}\rangle\rangle \\
=&\sum_{\mu\nu}\mathcal{D}_{\mu\nu}^{(\kappa)}\langle\langle\Pi_\mu^{(\kappa)}\delta\sigma_\mu^{(\kappa)}|\{\dot{\sigma}_\mu^{(\kappa)} + \mathcal{G}\sigma_\mu^{(\kappa)}\}\rangle\rangle. \qquad (3.79)
\end{aligned}$$

Similarly the right hand side of (3.78) can be rewritten as:

$$\begin{aligned}
&\sum_{\mu}\langle\langle\Pi_\mu^{(\kappa)}\delta\sigma_\mu^{(\kappa)}|\mathcal{L}(\rho)\rangle\rangle - \sum_{\mu}\sum_{T}\langle\langle\Pi_\mu^{(\kappa)}\delta\sigma_\mu^{(\kappa)}|\Omega_T\rangle\rangle\langle\langle\Omega_T|(\mathcal{L}+i\mathcal{G})\rho\rangle\rangle \\
&+ i\sum_{\mu\nu}\langle\langle\Pi_\mu^{(\kappa)}\delta\sigma_\mu^{(\kappa)}|\mathcal{G}\rho\rangle\rangle. \qquad (3.80)
\end{aligned}$$

Therefore the equations of motion for coefficients and single particle density operators can be summarised as:

$$\dot{\sigma}^{(\kappa)} = -i\mathcal{G}^{(\kappa)}\sigma^{(\kappa)} + (1-\mathcal{P}^{(\kappa)})(\mathcal{D}^{(\kappa)})^{-1}\langle\mathcal{L}+i\mathcal{G}\rangle^{(\kappa)}\sigma^{(\kappa)} \qquad (3.81)$$

$$\dot{B}_T = \sum_{T'}\langle\langle\Omega_T|(\mathcal{L}+i\mathcal{G})\Omega_{T'}\rangle\rangle B_{T'}. \qquad (3.82)$$

3.8 ML-MCTDH and ML-ρ-MCTDH derivation

The key to ML-MCTDH is expanding the SPFs recursively in an 'MCTDH-like' form to create 'layers'. First expand wavefunction in configurations that are products of SPFs to form the first layer (in the following nomenclature

based on Manthe [91]).

$$\Psi(q_1 \cdots q_f, t) = \sum_J A'_J(t)\phi'_J(q_1 \cdots q_f, t) \tag{3.83}$$
$$= \sum_{j_1 \cdots j_{d_1}} A'_{j_1 \cdots j_{d_1}}(t)\varphi_{j_1}^{1:1}(q^{1:1}, t) \cdots \varphi_{j_{d_1}}^{1:d_1}(q^{1:d_1}, t),$$

where the superscript 1 denotes the first layer, d_1 is the dimensionality of this layer (number of sets of SPFs) and $q^{1:\kappa} = (q_1 \dots q_{d^\kappa})$ denotes the set of coordinates for the κ-th set of SPFs (mode).

One SPF is then expanded in a second layer set of SPFs requiring an extra superscript:

$$\varphi_j^{1:\kappa} = \sum_k A_{j:k}^{2:\kappa}\phi_k^{2:\kappa} = \sum_{k_1 \cdots k_{d_\kappa}} A_{j:k_1 \cdots k_{d_\kappa}}^{2:\kappa}(t)\varphi_{k_1}^{2:\kappa 1}(q^{2:\kappa 1}, t) \cdots \varphi_{k_{d_\kappa}}^{2:\kappa d_\kappa}(q^{2:\kappa d_\kappa}, t), \tag{3.84}$$

where the superscript $2:\kappa$ denotes functions (and coefficients) in the second layer coming from the κ-th mode from the top layer. These functions can in turn be expanded:

$$\varphi_j^{2:\kappa\mu} = \sum_k A_{j:k}^{3:\kappa\mu}\phi^{3:\kappa\mu}$$
$$= \sum_{k_1 \cdots k_{d_{\kappa\mu}}} A_{j:k_1 \cdots k_{d_{\kappa\mu}}}^{3:\kappa\mu}(t)\varphi_{k_1}^{3:\kappa\mu 1}(q^{3:\kappa\mu 1}, t) \cdots \varphi_{k_{d_{\kappa\mu}}}^{3:\kappa\mu d_{\kappa\mu}}(q^{3:\kappa\mu d_{\kappa\mu}}, t), \tag{3.85}$$

etc. Note that the superscript contains the history of where the function comes from running down the expansion tree from the top layer ($\kappa\mu$) in addition to the layer number (3) and function number in that layer (e.g. 1). For simplicity pack this history into a single index and assume this can be correctly mapped, i.e. write

$$\varphi_j^{2:\kappa} = \sum_{k_1 \cdots k_{d_\kappa}} A_{j:k_1 \cdots k_{d_\kappa}}^{3:\kappa}(t)\varphi_{k_1}^{3:\kappa 1}(q^{3:\kappa 1}, t) \cdots \varphi_{k_{d_\kappa}}^{3:\kappa d_\kappa}(q^{3:\kappa d_\kappa}, t). \tag{3.86}$$

Note also that coefficients require a subscript, j, to denote which function in the layer above they relate to, or in general

$$\varphi_j^{m:\kappa}(q^{m:\kappa},t) = \sum_{k_1\cdots k_d} A^{m+1:k}_{j:k_1\cdots k_d}(t)\varphi_{k_1}^{m+1:\kappa 1}(q^{m+1:\kappa 1},t)\cdots\varphi_{k_d}^{m+1:\kappa d}(q^{m+1:\kappa d},t)$$

$$= \sum_K A^{m+1:\kappa}_{j:K}(t)\phi_K^{m+1:\kappa}(q^{m:\kappa},t). \tag{3.87}$$

Note that the history of the function on the left hand side, $\varphi_j^{m:\kappa}$ is implicit - this is simply the j-th function of the κ-th mode of the m-th layer with dimension d. History on the right hand side, $\varphi_{k_\lambda}^{m+1:\kappa\lambda}$, only explicitly goes up one layer - this is the k_λ-th function of the mode $\kappa\lambda$ in layer $m+1$, where $\kappa\lambda$ means the λ-th set of functions used to expand the κ-th mode of the layer above. The functions $\{\varphi_k^{\kappa\lambda}\}$ span the set of coordinates $q^{m+1:\kappa\lambda}$, which are a subset of $q^{m:\kappa}$. Equation (3.87) also defines layer configurations, $\phi_k^{m:\kappa}$. As a final note on the structure of the ML-MCTDH wavefunction, it should be mentioned that the recursive expansion is finished at the lowest layer with a basis set - either a time-independent DVR or a GWP basis. Two diagrams which show explicit examples of possible structures for an ML-MCTDH wavefunction are shown in Figure 3.1.

It is useful to define layer single hole functions. As for MCTDH, the top layer wavefunction can be written as

$$\Psi(q_1\cdots q_f,t) = \sum_j \psi_j^{1:\kappa}\varphi_j^{1:\kappa} \tag{3.88}$$

with the SHF $\psi_j^{1:\kappa}$ the wavefunction ignoring the SPFs for mode κ. Expanding $\varphi_j^{1:\kappa}$ using (3.87),

$$\Psi = \sum_j \psi_j^{1:\kappa}\sum_{k_1\cdots k_d} A^{2:\kappa}_{j:k_1\cdots k_d}\varphi_{k_1}^{2:\kappa 1}\cdots\varphi_{k_\lambda}^{2:\kappa\lambda}\cdots\varphi_{k_d}^{2:\kappa d} \tag{3.89}$$

$$= \sum_k \psi_k^{2:\kappa\lambda}\phi_k^{2:\kappa\lambda} \tag{3.90}$$

where (3.89) and (3.90) define the relationship between SHFs on different layers. The generalisation of (3.90) is:

$$\Psi = \sum_k \psi_k^{m:\kappa\lambda} \varphi_k^{m:\kappa\lambda} \tag{3.91}$$

$$= \sum_k \psi_k^{m:\kappa\lambda} \sum_J A_{k:J}^{m+1:\lambda} \phi_J^{m+1:\lambda}. \tag{3.92}$$

The equations of motion are obtained as usual from the Dirac-Frenkel variational principle

$$\langle \delta\psi | H - i\frac{\partial}{\partial t} | \Psi \rangle = 0. \tag{3.93}$$

First vary the top layer coefficients $\delta A'_J$:

$$\langle \phi_J | H - i\frac{\partial}{\partial t} | \Psi \rangle = 0 \tag{3.94}$$

$$i\langle \phi_J | \dot{\Psi} \rangle = \langle \phi_J | H | \Psi \rangle \tag{3.95}$$

$$i\langle \phi_J | \sum_K \phi_K \dot{A}_K + \dot{\phi}_K A_K \rangle = \sum_K \langle \phi_J | H | \phi_K \rangle A_K \tag{3.96}$$

and taking the common MCTDH gauge constraint $\langle \phi_J | \dot{\phi}_K \rangle = 0$ to retain orthonormality of the SPFs, we obtain the usual MCTDH equations of motion

$$i\dot{A}_J = \sum_K \langle \phi_J | H | \phi_K \rangle A_K. \tag{3.97}$$

Now varying the basis functions is equivalent to varying all of the expansion coefficients on all of the layers - these are the remaining 'parameters' that define the wavefunction. These can be best accessed using the SHF of (3.92). Vary $\delta A_{j:k}^{m:\lambda}$:

$$\langle \psi_j^{m-1:\kappa\lambda} \phi_k^{m:\lambda} | H - i\frac{\partial}{\partial t} | \Psi \rangle = 0, \tag{3.98}$$

i.e.

$$i\langle \psi_j^{m-1:\kappa\lambda} \phi_k^{m:\lambda} | \sum_{j'k'} \dot{\psi}_{j'}^{m-1:\kappa\lambda} \phi_{k'}^{m:\lambda} A_{j'k'}^{m:\lambda} + \psi_{j'}^{m-1:\kappa\lambda} \dot{\phi}_{k'}^{m:\lambda} A_{j'k'}^{m:\lambda}$$

$$+ \psi_{j'}^{m-1:\kappa\lambda} \phi_{k'}^{m:\lambda} \dot{A}_{j'k'}^{m:\lambda} \rangle = \langle \psi_j^{m-1:\kappa\lambda} \phi_k^{m:\lambda} | H | \sum_{j'k'} \psi_{j'}^{m-1:\kappa\lambda} \phi_{k'}^{m:\lambda} \rangle A_{j'k'}^{m:\lambda}. \tag{3.99}$$

Due to gauge of $\langle\phi_k^{m:\lambda}|\dot{\phi}_{k'}^{m:\lambda}\rangle = 0$, and $\langle\phi_k^{m:\lambda}|\phi_{k'}^{m:\lambda}\rangle = \delta_{kk'}$, this becomes

$$\sum_{j'} i\langle\psi_j^{m-1:\kappa\lambda}|\dot{\psi}_{j'}^{m-1:\kappa\lambda}\rangle A_{j'k}^{m:\lambda} + i\langle\psi_j^{m-1:\kappa\lambda}|\psi_{j'}^{m-1:\kappa\lambda}\rangle \dot{A}_{j'k}^{m:\lambda}$$

$$= \sum_{j'k'}\langle\psi_j^{m-1:\kappa\lambda}\phi_k^{m:\lambda}|H|\psi_{j'}^{m-1:\kappa\lambda}\phi_{k'}^{m:\lambda}\rangle A_{j'k'}^{m:\lambda}. \quad (3.100)$$

In an analogous way to MCTDH, define the 'layer density matrices':

$$\rho_{jj'}^{m:\lambda} = \langle\psi_j^{m-1:\kappa\lambda}|\psi_{j'}^{m-1:\kappa\lambda}\rangle \quad (3.101)$$

and the layer 'mean-field matrices':

$$\mathcal{H}_{jj'}^{m:\lambda} = \langle\psi_j^{m-1:\kappa\lambda}|H|\psi_{j'}^{m-1:\kappa\lambda}\rangle. \quad (3.102)$$

Then (3.100) becomes

$$\sum_{j'} i\rho_{jj'}^{m:\lambda}\dot{A}_{j'k}^{m:\lambda} = \sum_{j'k'}\langle\phi_k^{m:\lambda}|\mathcal{H}_{jj'}^{m:\lambda}|\phi_{k'}^{m:\lambda}\rangle A_{j'k'}^{m:\lambda}$$

$$- \sum_{j'} i\langle\psi_j^{m-1:\kappa\lambda}|\dot{\psi}_{j'}^{m-1:\kappa\lambda}\rangle A_{j'k}^{m:\lambda}. \quad (3.103)$$

To evaluate the second term on the right hand side, multiply (3.103) by $A_{kK}^{m:\lambda*}$ and sum over K. (This is the same as in MCTDH multiplying by an SPF and integrating in a DVR, i.e. $\langle\varphi_i|\varphi_j\rangle = \sum_\alpha A_{i\alpha}^*\langle\chi_\alpha|\chi_\alpha\rangle A_{j\alpha} = \delta_{ij}$.)

$$\sum_k\sum_{j'} i\rho_{jj'}^{m:\lambda}A_{kK}^{m:\lambda*}\dot{A}_{j'K}^{m:\lambda} = \sum_K\sum_{j'K'} A_{kK}^{m:\lambda*}\langle\phi_K^{m:\lambda}|\mathcal{H}_{jj'}^{m:\lambda}|\phi_{K'}^{m:\lambda}\rangle A_{j'K'}^{m:\lambda}$$

$$- \sum_K\sum_{j'} i\langle\psi_j^{m-1:\kappa\lambda}|\dot{\psi}_{j'}^{m-1:\kappa\lambda}\rangle A_{kK}^{m:\lambda*}A_{j'K}^{m:\lambda} \quad (3.104)$$

using the orthonormality of the SPFs,

$$\sum_K A_{kK}^{m:\lambda*}A_{j'K}^{m:\lambda} = \delta_{kj'} \text{ and } \sum_K A_{kK}^{m:\lambda*}\dot{A}_{j'K}^{m:\lambda} = 0, \quad (3.105)$$

and the term on the left hand side of (3.104) is zero, i.e. (3.104) becomes

$$i\langle\psi_j^{m-1:\kappa\lambda}|\dot{\psi}_k^{m-1:\kappa\lambda}\rangle = \sum_{j'KK'} A_{kK}^{m:\lambda*}\langle\phi_K^{m:\lambda}|\mathcal{H}_{jj'}^{m:\lambda}|\phi_{K'}^{m:\lambda}A_{j'K'}^{m:\lambda}. \quad (3.106)$$

Substitute (3.106) into (3.103) to get

$$\sum_{j'} i\rho^{m:\lambda}_{jj'}\dot{A}^{m:\lambda}_{j'K} = \sum_{j'K'}\langle\phi^{m:\lambda}_{K}|H^{m:\lambda}_{jj'}|\phi^{m:\lambda}_{K'}\rangle A^{m:\lambda}_{j'K'} - \sum_{j'j''K'K''} A^{m:\lambda *}_{j'K'}\langle\phi^{m:\lambda}_{K'}|\mathcal{H}_{jj''}|\phi^{m:\lambda}_{K''}\rangle A^{m:\lambda}_{j''K''}A^{m:\lambda}_{j'K} \tag{3.107}$$

and finally defining the SPF projector

$$P^{m:\lambda} = \sum_{j'}|\varphi^{m:\lambda}_{j'}\rangle\langle\varphi^{m:\lambda}_{j'}| \tag{3.108}$$

$$= \sum_{j'KK'}|\phi^{m:\lambda}_{j'K}\rangle A^{m:\lambda}_{j'K}A^{*}_{j'K'}\langle\phi^{m:\lambda}_{K'}| \tag{3.109}$$

we can write (3.107), after multiplying by $(\rho^{m:\lambda}_{\ell j})^{-1}$, as

$$i\dot{A}^{m:\lambda}_{\ell K} = (\rho^{m:\lambda}_{\ell j})^{-1}\sum_{j'K'}\langle\phi^{m:\lambda}_{K}|(1-P^{m:\lambda})\mathcal{H}^{m:\lambda}_{jj'}|\phi^{m:\lambda}_{K'}\rangle A^{m:\lambda}_{j'K'}. \tag{3.110}$$

Note that (3.110) is identical to the usual MCTDH equations of motion for the SPFs except that the basis representation of the SPFs is explicit. (3.97) and (3.110) are the full ML-MCTDH equations of motion, which can be implemented using the recursive structure of Manthe.

3.8.1 ML-ρ-MCTDH(I)

The ρ-MCTDH(I) density matrix is written in terms of SPDOs:

$$\rho(q_1\cdots q_f, q'_1\cdots q'_f, t) = \sum_{j_1\cdots j_\rho} A_{j_1\cdots j_\rho}\sigma^{(1)}_{j_1}\cdots\sigma^{(\rho)}_{j_\rho}$$

and is isomorphic with MCTDH, but using the Hilbert-Schmidt norm (Raab et al [61,62]). Thus the variational derivation above is valid with the following

substitutions:

$$\langle\delta\Psi|(H-i\frac{\partial}{\partial t})\Psi\rangle=0\longmapsto\langle\langle\delta\rho|(\hat{\mathcal{L}}-i\frac{\partial}{\partial t})\rho\rangle\rangle=0,$$

$$\Psi=\sum_J A'_J\phi'_J\longmapsto\rho=\sum_J A'_J\Omega'_J \text{ top layer},$$

$$\phi_J^{m:\kappa}=\varphi_{j_1}^{m:\kappa}\cdots\varphi_{j_{d_\kappa}}^{m:\kappa}\longmapsto\Omega_J^{m:\kappa}=\sigma_{j_1}^{m:\kappa}\cdots\sigma_{j_{d_\kappa}}^{m:\kappa} \text{ layer configurations},$$

$$\varphi_j^{m:\kappa}=\sum_J A_J^{m+1:\kappa}\phi_J^{m+1:\kappa}\longmapsto\sigma_j^{m:\kappa}=\sum_J A_J^{m+1:\kappa}\sigma_J^{m+1:\kappa} \text{ SPDO expansion},$$

$$\Psi=\sum_j\psi_j^{m:\kappa\lambda}\varphi_j^{m:k\lambda}\longmapsto\rho=\sum_j\Pi_j^{m:\kappa\lambda}\sigma_j^{m:\kappa\lambda} \text{ single-hole SPDOs},$$

etc. Thus we can immediately write down that the top layer equation (from (3.97)) is

$$i\dot{A}_J=\sum_K\langle\langle\Omega_J|\mathcal{L}(\Omega_K)\rangle\rangle A_K \tag{3.111}$$

and the lower layer coefficient (from (3.110)),

$$i\dot{A}_{\ell K}^{m:\lambda}=(D_{\ell j}^{m:\lambda})^{-1}\sum_{j'K'}\langle\langle\sigma_K^{m:\lambda}|(1-P^{m:\lambda})\langle\mathcal{L}\rangle_{jj'}^{m:\lambda}\sigma_{j'}^{m:\lambda}\rangle\rangle A_{j'K'}^{m:\lambda} \tag{3.112}$$

where we have defined the following quantities for the layers:

$$D_{\ell j}^{m:\lambda}=\langle\langle\Pi_\ell^{m:\lambda}|\Pi_j^{m:\lambda}\rangle\rangle \text{ 'reduced density matrices'} \tag{3.113}$$

$$\langle\mathcal{L}\rangle_{jj'}^{m:\lambda}=\langle\langle\Pi_j^{m:\lambda}|\mathcal{L}(\Pi_{j'}^{m:\lambda})\rangle\rangle \text{ 'mean-field Liouville'} \tag{3.114}$$

and the projector

$$P^{m:\lambda}=\sum_k|\sigma_k^{m:\lambda}\rangle\rangle\langle\langle\sigma_k^{m:\lambda}|. \tag{3.115}$$

3.8.2 ML-ρ-MCTDH(II)

For type II the density matrix is written in terms of SPFs:

$$\rho=\sum_{JK}|\phi'_J\rangle B'_{JK}\langle\phi'_K| \text{ top layer} \tag{3.116}$$

with configurations ϕ'_K as for ML-MCTDH and a matrix of coefficients. Following Raab et al and extending to ML, the top layer coefficients equations of motion comes from (3.111) to give

$$i\dot{B}_{JL} = \langle \phi_J | \mathcal{L}(\rho) | \phi_L \rangle \tag{3.117}$$

and the SPFs come from (3.110) to give

$$i\dot{A}^{m:\lambda}_{\ell K} = (D^{(2)m:\lambda}_{\ell j})^{-1} \sum_{j'K'} \langle \phi^{m:\lambda}_K | (1 - P^{m:\lambda}) \operatorname{Tr}\{\mathcal{L}(\rho)\rho\}_\lambda | \phi^{m:\lambda}_{K'} \rangle A^{m:\lambda}_{jK'}. \tag{3.118}$$

3.9 Discussion

This chapter shows the derivation of the ML-ρ-MCTDH EOM for the first time in order to show that they are well defined and that the ρ-MCTDH scheme can be incorporated into the multilayer formalism. The step by step derivations for the EOM of both the type I and II ML-ρ-MCTDH are detailed, which extends on the brief overview of this which was previously published in Raab et al [61, 62]. This extensive derivation was required in order to check whether the ρ-MCTDH and ML-ρ-MCTDH schemes are compatible and can be combined. This the first proof that ML-MCTDH can be used for density matrices in an ML-ρ-MCTDH (I) or ML-ρ-MCTDH (II) algorithm.

It is important to note that the ML-ρ-MCTDH method is analogous to ρ-MCTDH, as ML-MCTDH is to the MCTDH method, and the ML-ρ-MCTDH method allows much larger systems to be treated than the standard ρ-MCTDH method could. An advantage of the MCTDH wavefunction is that since it is governed by the Dirac-Frenkel variational principle, it conserves both total probability and energy. These quantities are not conserved for density matrices, although the energy becomes increasingly preserved with

convergence. The main computational effort for the type I formalism is linked to the number of SPDOs used in a calculation whereas the computational effort for the type II is linked to the number of coefficients.

For small systems, the overhead due to the additional equations of motion required to solve the wavefunction in the multi-layer form makes it more expensive to solve the wavefunction in this way. This is not specific to the ML-ρ-MCTDH method, but the ML-MCTDH method in general. It is also important to remember that the way the ML-tree is set up has a significant impact on the efficiency of the ML calculations, both for wavefunctions and density matrices. The system-specificity of the ML-tree is also one of the main disadvantages of this method, although the payoff that is seen in terms of the speedup of calculations makes this method a very powerful approach for studying quantum dynamics of large systems.

As a final note on scaling, for ρ-MCTDH, type I is more efficient for high temperature systems as thermalisation is included in the SPDOs, whereas type II uses the expansion coefficients to represent this. At low temperatures, however, type II will scale better due to the more compact SPF basis. In ML-ρ-MCTDH, it is likely that type I will scale better for all large systems as the basis functions dimensionality plays less of a role and the main effort goes into the top layer coefficients, which scale linearly with basis set size for type I and quadratically for type II.

Chapter 4

Exact propagation of wavepackets and density matrices

4.1 Introduction

This chapter introduces a new numerical integrator which allows the exact propagation of density matrices based on an extension to the well-known Chebyshev integrator used to solve the TDSE and propagate wavepackets. The capability of propagating exact density matrices within the Quantics [92] package, was not previously possible. The term exact in this context means numerically exact, where the nuclear wavefunction is expanded straight onto the full grid rather than parametrised into basis functions, as is typical in the MCTDH method. In a numerically exact calculation the only error comes from using numerical integration rather than the full analytic integral. In

this chapter, the numerical error resulting from the choice of integrator and variables which affect the error is discussed. This new method is implemented in Quantics and tested for a model of pyrazine based on previous studies [34, 93] using MCTDH [94].

4.2 Chebyshev integration method

The purpose of an integrator in quantum dynamics simulations is to solve the TDSE using a numerical integration method. Existing integrators in MCTDH include the Lanczos [95, 96], Runga-Kutta and Adams-Bashforth-Moulton methods. In this section, we describe how the Chebyshev numerical integration method [97] has been implemented into the Quantics package. As mentioned above, the Chebyshev integrator allows the propagation of the exact density matrix, which was not previously possible. This method, which uses Chebyshev polynomials to approximate the time evolution operator, is based on a paper by Leforestier et al [98],

$$\hat{U}(t) = e^{(-i/\hbar)\hat{H}t} \approx \sum_{n=0}^{N} a_n T_n \left(-\frac{i}{\hbar}\hat{H}t \right), \tag{4.1}$$

along with expansion coefficients a_n which are based on Bessel functions. In contrast to the other integrators, the Chebyshev integrator can be used to calculate the time evolution of the system in just 1 timestep from $t_{initial}$ to t_{final}, without the need to determine any intermediate timesteps. It is an iterative scheme that converges on the exact solution to the TDSE over the integration interval chosen.

Various properties of the Chebyshev polynomials make them useful as a basis, such as their orthonormality and the fact that they can be generated recursively as follows:

$$\begin{aligned} T_0(x) &= 1, \\ T_1(x) &= 2x, \\ &\vdots \\ T_{n+1}(x) &= 2xT_n(x) - T_{n-1}(x). \end{aligned} \tag{4.2}$$

This simple recursion relation means that just two terms T_N and T_{N-1} need to be stored during computation. The second aspect of this method is the use of Bessel functions, which are a series of infinite series functions defined by the fact that they are canonical solutions to the Bessel differential equation:

$$x^2y'' + xy' + (x^2 + \alpha^2)y = 0. \tag{4.3}$$

The corresponding solutions to this differential, Bessel functions, are of the following form:

$$y_\alpha(x) = \sum_{m=0}^{\infty} \frac{(-1)^m}{m!\Gamma(m+\alpha+1)} \left(\frac{x}{2}\right)^{2m+\alpha}. \tag{4.4}$$

In general $\alpha \in \mathbb{R}$, but in this case we simply require α to be of integer order. Renaming $\alpha = n \in \mathbb{Z}$ and using the fact that the gamma function of an integer resolves to

$$\begin{aligned} \Gamma(n) &= \int_0^\infty x n^{-1} e^{-x} dx \\ &= (n-1)!, \end{aligned} \tag{4.5}$$

then the Bessel functions simplify so that:

$$
\begin{aligned}
y_0(x) &= \sum_{m=0}^{\infty} \frac{(-1)^m}{(m!)(m+1)!} \left(\frac{x}{2}\right)^{2m} \\
y_1(x) &= \sum_{m=0}^{\infty} \frac{(-1)^m}{m!(m+2)!} \left(\frac{x}{2}\right)^{2m+1} \\
&\vdots \\
y_n(x) &= \sum_{m=0}^{\infty} \frac{(-1)^m}{m!(m+n+1)!} \left(\frac{x}{2}\right)^{2m+n},
\end{aligned} \tag{4.6}
$$

where the n-th Bessel function can be determined from lower order functions using the recurrence relation

$$
y_{n+1}(x) = \frac{2n}{x} y_n(x) - y_{n-1}(x). \tag{4.7}
$$

An important property of Chebyshev polynomials which must be taken into account is that the domain must be contained in the interval $[0, 1]$, which means that it is necessary to rescale the system Hamiltonian so that eigenvalues are between 0 and 1:

$$
\hat{H}_{norm} = 2 \left[\frac{\hat{H} - \hat{I}(\Delta E_{grid}/2 + E_{min})}{\Delta E_{grid}} \right]. \tag{4.8}
$$

Here I is the identity matrix, E_{min} and E_{max} are (in practice, initial estimates) of the minimum and maximum eigenvalues of the system and $\Delta E_{grid} = E_{max} - E_{min}$.

Now the evolution of the wavefunction in terms of Chebyshev polynomials can be written in the following way;

$$
\Psi(t) \approx e^{(-i/\hbar)[\Delta E_{grid}/2 + E_{min}]} + \sum_{n=0}^{N} a_n(\alpha)[T_n(-i\hat{H}_{norm})\Psi(t_0)], \tag{4.9}
$$

with $\alpha = \frac{\Delta E_{grid} t}{2\hbar}$. The expansion coefficients a_n are related to Bessel functions

according to

$$a_n(\alpha) = \begin{cases} y_0(\alpha) & \text{if } \alpha = 0, \\ 2y_n(\alpha) & \text{if } \alpha \neq 0. \end{cases} \tag{4.10}$$

The number of iterations N required is determined by the theoretical limit $N \geq \frac{\Delta E_{grid} t}{2\hbar}$. For $n > N$ Bessel functions are vanishingly small and since by definition $T_n \leq 1$ the neglection of these terms results in negligible error. Therefore the numerical error mostly arises from the truncation of individual Bessel functions which are each, in theory, infinite sums. Using the fact that for small α, the terms in a Bessel function are monotonically decreasing, a certain tolerance can be set in the code, for instance to 10^{-6}, so that the iteration only stops when this level of accuracy has been achieved.

To set up the Chebyshev integrator in MCTDH it is necessary to evaluate the operation of $T_n(x)$ on $\Psi(t_0)$ to avoid higher order polynomial operations on $\hat{H}_{norm}$. To do this, it is useful to reformulate the above recursion relation of the Chebyshev polynomials in relation to this procedure. If we define a new set of functions indexed by the same n by $P_n = T_n(-i\hat{H}_{norm})\Psi(0)$ then

$$\begin{aligned} P_0 &= T_0\Psi(0) \\ &= 1 \cdot \Psi(0) = \Psi(0) \\ P_1 &= T_1\Psi(0) \\ &= -i\hat{H}_{norm}\Psi(0) \\ \therefore P_{n+1} &= -2i\hat{H}_{norm}P_n + P_{n+1}. \end{aligned} \tag{4.11}$$

This procedure has been implemented in the Quantics package for wavefunctions and results using this integrator are discussed later in this chapter.

In order to adapt the Chebyshev integrator so that it is compatible with ρ-MCTDH, recall the Liouville equation (LE);

$$i\dot{\rho} = [H, \rho] = \mathcal{L}(\rho). \tag{4.12}$$

Recall that ρ is a matrix. In order to relate this to the TDSE, write ρ as a vector within Liouville space, expanded in a basis $|I\rangle\rangle = |i\rangle\langle j|$. Then $i\dot{\rho} = \hat{\mathcal{L}}\rho$ where $\mathcal{L}$ is the matrix of an operator:

$$\begin{aligned}
\langle\langle I|\hat{\mathcal{L}}|J\rangle\rangle &= \mathrm{Tr}\left\{|j\rangle\langle i|\hat{\mathcal{L}}|k\rangle\langle m|\right\} \\
&= \mathrm{Tr}\left\{|j\rangle\langle i|\hat{H}|k\rangle\langle m| - |j\rangle\langle i|k\rangle\langle m|\hat{H}\right\} \\
&= H_{ik}\delta_{jm} \cdot \delta_{ik}H_{mj} \\
&= H_{ik}\delta_{jm} - H^*_{jm}\delta_{ik}.
\end{aligned} \tag{4.13}$$

Then the solution to the LE, analogous to the TDSE is

$$\rho(t) = e^{-i\hat{\mathcal{L}}(t)}\rho(0). \tag{4.14}$$

As with the case above for wavefunctions, this expression can be expanded in a basis of Chebyshev polynomials with (4.13) substituted for $\hat{H}$. Previously it was not possible to do exact calculations using the density matrix in Quantics, so the implementation of the Chebyshev integrator adapted for density matrices adds this new capability. As before scaling is needed to ensure that the domain of the polynomials is in $[0, 1]$, so maximum and minimum eigenvalues of $\hat{\mathcal{L}}$ are needed. Using eigenvectors of $\hat{H}$ as a basis

$$H|i\rangle = \varepsilon_i|i\rangle, \tag{4.15}$$

there are several cases to consider.

Firstly if $k = i$, $m = j$,

$$\mathcal{L}_{ij,km} = \mathcal{L}_{ij,ij} = H_{ii}\delta_{jj} - H^*_{jj}\delta_{ii}$$

$$= \varepsilon_i - \varepsilon_j. \tag{4.16}$$

If $k = i$, $m \neq j$,

$$\mathcal{L}_{ij,im} = -H^*_{mj} = 0. \tag{4.17}$$

If $k \neq i$, $m = j$,

$$\mathcal{L}_{ij,kj} = H_{ik} = 0. \tag{4.18}$$

If $k \neq i$, $m \neq j$,

$$\mathcal{L}_{ij,km} = 0. \tag{4.19}$$

Thus in the eigenvalue basis $\mathcal{L}$ is diagonal with values $\varepsilon_j - \varepsilon_i$ for all i, j. Then the maximum and minimum eigenvalues are

$$\ell_{max} = \varepsilon_{max} - \varepsilon_{min}, \tag{4.20}$$

$$\ell_{min} = \varepsilon_{min} - \varepsilon_{max}. \tag{4.21}$$

This scaling means that the Chebyshev integrator can be used to propagate the density matrix. This has been implemented in Quantics for the type I density matrix and the next section discusses some results which test this new approach.

4.3 2-mode pyrazine: a test case

As a test for the Chebyshev integration scheme a 2-dimensional, 2-state model of pyrazine using the model Hamiltonian of [93] is used, consisting

of vibrational modes ν_{10a} and ν_{6a}. This system is set up with 10 SPFs per mode for each state, starting in the excited state.

To test the Chebyshev integrator, a measure of its accuracy should be ascertained. In general for this integrator, the number of iterations N required is determined by the theoretical limit $N \geq \frac{\Delta E_{grid} t}{2\hbar}$. For $n > N$ Bessel functions are vanishingly small and since by definition $T_n \leq 1$ the neglection of these terms results in negligible error. Therefore the numerical error mostly arises from the truncation of individual Bessel functions which are each, in theory, infinite sums.

Using the fact that for small α, the terms in a Bessel function are monotonically decreasing, a certain tolerance can be set in the code, for instance selecting $err = 10^{-6}$, means that the iteration continues up until this level of accuracy has been achieved. Here three different error tolerances are considered: $err = 10^{-6}$, $err = 10^{-5}$ and $err = 10^{-4}$. While the norm and total energy (E_{tot}) values for a system are conserved by default for existing integrators ABM and SIL, the iterative form of the Chebyshev integrator means that there can be a loss in these quantities over time.

Pyrazine was propagated using the Chebyshev integrator for 120fs, and in Figure 4.1 the total energy for these 3 different values of *err* are plotted against time. For the same calculation, the loss in the norm over these 3 values of the *err* are plotted in Figure 4.1. For comparison purposes, the calculation is repeated using MCTDH along with the default ABM integrator, then an exact propagation using ABM again, and finally exact along with the Lanczos integrator. Note that ABM MCTDH is not exact, meaning that the

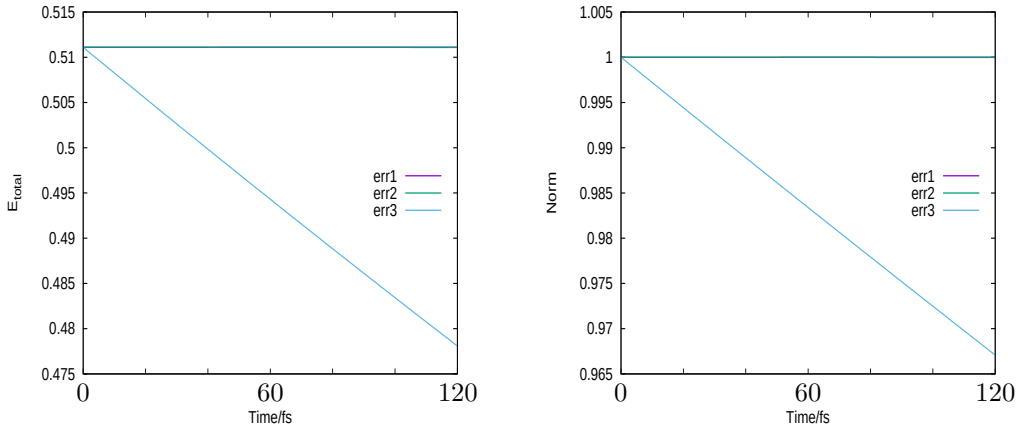

Fig. 4.1: Left: 2D pyrazine plot of the change in the energy during a propagation of a 2D model for pyrazine photo-excitation for exact calculation with the Chebyshev integrator. Right: change in the norm for the same calculation. In both plots the system was propagated for 120fs

wavefunction is expanded into a basis of SPFs in the usual way. The ABM Exact method uses the ABM integrator to propagate the full wavefunction on the grid. The results of these are summarised in Table 4.1.

We see that the Chebyshev integrator is faster than ABM but slower than SIL. Considering that the number of iterations is proportional to the computational effort and a dominant factor in the efficiency is the number of times that $H\Psi$ is calculated, Table 4.2 summarises the iterations needed for each of the Chebyshev calculations. The figures show that, as expected, the calculations with a larger value of *err* are faster but result in a greater loss of norm and energy.

The fact that each figure is a straight line shows that the loss in accuracy

Integrator	**CPU**	E_{tot}	**Norm**
ABM MCTDH	6.120	0.511105000	1.000000000
ABM Exact	2.516	0.511105000	1.000000000
SIL Exact	0.564	0.511105000	1.000000000
Chebyshev Exact, $err1 = 10^{-6}$	0.964	0.511114915	1.00008446
Chebyshev Exact, $err2 = 10^{-5}$	0.932	0.511087311	0.999977334
Chebyshev Exact, $err3 = 10^{-4}$	0.556	0.478087110	0.967083781

Table 4.1: CPU time, final energy and final norm for a set of wavepacket simulations of a 2D model of pyrazine photo-excitation using different integration schemes.

Dimension	**Iterations per timestep**
2D $err1 = 10^{-6}$	17
2D $err2 = 10^{-5}$	16
2D $err3 = 10^{-4}$	12
2D density 1 $err1 = 10^{-6}$	26
4D $err1 = 10^{-6}$	21
4D $err2 = 10^{-5}$	19

Table 4.2: Number of iterations per timestep for the Chebyshev simulations of the 2D and 4D model of pyrazine photo-excitation using different set tolerance values, err.

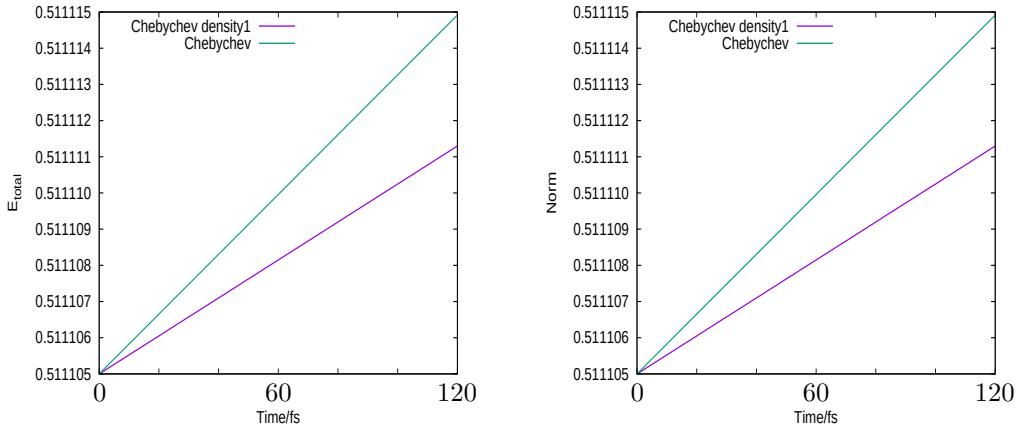

Fig. 4.2: Left: Exact density 1 propagation of 2D pyrazine, plotting total energy over time using the Chebyshev integrator. Right: Exact density 1 propagation of 2D pyrazine, plotting total norm over time using the Chebyshev integrator.

is accumulated at a constant rate over each timestep. Interestingly, the MCTDH calculation is slower than its exact counterpart, due to overheads from the extra basis layer which is unnecessary for this size of model, but a speedup is seen for larger systems. In Figure 4.1 the norm is conserved well for an $err \leq 10^{-5}$ but reduces sharply for $err = 10^{-4}$ over a period of 120fs. The difference in CPU cost of the two more accurate err values is minimal, therefore the default is set to $err = 10^{-6}$.

4.4 Density matrix dynamics

The 2D model of pyrazine is used again here to test the implementation of the Chebyshev integrator for the density matrix. Prior to the implementation of the new Chebyshev integrator it was not previously possible to conduct an exact calculation using density operators using the Quantics program. Note

Integrator	CPU	E_{tot}	Norm
ABM ρ-MCTDH	306.368	0.511105000	1.000000000
Chebyshev Exact	618.124	0.511111297	1.000012319

Table 4.3: CPU time, final energy and final norm for the density matrix simulations of the 2D model of pyrazine photo-excitation using different integration schemes.

here that by "exact" propagation we mean the density matrix is expanded directly on the grid rather than using the time-dependent basis functions of ρ-MCTDH. It may have an integration error but does not require convergence with respect to the basis set and is thus a useful test of performance. In contrast, the ρ-MCTDH propagation using the ABM integrator is not exact which is why the Chebyshev integrator is needed.

Once again we consider how well this scheme conserves the total energy and norm. The total energy increases incrementally over the 120fs propagation time, as does the norm (in comparison to the Chebyshev calculation with the highest accuracy). The CPU time for the exact density type I calculation is roughly double the non-exact equivalent, which is shown in Table 4.3, which also lists final total energy and norm value at the end of the 120fs propagation. All density matrix calculations take a lot longer than the equivalent wavepacket calculations seen in the previous section as we have effectively gone from 3 state 2D system to a 9 state 4D system which squares the effort.

4.5 4-mode pyrazine

The calculations are repeated for 4D pyrazine, the results of which are summarised in Table 4.4. The total energy value starts at 0.65255000 and

Integrator	CPU	E_{tot}	Norm
ABM MCTDH	54.564	0.65255000	1.000000000
ABM Exact Wavepacket	532.496	0.65255000	1.000000000
SIL Exact Wavepacket	96.676	0.65255000	1.000000000
Chebyshev Exact density matrix, accuracy 10^{-6}	132.968	0.650278825	1.000018523

Table 4.4: CPU time, final energy and final norm for a set of simulations of a 4D model of pyrazine photo-excitation using different integration schemes.

increases with the Chebyshev integrator by 0.002271175. The norm does not increase significantly, and the small error in the energy is proportionate to the error tolerence function which truncates the Chebyshev order to reduce the cost of the simulations. As before, the SIL calculation is faster, but the Chebyshev integrator sees an improvement on the ABM exact calculation.

Figure 4.3 shows the 4D spectrum calculated using MCTDH and the equivalent spectrum resulting from the density matrix approach. The spectrum calculated using the density matrix has less defined peaks and is closer to the more diffuse spectrum for the full 24D model of pyrazine which implies that the effect of the density matrix is to partially account for these missing bath modes.

4.6 Discussion

This chapter presents a study into whether the efficiency of propagating density matrices can be improved by the choice of numerical integrator. A new integrator which uses the Chebyshev integration scheme is developed, implemented and tested in the Quantics package against several of the existing integrators. The main advantage of the Chebyshev integrator is that

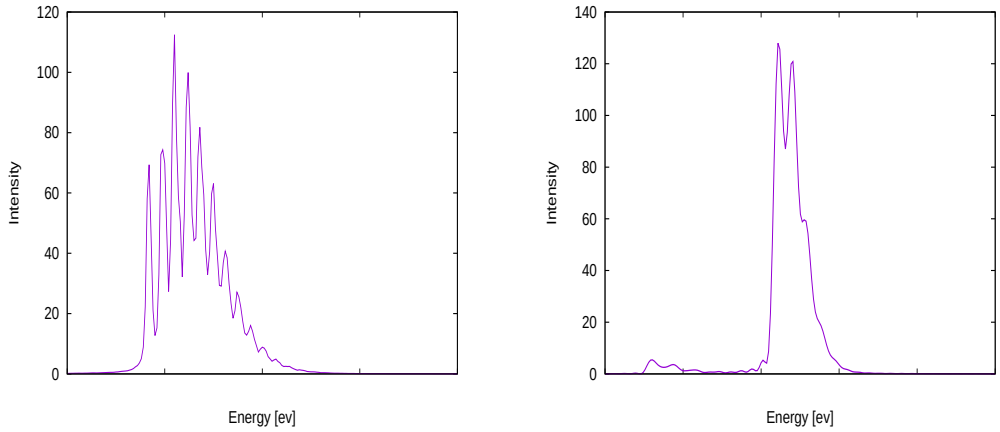

Fig. 4.3: S1 absorption spectrum for the 4 mode pyrazine model, and the 4 mode spectrum calculated using ρ-MCTDH.

it allows exact density matrix calculations for the first time. Although the terminology "exact' here may seem a bit confusing since the error introduced by the Chebyshev integrator is not insignificant in these studies, the error can be set to be smaller at the cost of more computational effort. Another motivation for exploring the utility of the Chebyshev integrator is that unlike most iterative numerical integrators which require small timesteps in order to be accurate, the Chebyshev scheme can easily propagate long timesteps (e.g 120fs at once) without losing accuracy unlike all other integration techniques which are not able to propagate longer timesteps. However, since the MCTDH method is set up to record results at regular small timesteps this is not immediately useful but nevertheless the integrator is freely available and could be adapted for use in a different QD method. In MCTDH the imaginary time propagator, which is used for relaxing a molecule to zero temperature, uses just 1 timestep so the Chebyshev integrator could potentially be adapted to improve the efficiency of this procedure. The results showed

that the newly implemented Chebyshev integrator worked well although it is not a significant improvement on the existing integrators in Quantics. The integrator could potentially be suitable for use with a QD method which uses a longer timestep.

Chapter 5

Models of thermalised proton transfer

The development of the multilayer density matrix ML-ρ-MCTDH method aims to reduce the effort of modelling the non-equilibrium dynamics which the density matrix approach is able to describe. In this chapter, the newly implemented ML-ρ-MCTDH is tested against the MCTDH, ML-MCTDH and ρ-MCTDH methods through the study of three different PT systems. The first system is based on a simple PT model where the reaction coordinate lies along a symmetric double-well PES. Wavepacket calculations were performed for various bath sizes and over a range of temperatures.

Secondly, salicylaldimine is considered, where the PT occurs across an asymmetrical double-well. Quantum dynamics simulations were performed to model PT in salicylaldimine, starting with the two dimensional model of the molecule, which is scaled up to 4D in order to assess the scalability of this new method. Different approaches to thermalisation are applied, and the

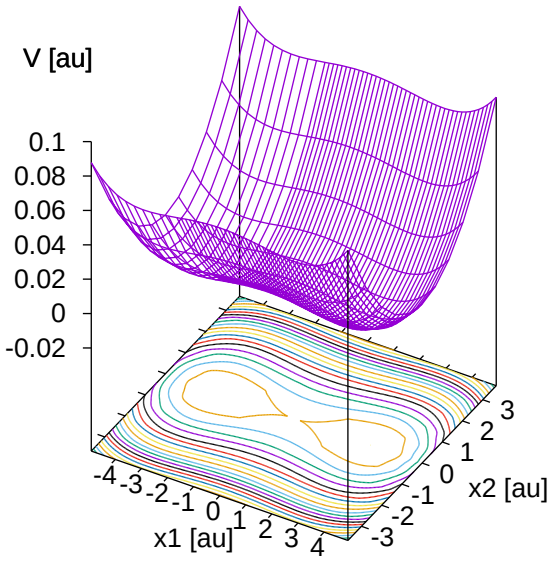

Fig. 5.1: Potential energy surface of the symmetric system for the PT mode and the most strongly coupled bath mode.

resulting rates of flux are presented. Finally, a double PT in porphycene is studied showing the change in rate of PT with both temperature and system size.

5.1 A model for symmetric double well proton transfer

A symmetric PT model is used, where a 1D double-well 'system' is weakly coupled to a 'bath' of 1D harmonic oscillators parametrised to typify a condensed phase environment. Figure 5.1 shows the PES for the PT mode and the most strongly coupled bath mode.

The model which is based on one used by Craig et al, represents PT (across the double-well barrier) in a solvent phase. The model is defined by the following Hamiltonian:

$$\hat{H} = \frac{\hat{p}_s^2}{2} + V_s(\hat{s}) + \sum_j^N \left[\frac{\hat{p}_j^2}{2} + \frac{1}{2}\omega_j^2 \left(\hat{Q}_j - \frac{c_j \hat{s}}{\omega_j^2} \right)^2 \right], \tag{5.1}$$

with the following potential:

$$V_s(\hat{s}) = -\frac{1}{2}\omega_b^2 \hat{s}^2 + \frac{\omega_b^4}{V_0^\ddagger} \hat{s}^4. \tag{5.2}$$

Bath and coupling parameters are given by $\omega_j = \omega_c \tan\left(\frac{\pi}{2}\frac{j}{N+1}\right)$, $c_j = \sqrt{\frac{\eta\omega_c}{N+1}}\omega_j$, and for a solvent $\omega_b = 500\text{cm}^{-1}$, $\omega_c = 100\text{cm}^{-1}$, $V_0 = 1043$ and $c_j = 25\text{cm}^{-1}$. To begin with, the initial conditions are implemented in a rudimentary way with each bath mode perturbed by displacing it from its equilibrium geometry so that they feed energy into the system mode through the coupling. A feature of this model is that the magnitude of the coupling terms for the bath modes is set up to scale with system size, meaning that a greater number of bath modes results in weaker coupling to the system mode. Later the initial conditions are set up more rigorously, to model the system over a range of temperatures.

Note that for consistency, the model is quoted in mass scaled coordinates, however issues with the grid lengths in this coordinate system meant that it was necessary to convert to mass-frequency-scaled coordinates before any accurate calculations could be made.

5.2 ML-MCTDH, increasing model size

Firstly, the 7-mode (Figure 5.2) and 17-mode models were adapted for ML-MCTDH and the convergence and in particular the multilayer basis specifi-

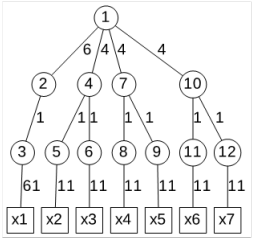

Fig. 5.2: ML-MCTDH tree representing the basis set contraction for a 7-mode PT model.

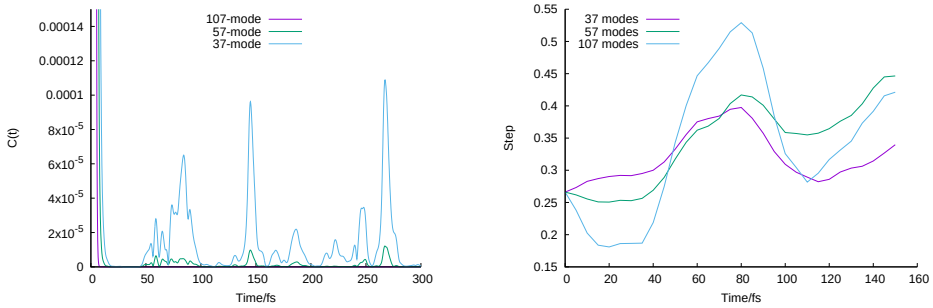

Fig. 5.3: PT dynamics for different bath sizes. Left: Autocorrelation function and Right: The expectation value of the step function each of the 3 bath sizes.

cation was considered. For the 17-mode model it was clear that the choice of mode groupings had a significant effect on computational efficiency (although not necessarily on precision). Because of the way that the bath mode couplings are scaled in the model, it is expected that the autocorrelation should converge with system size, however this is not seen here because the initial conditions for each bath mode were identically specified meaning that total energy increases with system size. Note that this is not the usual thermal distribution based on random sampling of the Boltzmann distribution as the initial conditions here were set up as a suitable test, and later in this chapter the initial conditions are set up more precisely.

Figure 5.3 shows the PT dynamics for different bath sizes; the dynamics was calculated for 36, 56 and 106 bath modes. The plot on the left is the autocorrelation function

$$c(t) = \langle \psi(0) | \psi(t) \rangle \tag{5.3}$$

of each of the three calculations. The autocorrelation function is the overlap between the initial and final wavefunction, which gives a measure of how the system evolves compared to its initial state. On the right, the expectation value of a step function placed at the transition state is shown. This gives a measure of the extent of the proton transferred. Therefore we see in Figure 5.3 that the increase in energy along with system size results in the dynamics being less correlated, although the oscillatory structure is similar over the three propagations. The trend seen for the autocorrelation function progresses consistently with system size. The step function illustrates that the initial conditions for the position of the wavepacket are identical. However, the wavepacket for the 107 mode system recedes first into the well that it starts from before transferring more completely across the barrier before dissipating back into the first well. Since the initial conditions are inconsistent with the earlier paper looking at this model, in particular due to rescaling of the model, it is therefore difficult to directly compare the results here to what has previously been observed.

The results show that the larger bath sizes, which have more energy (are "hotter") display a greater mobility. The autocorrelation function for the 37 mode calculation displays recurrences, when the wavepacket returns to its initial position, which are damped in the larger calculations. The degree of PT is also seen to increase with increasing system size as the energy from the bath feeds into the PT mode and the system can overcome the barrier. The degree of PT oscillates, but is seen to increase with time in all calculations.

5.3 G-ML-MCTDH

A long term aspiration in the field of quantum dynamics simulations is to develop a "black-box" method, where the dynamics of a system can be calculated without the need for system specific pre-calculated PES. Within the quantics package, the relatively recently developed direct-dynamics method is designed to do this. This approach is based on the G-MCTDH method in which the grid-based single-particle function basis is replaced by a basis set of parametrised Gaussian functions [87]. As it is not a grid-based method the basis set of variational multiconfigurational gaussians can be used to estimate both the local PES and nuclear dynamics on the fly. If the density matrix can be set up to work in this way with the direct-dynamics approach, then this could potentially be a very useful technique. G-ML-MCTDH uses exactly the same procedure as G-MCTDH and replaces SPFs with Gaussian functions. This can then in principle be extended to provide a Gaussian based G-ML-ρ-MCTDH scheme to enable on the fly density matrix calculations.

The first step towards this is to investigate how well G-ML-MCTDH works with a basis of static GWPs. In order to test the G-ML-MCTDH scheme against the benchmark of MCTDH, the 17-mode model was considered since the 37-mode system would result in scaling issues on a full MCTDH grid. In Figure 5.4 the autocorrelation function for each of these three schemes is compared after 150fs propagation time and with identical initial conditions. We see that it is difficult to converge the G-ML-MCTDH calculation fully, which is one of the major drawbacks of this method. However, the advantage of using a GWP basis is the flexibility, which can make it a powerful approach depending on the properties of the system being studied.

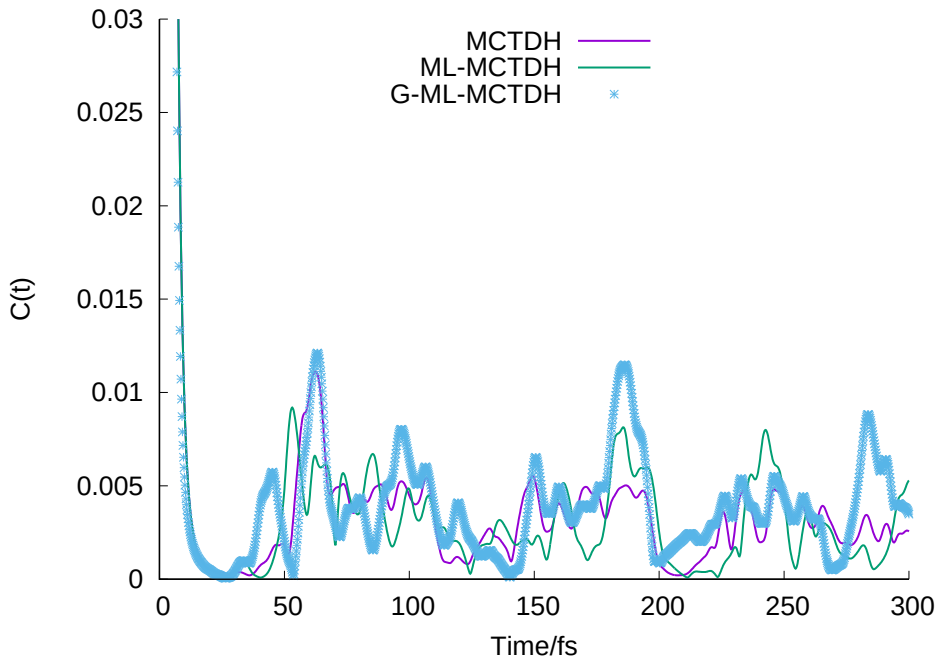

Fig. 5.4: The autocorrelation function from a 17-mode PT model using methods MCTDH, ML-MCTDH and G-ML-MCTDH.

The trend that is seen for the three methods is roughly similar given the sensitivity of a measure such as autocorrelation and a certain amount of accuracy is to be expected to be lost where Gaussian wavepackets are used in substitute for the full propagation on the grid. This initial finding suggests that the G-ML-MCTDH routine can be expected to work well and one advantage is that it is more generally applicable to problems where the full solution on the grid is inefficient.

5.4 Effects of temperature

We saw earlier in the chapter how the larger bath size resulted in more energy transfer into the system mode given that the initial conditions for each

bath mode were identically specified meaning that total energy scales with system size. It would be possible to scale initial conditions so that the total energy remains the same regardless of system size.

Note however that the coupling strength of bath modes does scale with system size, for instance bath modes which are labeled with higher numbers will couple less strongly to the system, so this must be taken into account when controlling for bath temperature. To explore the temperature dependence of the dynamics, and to test the new code, calculations were run at a range of temperatures using ρ-MCTDH(I) and ML-ρ-MCTDH(I). Thermalisation was achieved by propagating in imaginary time. Formally, propagation of a wavepacket can be written as

$$\Psi(t) = \exp(-iHt)\Psi(0), \tag{5.4}$$

The propagation in time can be changed to a propagation in temperature, where time 0 is effectively infinite temperature. Therefore a propagation in imaginary time relaxes the system from infinite temperature to a chosen finite temperature using the transformed time $it \rightarrow \frac{1}{kT}$ so that

$$\Psi(T) = \exp\left(-\frac{H}{kT}\right)\Psi(\infty). \tag{5.5}$$

For a density matrix propagation, using the Liouville von-Neumann equation results in a thermalised density matrix with the form

$$\rho(T) = \exp\left(\frac{H}{2kT}\right)\rho(\infty)\exp\left(-\frac{H}{2kT}\right). \tag{5.6}$$

This means that starting with a density matrix in which all states are equally populated (infinite temperature), propagation to temperature T provides the thermalised density.

Thermalisation calculations were run for the 2D system using ρ-MCTDH(I), and the 7D system using ML-ρ-MCTDH(I) at 0K, 500K, 1000K, 1500K and 2000K. During thermalisation, the system was localised in the left hand (negative coordinate) energy well by adding a step function to the potential centered at the transition barrier. This effectively places a high wall, masking out the right hand well. The step function is defined as follows, with respect to the location of the TST which is defined as displacement 0 ($x = 0$).

$$\Theta(\nu_1) = \begin{cases} 1, & \text{if } x > 0, \\ \\ 0, & \text{if } x < 0, \end{cases} \tag{5.7}$$

The expectation value of a step function placed at the barrier, provides the density that has crossed to the right hand well. In Figure 5.5 the expectation of the step function at the different temperatures is plotted over time. The bath and system are at the same temperature so it appears that there is very little energy flow between them, as is illustrated in the right hand figure.

5.5 Proton transfer in an asymmetric double well: Salicylaldimine

This section uses a model for salicylaldimine based on previous work by [99, 100] using a model from Polyak et al [101]. This molecule was used previously to study hydrogen bonding. The two most stable tautomers of salicylaldimine, also known as 2-hydroxybenzaldimine are the enol and keto forms, as seen in Figure 5.6. An intramolecular PT occurs if the molecule has sufficient energy. The enol form is the most stable and is calculated to be 0.39ev below the transition state while the keto form is 0.22ev.

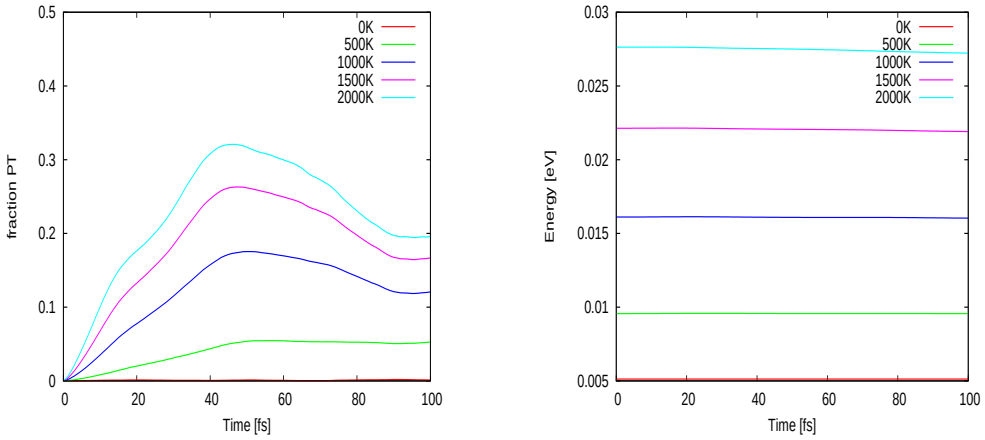

Fig. 5.5: Left: expectation value of the step functions for a range of thermalised 7D propagations. Right: total energy of the bath modes for the 7D propagation at a range of temperatures.

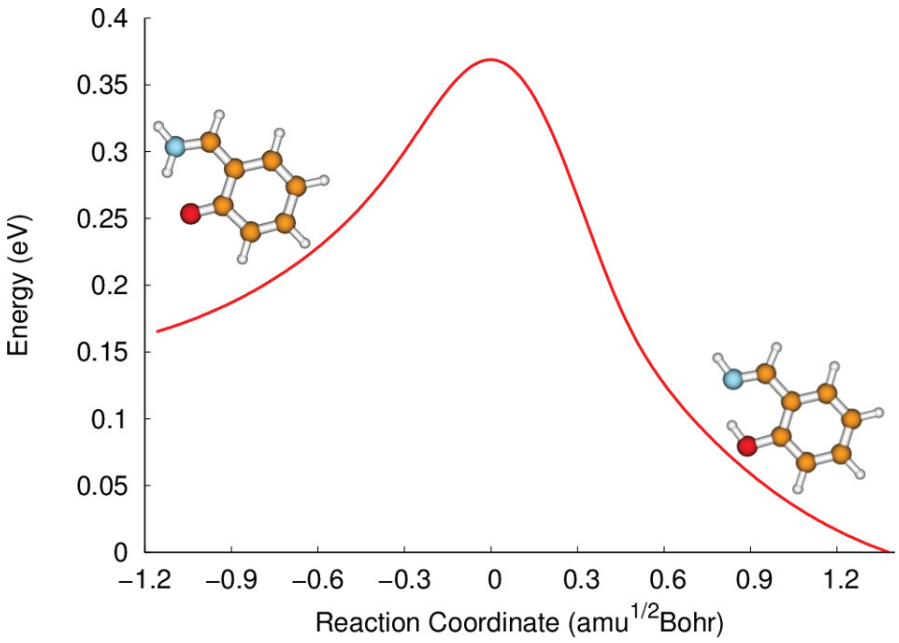

Fig. 5.6: Reaction coordinate taken from [101].

A full PES for salicylaldimine C_7H_7ON is described by 42 normal modes, but the previous work by Polyak et al selects the 13 which contribute the most to the reaction. ν_1 is the transition pathway and ν_{36} is the in-plane proton motion perpendicular to ν_1. In the previous study, the model starts close to the enol form with the bond slightly stretched to give it enough energy for the reaction to occur.

Before any further calculations on this model took place, it was initially verified that the result for the 2D exact calculation in this model corresponded to the results published by Polyak et al. They did indeed correspond and all further calculations used different initial conditions where the temperature has been precisely defined, as was discussed in the previous section. At cold temperatures it is unlikely that the proton would have sufficient energy to cross the barrier but as the system is thermalised above the barrier we should get movement. When the system is relaxed to 0K, the energy difference to the stretched molecule is found to be 0.05182ev for the 2D model. Using that $T = E/k_b$ where E is the energy in Joules, this is equivalent to a temperature of 601.22K. Similarly, the energy gap between the stretched and relaxed 4D model was found to be equivalent to a temperature of 1137.59K.

Thermalisation calculations were run for the 2D system using ρ-MCTDH(I) to 0K, 500K, 1000K and 1500K. The expectation value of a step function placed at the barrier, provides the density that has crossed to the high energy well. This is plotted in Figure 5.7. It can be seen that at 0K the density is localised in the low energy, keto, well. PT then occurs by tunnelling through the barrier to the enol well. At higher temperatures, more density is found in the high energy well, but no dynamics takes place, showing that

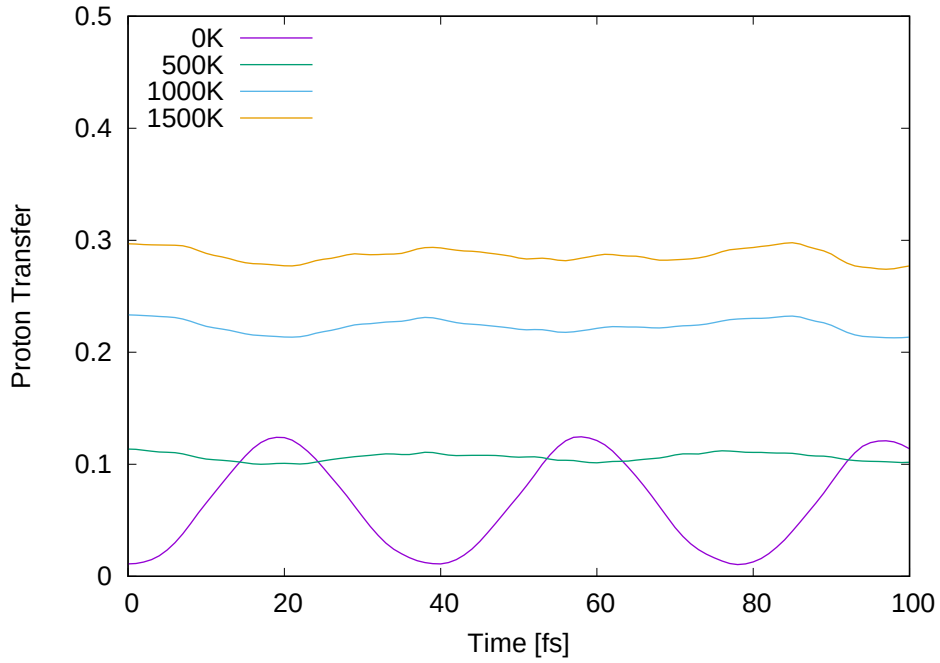

Fig. 5.7: Fraction of the density in the high-energy well of a 2D model of salicylaldimine at a range of temperatures.

the thermalisation has provided a good approximation to the thermalised stationary state. As shown earlier, these calculations are converged and so are the same as an exact result.

To test the effect of increasing the bath size on performance and system behaviour a similar set of calculations was carried out for a 6D model, in which the modes $\nu_{10}, \nu_{11}, \nu_{13}$ and ν_{32} were added to the main PT modes of ν_1 and ν_{36} used in the 2D model. The resulting fraction of PT is shown in Figure 5.8. A similar behaviour is seen, but the degree of tunnelling at 0K is much less, indicating the higher barrier height. The high temperature densities are also less constant, perhaps indicating that the calculations are

not fully converged. These results show that the trend previously seen in the 2D systems is replicated here, where an increase in the dynamics is seen as the temperature increases. The only movement of the system at zero Kelvin is due to proton tunnelling. In this case, the wavepacket partially crosses the barrier from the global minimum (enol) to the less stable minimum (keto). When the temperature is increased to 500K and to 1000K the dynamics of the system is not significantly altered. The change in the dynamics between the 500K and 1000K propagations can be rationalised by the fact that the system at 1000K has enough energy to traverse the lower activation energy barrier for the return keto-enol tautomerisation, and hence the dynamics can no longer be attributed entirely to tunnelling. The most significant change in dynamics occurs when the temperature increases from 1000K to 2000K.

As a note on computational effort, a 2D propagation using ρ-MCTDH(I) for 100fs on a Xenon 12 core machine took 11,328s (3 hours 8 mins), while a 6D calculation took 204 hours. This demonstrates the huge increase in resource required by density matrix calculations. In contrast, the 6D calculation on the same machine using ML-ρ-MCTDH(I) took only 26,508s (7 hours 21 mins), a huge saving in effort. The ML-ρ-MCTDH (II) method required much longer and a comparison between the scaling for type I to type II methods is given in the next section.

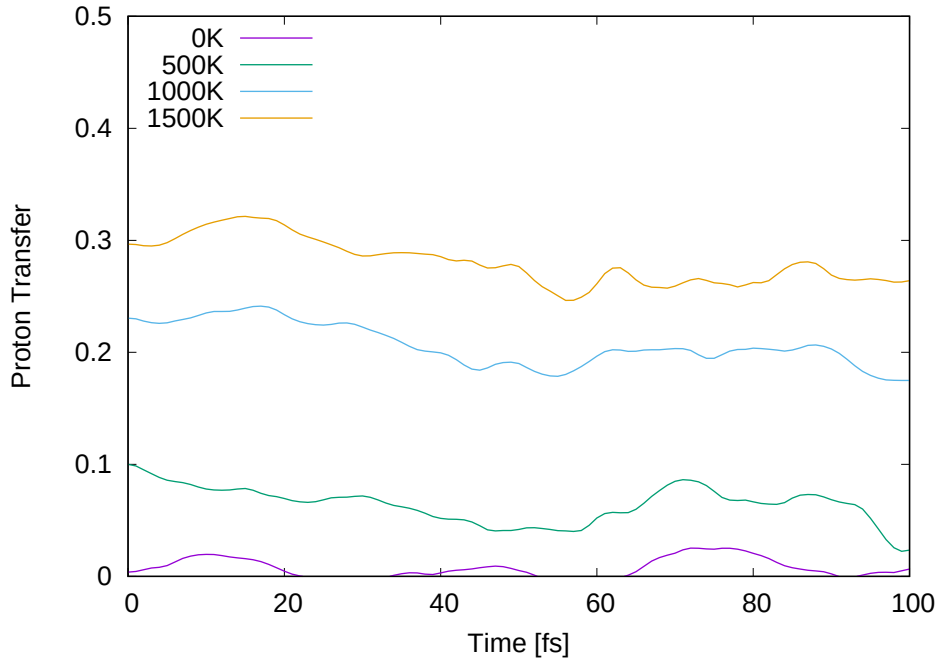

Fig. 5.8: Fraction of the density in the high-energy well of a 6D model of salicylaldimine at a range of temperatures.

Parameter	Value
U_0	876.0 cm^{-1}
g	0.435
x_0	0.624 Bohr
α_{trans}	0.0095
α_{cis}	0.034

Table 5.1: Parameters for the porphycene double PT potential of Abdel-Latif and Kühn [103].

5.6 The porphycene model Hamiltonian

Abdel-Latif and Kühn [102, 103] provide a two-dimensional model Hamiltonian for the double PT in porphycene using a symmetric and anti-symmetric PT coordinates and a potential form that provides four minima. The Hamiltonian is

$$H = -\frac{\hbar^2}{2m_H}\left(\frac{\partial^2}{\partial x_s^2}+\frac{\partial^2}{\partial x_a^2}\right)++U_{sym}+U_{asym}; \tag{5.8}$$

$$U_{sym} = 2U_0+\frac{U_0}{x_0^2}\left[(g-4)x_a^2-(g+4)x_s^2\right] + a\frac{2U_0}{x_0^4}\left(x_s^4+x_a^4+6x_a^2x_s^2\right); \tag{5.9}$$

$$U_{asym} = \frac{\alpha_{\text{trans}}U_0}{x_0}x_a+\frac{\alpha_{\text{cis}}U_0}{x_0}x_s. \tag{5.10}$$

Double PT in porphycene has also been studied in an application of a path-integral ring-polymer method [104]. The parameters were calculated at the B3LYP/6-31+G** level of theory and are listed in Table 5.1. The potential is shown in Figure 5.9.

This Hamiltonian was extended to include the remaining 106 vibrations of

(a) (b)

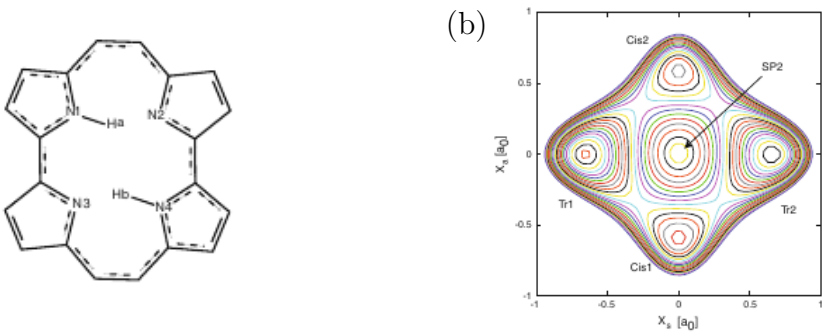

Fig. 5.9: (a) porphycene and (b) the double well potential surface for porphycene used to describe the double PT. Taken from [103].

porphycene as a bath of harmonic oscillators coupled to the system modes.

$$H = H_s + H_b + H_{sb} \tag{5.11}$$

with the bath modes described by a set of harmonic oscillators in mass-frequency scaled coordinates

$$H_b = \sum_{i=3}^{108} -\frac{\omega_i}{2}\frac{\partial^2}{\partial q_i^2} + \frac{1}{2}\omega_i q_i^2. \tag{5.12}$$

To parameterise the extended model, the transition state structure was first optimised using the same level of theory used by Abdel-Latif and Kühn. This structure has D_{2h} symmetry and the "symmetric" and "anti-symmetric" double-proton vibrations are found to have imaginary frequencies and b_{2u} and b_{3g} symmetry, respectively. These vibrations are shown in Figure 5.10.

Taking symmetry into account, coupling between the two system modes and the bath can be written

$$H_{sb} = \sum_{si} \gamma_{si} x_s q_i + \sum_{aj} \gamma_{aj} x_a q_j + \sum_{sk} \gamma_{sk} x_s^2 q_k + \sum_{sk} \gamma_{ak} x_a^2 q_k \tag{5.13}$$

where i are the 16 b_{2u} vibrations, j are the 17 b_{3g} vibrations, and k the 17

(a) (b)

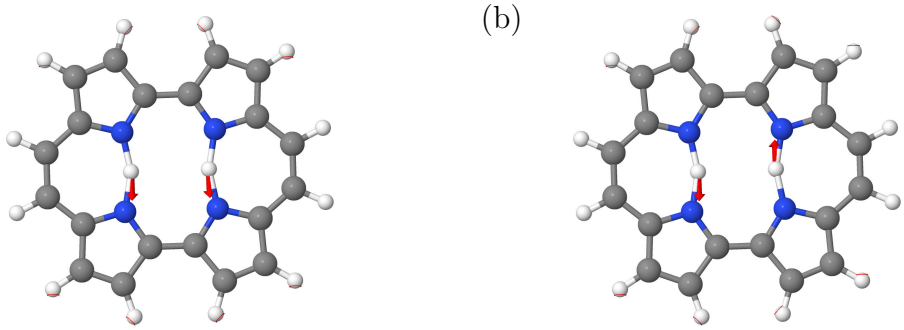

Fig. 5.10: The (a) symmetric, x_s, and (b) anti-symmetric, x_a, PT vibrational modes of porphycene, calculated at the B3LYP/6-31+G** level of theory.

a_{1g} vibrations. The final model Hamiltonian thus include 55 modes.

The parameters for the system-bath coupling can be obtained by taking the derivative of the full potential at the minimum energy structures with respect to one of the bath modes. For modes of b_{2u} symmetry, the derivative is

$$\frac{\partial V}{\partial q_i} = \omega_i q_i + \gamma_{si} x_{s,0} = 0 \tag{5.14}$$

for modes of b_{3g} symmetry

$$\frac{\partial V}{\partial q_j} = \omega_j q_j + \gamma_{aj} x_{a,0} = 0 \tag{5.15}$$

and for modes of a_{1g} symmetry

$$\frac{\partial V}{\partial q_k} = \omega_k q_k + \gamma_{sk} x_{s,0}^2 + \gamma_{ak} x_{a,0}^2 = 0 \tag{5.16}$$

where $x_{s,0}$ and $x_{a,0}$ are the symmetric and anti-symmetric coordinates at the minima. From these relationships the coupling parameters, γ, can be calculated from the geometry of the energy minima. The structures at the minima were obtained by optimising at the B3LYP/6-31+G** level and theory, and transformed to normal mode coordinates. The coupling parameters were

then obtained using equations (5.14-5.16). The values are listed in Tables 5.2, 5.3 and 5.4, along with the frequencies for the modes.

Mode	ω (eV)	γ_{si} (eV/Bohr)
12	0.0310	0.02569
20	0.0509	0.05882
26	0.0781	-0.03258
43	0.1050	-0.03199
55	0.1245	-0.08677
58	0.1303	0.09544
61	0.1364	-0.04995
68	0.1517	-0.01423
74	0.1640	-0.00573
75	0.1676	-0.00745
80	0.1762	0.01957
86	0.1888	-0.00684
89	0.1948	-0.00024
94	0.2020	0.01869
97	0.3934	-0.00136
103	0.4025	-0.00192
107	0.4050	-0.00218

Table 5.2: Frequencies and coupling parameters for the bath modes in the porphycene model with b_{2u} symmetry.

Mode	ω (eV)	γ_{aj} (eV/Bohr)
8	0.0194	-0.01773
22	0.0616	0.00151
25	0.0764	-0.05334
44	0.1053	0.04010
49	0.1129	-0.08953
56	0.1296	-0.09407
60	0.1358	-0.06313
64	0.1432	-0.00426
72	0.1615	-0.02938
78	0.1729	-0.01279
79	0.1742	0.00291
83	0.1797	-0.00477
88	0.1918	-0.00633
92	0.1995	-0.01916
98	0.3934	-0.00212
101	0.4023	0.00226
105	0.4046	-0.00305

Table 5.3: Frequencies and coupling parameters for the bath modes in the porphycene model with b_{3g} symmetry.

Mode	ω (eV)	γ_{sk} (eV/Bohr^2)	γ_{ak} (eV/Bohr^2)
13	0.0346	0.2222	0.2002
17	0.0457	0.0696	0.0746
18	0.0466	-0.1551	-0.1620
31	0.0852	-0.0637	-0.0624
54	0.1228	0.0044	0.0140
57	0.1301	0.1974	0.1895
62	0.1372	0.1006	0.1018
66	0.1489	0.0219	0.0136
70	0.1530	-0.0223	-0.0279
76	0.1696	0.2061	0.1879
77	0.1716	-0.0005	0.0200
82	0.1796	-0.0370	-0.0403
85	0.1883	0.0819	0.0620
91	0.1984	-0.0714	-0.0523
93	0.2016	-0.0775	-0.0771
96	0.2263	0.2932	0.3116
100	0.3955	-0.0024	-0.0007
104	0.4026	0.0000	0.0027
108	0.4050	-0.0142	-0.0101

Table 5.4: Frequencies and coupling parameters for the totally symmetric (a_{1g}) bath modes in the porphycene model.

5.7 Double proton transfer in the porphycene model

The porphycene PT model Hamiltonian was used in a series of calculations to test the potential of the ML-ρ-MCTDH methods. This consisted of different dimensional systems at a range of temperatures to demonstrate the scaling as well as the changes in physical behaviour. In all cases, an initial energy relaxation calculation was made to thermalise the system to the desired temperature, followed by a propagation of 500fs. The number of basis functions was chosen such that all natural populations were below 0.001 after 250fs. I.e. the initial dynamics is well represented.

As a benchmark for the system dynamics, initially 2D calculations including the x_s and x_a PT modes were ran at 0, 500, 1061, 1500 and 200K. The barrier height is 1061K. The initial relaxation localised the density in one well centred at $(x_s, x_a) = (-0.607, 0.0)$. This was done by including a step function in the Hamiltonian during the relaxation to create a high wall at $x_s = 0.0$. This wall was then removed for the propagation, but the expectation value of the step function as a function of time was used to calculate the amount of PT taking place.

This PT at varying temperatures is shown in Figure 5.11. At 0K (purple line), there is a slow transfer, which is almost complete after 300fs before returning to the initial well. This is due to tunnelling. As the temperature increases, the transfer is faster, and the amount decreases.

Snapshots of the density at different times are shown in Figure 5.12 and

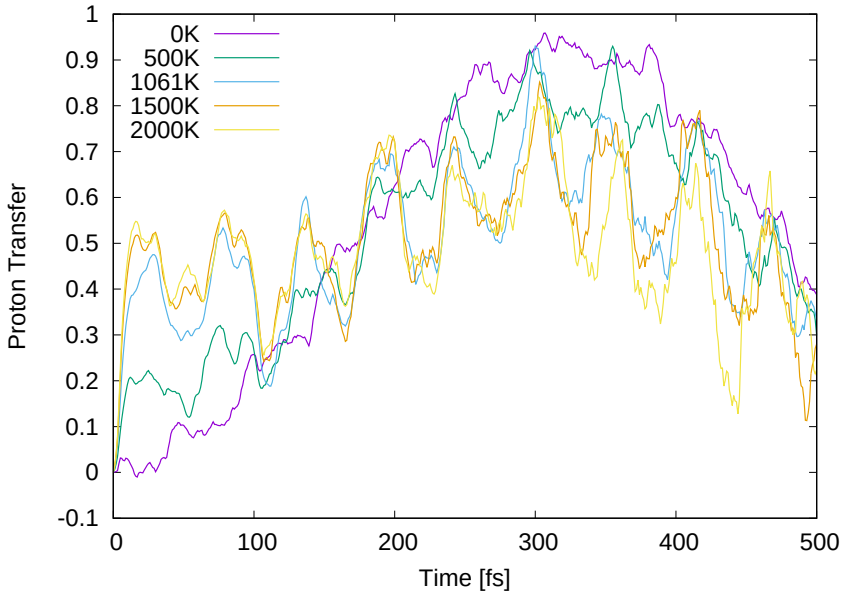

Fig. 5.11: Transfer of density between PT minima in the 2D porphycene model at different temperatures, starting in one minima.

Figure 5.13. The density is taken from the trace of the time-evolving density matrices. At 0K, the initially localised density is seen to move towards and then cross the barrier. At 1061K, the initial density is again localised in the one well, but vibrationally excited in the x_a mode, as seen by the structure. In contrast to the 0K case, this hot density flows quickly around the maximum of the potential at $(x_s, x_a) = (0, 0)$ to undergo the double PT. At 20fs it is seen to be occupying all four wells, after which the density oscillates back and forth between the two minima at $(x_s, x_a) = (\pm 0.6, 0)$.

A 4D system was then studied, including the 2 bath modes with the strongest coupling ν_{13} and ν_{18}. The amount of PT for this system as a function of time at different temperatures is shown in Figure 5.14. The bath modes have a strong effect in slowing down the transfer. The tunnelling at 0K is still taking place at 500fs. Even at the barrier height temperature the transfer is increasing in a similar way to the tunnelling. Only when well above the

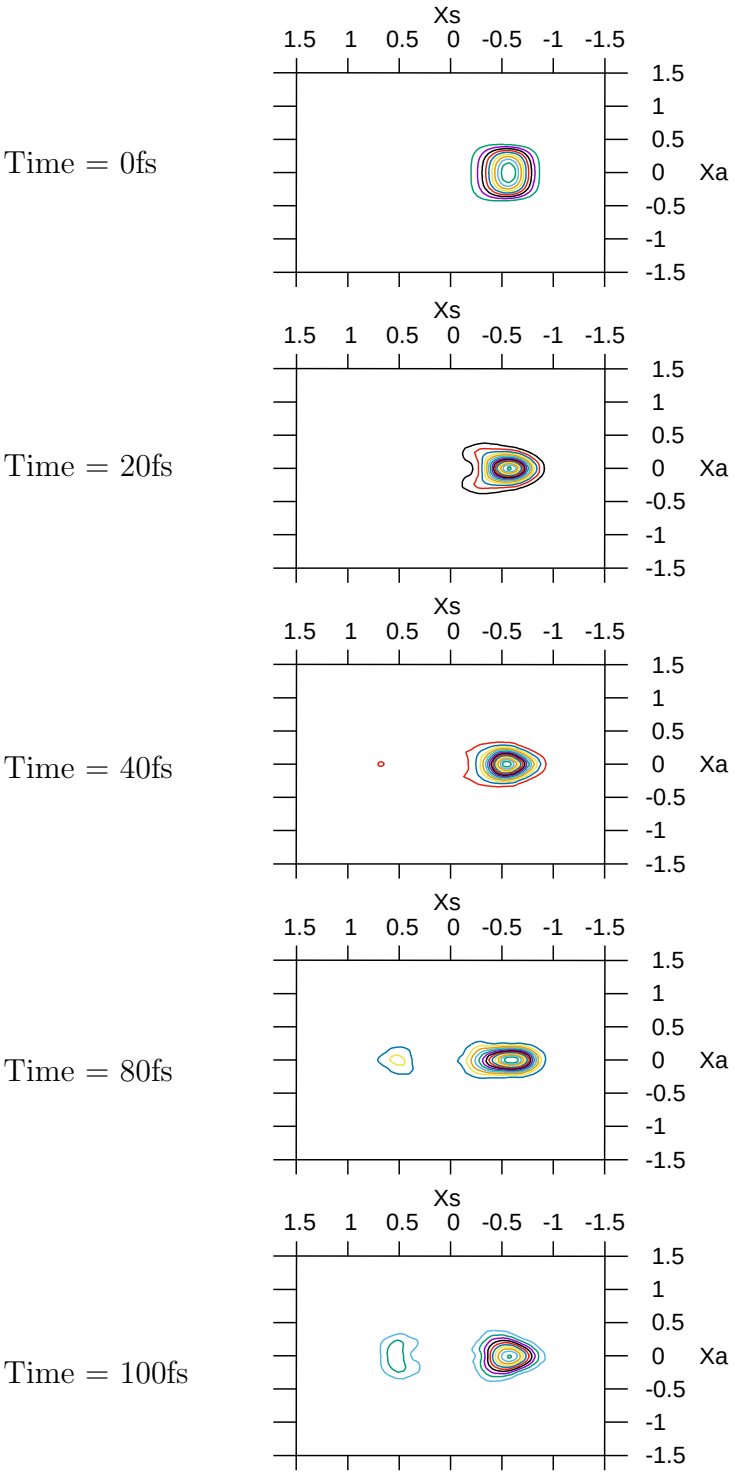

Fig. 5.12: Snapshots of the density of the 2D porphycene model at different times, starting in one minima at 0K.

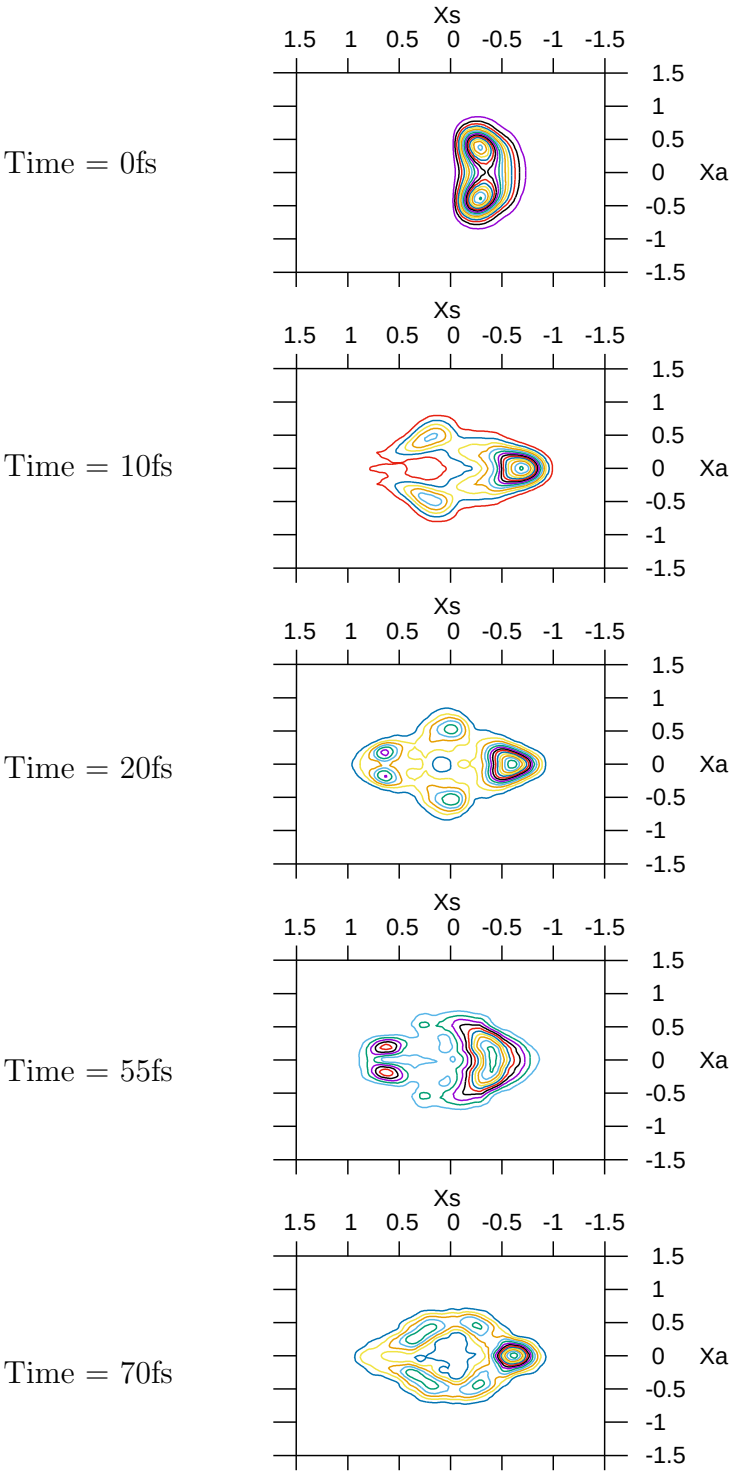

Fig. 5.13: Snapshots of the density of the 2D porphycene model at different times, starting in one minima at 1061K.

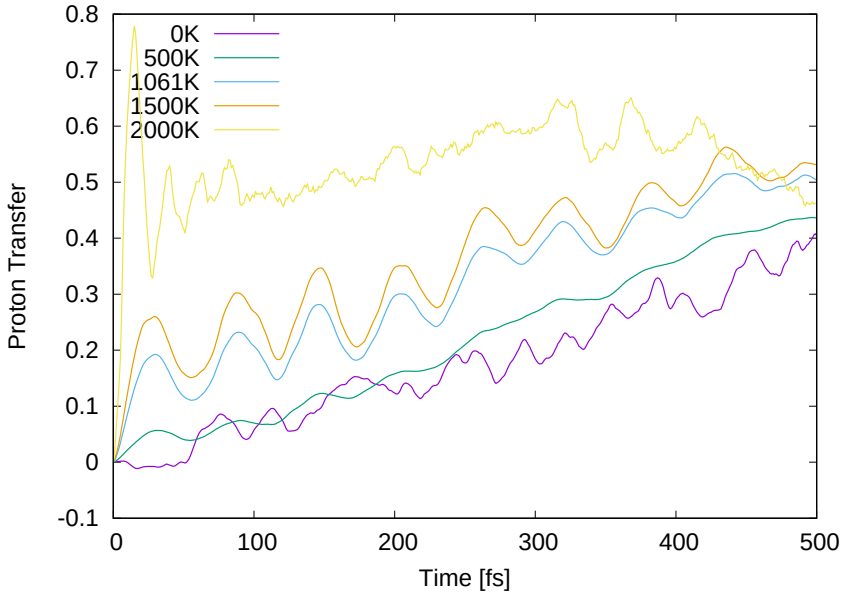

Fig. 5.14: Transfer of density between PT minima in the 4D porphycene model at different temperatures, starting in one minima.

barrier at 2000K does the transfer now take place in less than 100fs, reaching 50% transfer and staying there, indicating the density is spread across the minima equally. The zero temperature propagation briefly dips negative in this calculation which is an artefact of a small numerical error in the calculation. It is possible to see some PT occurs in the low temperature calculation where the energy of the system is below the barrier height, which indicates that tunnelling plays a significant role in the reaction at lower temperatures. When the temperature of the system is set to be equivalent to the barrier height, T=1061K, and also for the 1500K propagation, clear oscillations are seen as the wavepacket oscillates back and forth between the two states. At the higher energy, 2000K propagation, the wavepacket transfers more quickly over the barrier.

Finally, a 6D system adding the modes ν_{17} and ν_{57} and a 10D system adding $\nu_{12}, \nu_{20}, \nu_{8}$, and ν_{25} were examined to show the performance of the ML-ρ-

MCTDH methods. The CPU-times for calculations on the 4 systems at 0K using the different algorithms are listed in Table 5.5. All 4 methods could be applied to the 4D system, and the huge saving in time by the ML-ρ-MCTDH(I) algorithm is clear.

The large number of expansion coefficients in the matrix top layer of ML-ρ-MCTDH(II) is the reason for the advantage of the type I density matrices. This difference in effort is even more pronounced for the 6D case, for which regular ρ-MCTDH(II) is prohibitively slow, and for ρ-MCTDH(I) is not feasible. For the 10D system, only the ML-ρ-MCTDH(I) is feasible, and impressively fast, taking only 6731s for a 500fs propagation. The key thing to note here is that ML-ρ-MCTDH(I) scales much better with the larger model. This is consistent with the trends seen in the earlier calculations looking at salicylaldimine. The 6D ρ-MCTDH(I) calculation has a CPU time of 1.030×10^6 seconds in comparison to just 4993 seconds for the same calculation using ML-ρ-MCTDH(I), which demonstrates how much more efficient this scheme is. The purpose of these calculations is to verify that new method gives consistent results to existing methods, i.e. to test that the code actually works as intended. While it is not easy to compare the calculations directly to previous studies as the models are set up differently and have incomparable initial conditions, the dynamics predictions of ML-ρ-MCTDH has been shown in this chapter to replicate existing dynamics approaches. Repeating earlier density matrix calculations using the exact method to show that the dynamics is identical verifies that this method is reliable. Building on this, the ρ-MCTDH and ML-ρ-MCTDH calculations were found to give consistent results, which shows that this method can be successfully used to predict the dynamics of these systems.

Method	2D	4D	6D	10D
ρ-MCTDH(I)	5855	8866	1.030×10^6	
ρ-MCTDH(II)	4875	14298		
ML-ρMCTDH(I)		967	4993	13275
ML-ρMCTDH(II)		6700	7014	

Table 5.5: CPU Time in seconds for various dimensional porphycene model systems using different algorithms. All calculations were ran on a xenon 12 core compute node.

5.8 Discussion

In this chapter ML-ρ-MCTDH is applied in three studies of PT. The first model considered is a symmetric PT system, which is well adapted to be represented with the ML-MCTDH basis and in previous studies it has been scaled up and propagated with more than 100 degrees of freedom. The second application is to asymmetric PT in salicylaldimine, where ML-ρ-MCTDH is tested with a new way of producing thermalised density matrices.

Finally, the phenomenon of double PT in porphycene is evaluated in a third application of the method. Porphycene was interesting to study as it exhibits stronger nonlinear coupling, which makes it more challenging to propagate within the multilayer basis setup. Despite this the capability of ML-ρ-MCTDH to propagate this system efficiently is clearly demonstrated, with a remarkable speedup in comparison to equivalent calculations using ρ-MCTDH.

Chapter 6

Summary

This thesis set out to improve efficiency in the Quantics version of the density matrix propagator, ρ-MCTDH, in order to allow the possibility of treating larger and more realistic quantum systems thermally. This led to the development and implementation of the novel ML-ρ-MCTDH scheme which has been successfully tested and applied to interesting and challenging systems. The potential of this method to treat much larger systems than were previously possible within the density matrix formalism has been demonstrated, which is an exciting development with many more potential applications.

Chapter 3 derives the ML-ρ-MCTDH EOM for the first time in order to show that they are well defined and that the ρ-MCTDH scheme can be incorporated into the multilayer formalism. The step by step derivations for the EOM of both the type I and II ML-ρ-MCTDH are detailed, which extends on the brief overview of this which was previously published in Raab et al [61, 62]. This extensive derivation was required in order to check whether the ρ-MCTDH and ML-ρ-MCTDH schemes are compatible and can be combined.

Chapter 4 presents a study into whether the efficiency of propagating density matrices can be improved by the choice of numerical integrator. A new integrator which uses the Chebyshev integration scheme is developed, implemented and tested in the Quantics package against several of the existing integrators.

In Chapter 5 ML-ρ-MCTDH is applied in three studies of PT, in order to better understand the crucial role the environment plays in this process, and the three methods MCTDH, ρ-MCTDH and ML-MCTDH are compared. The first study looks at a model of symmetric PT, the second is a study into salicylaldimine and a third looks at porphycene. The symmetric PT system was selected as a demonstration of the effect of an environment and since it is well adapted for the ML-MCTDH scheme, where it has previously been scaled up and propagated for more than 100 degrees of freedom. The second system examined is the asymmetric PT in salicylaldimine. ML-ρ-MCTDH is tested along with a new way of producing thermalised density matrices. Finally, a double PT in porphycene is studied showing the change in rate of PT with both temperature and system size. This molecule was of interest as it is a more complex system with stronger nonlinear coupling, and this property makes it more difficult to propagate within the multilayer basis setup.

The key advantage of the ML-ρ-MCTDH approach is that it brings the power of MCTDH to simulations of open systems, including allowing partitioning of degrees of freedom into a primary system, secondary bath and "dissipative" modes that can then be included using dissipation operators. In future work, the method could be applied to investigate the open system dynamics of a

molecule, for example using a Lindblad operator to model the dissipative environment.

It would also be interesting to apply the method to larger systems. An alternative approach to thermalisation is to use wavepacket dynamics with the MCTDH method treating the bath modes of the thermalised environment explicitly, with repeated dynamics calculations stochastically, sampling initial conditions from the Boltzmann distribution. In future work it could be interesting to compare this approach with the density matrix treatment of molecular systems.

Bibliography

[1] L. Masgrau, A. Roujeinikova, L. O. Johannissen, P. Hothi, J. Basran, K. E. Ranaghan, A. J. Mulholland, M. J. Sutcliffe, N. S. Scrutton, and D. Leys. Atomic description of an enzyme reaction dominated by proton tunneling. *Science*, 312:237–241, 2006.

[2] J. Mavri, H. Liu, M. H. M. Olsson, and A. Warshel. Simulation of tunneling in enzyme catalysis by combining a biased propagation approach and the quantum classical path method: application to lipoxygenase. *J. Phys. Chem. B*, 112:5950–5954, 2008.

[3] B. O'Regan and M. Grätzel. A low-cost, high-efficiency solar cell based on dye-sensitized colloidal TiO2 films. *Nature*, 353:737–740, 1991.

[4] T.V. Arjunan and T.S. Senthil. Review: Dye sensitised solar cells. *Mater. Technol.*, 28:9–14, 03 2013.

[5] J. Cao and G. A. Voth. The formulation of quantum statistical mechanics based on the Feynman path centroid density. I. Equilibrium properties. *J. Chem. Phys.*, 100(7):5093–5105, 1994.

[6] J. Cao and G. A. Voth. The formulation of quantum statistical mechanics based on the Feynman path centroid density. II. Dynamical properties. *J. Chem. Phys.*, 100(7):5106–5117, 1994.

[7] I. R. Craig and D. E. Manolopoulos. Quantum statistics and classical mechanics: real time correlation functions from ring polymer molecular dynamics. *J. Chem. Phys.*, 121:3368–3373, 2004.

[8] B. J. Braams and D. E. Manolopoulos. On the short-time limit of ring polymer molecular dynamics. *J. Chem. Phys.*, 125(12):124105, 2006.

[9] J. Cao and G. A. Voth. The formulation of quantum statistical mechanics based on the Feynman path centroid density. III. Phase space formalism and analysis of centroid molecular dynamics. *J. Chem. Phys.*, 101(7):6157–6167, 1994.

[10] I. R. Craig and D. E. Manolopoulos. Inelastic neutron scattering from liquid para-hydrogen by ring polymer molecular dynamics. *Chem. Phys.*, 322(1-2):236–246, 2006.

[11] D. R. Reichman, P.-N. Roy, S. Jang, and G. A. Voth. A Feynman path centroid dynamics approach for the computation of time correlation functions involving nonlinear operators. *J. Chem. Phys.*, 113(3):919–929, 2000.

[12] E. Geva, Q. Shi, and G. A. Voth. Quantum-mechanical reaction rate constants from centroid molecular dynamics simulations. *J. Chem. Phys.*, 115(20):9209–9222, 2001.

[13] A. Horikoshi and K. Kinugawa. Effective potential analytic continuation approach for real time quantum correlation functions involving nonlinear operators. *J. Chem. Phys.*, 122(17):174104, 2005.

[14] V. Kapil, E. Engel, M. Rossi, and M Ceriotti. Assessment of approximate methods for anharmonic free energies. *J. Chem. Theory Comput.*, 15(11):5845–5857, 2019.

[15] B. Hirshberg, V. Rizzi, and M. Parrinello. Path integral molecular dynamics for bosons. *Proc. Natl. Acad. Sci. U. S. A.*, 116(43):21445–21449, 2019.

[16] V. Kapil, D. M. Wilkins, J. Lan, and M. Ceriotti. Inexpensive modeling of quantum dynamics using path integral generalized Langevin equation thermostats. *J. Chem. Phys.*, 152(12):124104, 2020.

[17] G. Trenins, M. J. Willatt, and S. C. Althorpe. Path-integral dynamics of water using curvilinear centroids. *J. Chem. Phys.*, 151(5):054109, 2019.

[18] S. J. Buxton and S. Habershon. Accelerated path-integral simulations using ring-polymer interpolation. *J. Chem. Phys.*, 147(22):224107, 2017.

[19] W. Fang, M. J. Thapa, and J. O. Richardson. Nonadiabatic quantum transition-state theory in the golden-rule limit. II. Overcoming the pitfalls of the saddle-point and semiclassical approximations. *J. Chem. Phys.*, 151(21):214101, 2019.

[20] J. E. Lawrence, T. Fletcher, L. P. Lindoy, and D. E. Manolopoulos. On the calculation of quantum mechanical electron transfer rates. *J. Chem. Phys.*, 151(11):114119, 2019.

[21] I. R. Craig and D. E. Manolopoulos. Chemical reaction rates from ring polymer molecular dynamics. *J. Chem. Phys.*, 122(8):084106, 2005.

[22] T. F. Miller III and D. E. Manolopoulos. Quantum diffusion in liquid para-hydrogen from ring-polymer molecular dynamics. *J. Chem. Phys.*, 122(18):184503, 2005.

[23] I. R. Craig and D. E. Manolopoulos. A refined ring polymer molecular dynamics theory of chemical reaction rates. *J. Chem. Phys.*, 123(3):034102, 2005.

[24] T. F. Miller III and D. E. Manolopoulos. Quantum diffusion in liquid water from ring polymer molecular dynamics. *J. Chem. Phys.*, 123(15):154504, 2005.

[25] J. Lobaugh and G. A. Voth. A quantum model for water: Equilibrium and dynamical properties. *J. Chem. Phys.*, 106(6):2400–2410, 1997.

[26] F. J. Bermejo, K. Kinugawa, C. Cabrillo, S. M. Bennington, B. Fåk, M. T. Fernandez-Diaz, P. Verkerk, J. Dawidowski, and R. Fernandez-Perea. Quantum effects on liquid dynamics as evidenced by the presence of well-defined collective excitations in liquid para-hydrogen. *Phys. Rev. Lett.*, 84(23):5359, 2000.

[27] Y. Yonetani and K. Kinugawa. Transport properties of liquid para-hydrogen: The path integral centroid molecular dynamics approach. *J. Chem. Phys.*, 119(18):9651–9660, 2003.

[28] T. D. Hone and G. A. Voth. A centroid molecular dynamics study of liquid para-hydrogen and ortho-deuterium. *J. Chem. Phys.*, 121(13):6412–6422, 2004.

[29] L. Hernández de la Peña and P. G. Kusalik. Quantum effects in light and heavy liquid water: A rigid-body centroid molecular dynamics study. *J. Chem. Phys.*, 121(12):5992–6002, 2004.

[30] L. Hernández de la Peña and P. G. Kusalik. Temperature dependence of quantum effects in liquid water. *J. Am. Chem. Soc.*, 127(14):5246–5251, 2005.

[31] K. K. Smith, J. A. Poulsen, G. Nyman, and P. J. Rossky. A new class of ensemble conserving algorithms for approximate quantum dynamics: Theoretical formulation and model problems. *J. Chem. Phys.*, 142:244112–14, 2015.

[32] K. K. G. Smith, J. A. Poulsen, G. Nyman, A. Cunsolo, and P. J. Rossky. Application of a new ensemble conserving quantum dynamics simulation algorithm to liquid para-hydrogen and ortho-deuterium. *J. Chem. Phys.*, 142:244113–10, 2015.

[33] J.A. Barker. A quantum-statistical Monte Carlo method; path integrals with boundary conditions. *J. Chem. Phys.*, 70(6):2914–2918, 1979.

[34] I. Burghardt, K. Giri, and G. A. Worth. Multimode quantum dynamics using Gaussian wavepackets: The Gaussian-based multiconfiguration time-dependent Hartree (G-MCTDH) method applied to the absorption spectrum of pyrazine. *J. Chem. Phys.*, 129:174104–174114, 2008.

[35] R. A. Marcus. On the theory of oxidation-reduction reactions involving electron transfer. I. *J. Chem. Phys.*, 24(5):966–978, 1956.

[36] B. Wolfseder, L. Seidner, G. Stock, and W. Domcke. Femtosecond pump-probe spectroscopy of electron-transfer systems: a nonperturbative approach. *Chem. Phys.*, 217:275–287, 1997.

[37] D. Egorova, M. Thoss, W. Domcke, and H. Wang. Modeling of ultrafast electron-transfer processes: Validity of multilevel Redfield theory. *J. Chem. Phys.*, 119:2761–2773, 2003.

[38] D. Egorova, M. F. Gelin, and W. Domcke. Time- and frequency-resolved fluorescence spectra of nonadiabatic dissipative systems: what photons can tell us. *J. Chem. Phys.*, 122:134504–15, 2005.

[39] D. Antoniou and S. D. Schwartz. Proton transfer in benzoic acid crystals: Another look using quantum operator theory. *J. Chem. Phys.*, 109:2287–2293, 1998.

[40] H. J. C. Berendsen and J. Mavri. Quantum simulation of reaction dynamics by density matrix evolution. *J. Phys. Chem*, 97:13464–13468, 1993.

[41] J. Mavri. Molecular dynamics with nonadiabatic transitions: A comparison of methods. *Mol. Sim.*, 23:389–411, 2000.

[42] J. Mavri, H. J. C. Berendsen, and W. F. van Gunsteren. Influence of solvent on intramolecular proton transfer in hydrogen malonate. Molecular dynamics simulation study of tunneling. *J. Phys. Chem.*, 97:13469–13476, 1993.

[43] D. Borgis and J. T. Hynes. Molecular-dynamics simulation for a model nonadiabatic proton transfer reaction in solution. *J. Chem. Phys.*, 94(5):3619–3628, 1991.

[44] N. Zettili. *Quantum Mechanics: Concepts and Applications.* Wiley, 2nd edition, 2009.

[45] D. J. Tannor. *Introduction to Quantum Dynamics - a Time Dependent Perspective.* University Science books, 1 edition, 2007.

[46] T. Pacher, L. S. Cederbaum, and H. Köppel. Adiabatic and quasidiabatic states in a gauge theoretical framework. *Adv. Chem. Phys.*, 84:293–391, 1993.

[47] M. Born and R. Oppenheimer. Zur quantentheorie der molekeln. *Ann. Phys.*, 84:457–484, 1927.

[48] F. Jensen. *Introduction to Computational Chemistry.* John Wiley & sons, 2 edition, 2007.

[49] K. Aidas, C. Angeli, K. L. Bak, V. Bakken, R. Bast, L. Boman, O. Christiansen, R. Cimiraglia, S. Coriani, P. Dahle, et al. The D alton quantum chemistry program system. *Wiley Interdiscip Rev Comput Mol Sci*, 4(3):269–284, 2014.

[50] E. Wigner. On the quantum correction for thermodynamics equilibrium. *Phys. Rev.*, 40:749–759, 1932.

[51] M. Hillery, R. F. O'Connell, M. O. Scully, and E. P. Wigner. Distribution functions in physics: Fundamentals. *Phys. Rep.*, 106:122–167, 1984.

[52] U. Fano. Density of states in quantum mechanics by density matrix and operator techniques. *Rev. Mod. Phys.*, 29:74–93, 1957.

[53] W. Barford. Lecture notes for advanced quantum mechanics. Technical report, Oxford University, 2014.

[54] K. Blum. *Density Matrix Theory and Applications*, volume 64 of *Springer Series on Atomic, Optical, and Plasma Physics.* Springer Berlin Heidelberg, Berlin, Heidelberg, 3rd edition, 2012.

[55] A. G. Redfield. The theory of relaxation processes. *Adv. Magn. Reson.*, 1:1–32, 1965.

[56] G. Lindblad. On the generators of quantum dynamical semigroups. *Commun. Math. Phys.*, 48:119–130, 1976.

[57] V. Gorini, A. Kossakowski, and E. C. G. Sudarshan. Completely positive dynamical semigroups of n-level systems. *Journal of Mathematical Physics*, 17(5):821–825, 1976.

[58] M. H. Beck, A. Jäckle, G. A. Worth, and H.-D. Meyer. The multiconfiguration time-dependent Hartree method: A highly efficient algorithm for propagating wavepackets. *Phys. Rep.*, 324:1–105, 2000.

[59] P. A. M. Dirac. Note on exchange phenomena in the Thomas atom. *Proc. Cambridge Philos. Soc.*, 26:376–385, 1930.

[60] J. Frenkel. *Wave Mechanics*. Clarendon Press, Oxford, U.K., 1934.

[61] A. Raab, I. Burghardt, and H.-D. Meyer. The multiconfiguration time-dependent Hartree method generalized to the propagation of density operators. *J. Chem. Phys.*, 111:8759–8772, 1999.

[62] A. Raab and H.-D. Meyer. A numerical study on the performance of the multiconfiguration time-dependent Hartree method for density operators. *J. Chem. Phys.*, 112:10718–10729, 2000.

[63] G. A. Worth, H.-D. Meyer, and L. S. Cederbaum. State filtering by a bath: Exact wavepacket dynamics treating 24 degrees of freedom. *Chem. Phys. Lett.*, 299:451–456, 1999.

[64] H. Wang and M. Thoss. Multilayer formulation of the multiconfiguration time-dependent Hartree theory. *J. Chem. Phys.*, 119:1289–1299, 2003.

[65] U. Manthe. On the integration of the multi-configurational time-dependent Hartree (MCTDH) equations of motion. *Chem. Phys.*, 329:168–178, 2006.

[66] Z. Wang, M. Liang, Y. Tan, L. Ouyang, Z. Sun, and S. Xue. Organic dyes containing dithieno $[2,3-d:2,3'-d']$ thieno $[3,2-b:3',2'-b']$ dipyrrole core for efficient dye-sensitized solar cells. *J. Mater. Chem.*, 3(9):4865–4874, 2015.

[67] I. R. Craig, M. Thoss, and H. Wang. Proton transfer reactions in model condensed-phase environments: Accurate quantum dynamics using the multilayer multiconfiguration time-dependent Hartree approach. *J. Chem. Phys.*, 127:144503, 2007.

[68] I. R. Craig, M. Thoss, and H. Wang. Accurate quantum-mechanical rate constants for a linear response Azzouz-Borgis proton transfer model employing the multilayer multiconfiguration time-dependent Hartree approach. *J. Chem. Phys.*, 135:64504, 2011.

[69] R. Welsch and U. Manthe. Reaction dynamics with the multi-layer multi-configurational time-dependent Hartree approach: $H+CH_4 \rightarrow H_2+ CH_3$ rate constants for different potentials. *J. Chem. Phys.*, 137(24):244106, 2012.

[70] L. Cao, S. Kronke, O. Vendrell, and P. Schmelcher. The multi-layer multi-configuration time-dependent Hartree method for bosons: Theory, implementation, and applications. *J. Chem. Phys.*, 139:134103, 2013.

[71] O. Vendrell and H.-D. Meyer. Multilayer multiconfiguration time-dependent Hartree method: Implementation and applications to a Henon-Heiles Hamiltonian and to pyrazine. *J. Chem. Phys.*, 134:44135, 2011.

[72] A. D. McLachlan. A variational solution of the time-dependent Schrödinger equation. *Mol. Phys.*, 8:39–44, 1964.

[73] H.-D. Meyer, U. Manthe, and L. S. Cederbaum. The multi-configurational time-dependent Hartree approach. *Chem. Phys. Lett.*, 165:73–78, 1990.

[74] H.-D. Meyer, F. Gatti, and G. A. Worth. *Multidimensional Quantum Dynamics: MCTDH Theory and Applications*. Wiley-VCH, Weinheim, Germany, 2009.

[75] U. Manthe, H.-D. Meyer, and L. S. Cederbaum. Wave-packet dynamics within the multiconfiguration Hartree framework: General aspects and application to NOCl. *J. Chem. Phys*, 97:3199–3213, 1992.

[76] M. H. Beck and H.-D. Meyer. An efficient and robust integration scheme for the equations of motion of the multiconfiguration time-dependent Hartree (MCTDH) method. *Z. Phys. D*, 42:113–129, 1997.

[77] G. A. Worth, H. D. Meyer, and L. S. Cederbaum. Relaxation of a system with a conical intersection coupled to a bath: A benchmark 24-dimensional wave packet study treating the environment explicitly. *J. Chem. Phys.*, 109:3518–3529, 1998.

[78] A. S. Dickinson and P. R. Certain. Calculation of matrix elements for one-dimensional quantum-mechanical problems. *J. Chem. Phys*, 49:4209, 1968.

[79] D. O. Harris, G. G. Engerholm, G. W. Gwinn, and W. D. Gwinn. Calculation of matrix elements for one-dimensional quantum-mechanical problems and the application to anharmonic oscillators. *J. Chem. Phys.*, 43:1515–1517, 1965.

[80] J. C. Light, I. P. Hamilton, and J. V. Lill. Generalized discrete variable approximation in quantum mechanics. *J. Chem. Phys.*, 82:1400–1409, 1985.

[81] J. C. Light. Discrete variable representations in quantum dynamics. In *Time-Dependent Quantum Mol. Dyn.*, pages 185–199, New York, 1992. Plenum.

[82] J.-Y. Fang and H. Guo. Multiconfiguration time-dependent Hartree studies of the CH_3I/MgO photodissociation dynamics. *J. Chem. Phys.*, 101(7):5831, 1994.

[83] G. A. Worth, H.-D. Meyer, and L. S. Cederbaum. The effect of a model environment on the S_2 absorption spectrum of pyrazine: A wavepacket study treating all 24 vibrational modes. *J. Chem. Phys.*, 105:4412–4426, 1996.

[84] G. A. Worth and I. Burghardt. Full quantum mechanical molecular dynamics using Gaussian wavepackets. *Chem. Phys. Lett.*, 368:502–508, 2003.

[85] B. Lasorne, M. A. Robb, and G. A. Worth. Direct quantum dynamics using variational multi-configuration Gaussian wavepackets. Implementation details and test case. *PCCP*, 9:3210–3227, 2007.

[86] G. A. Worth, M. A. Robb, and B. L. Lasorne. Solving the time-dependent Schrödinger equation for nuclear motion in one step: Direct dynamics of non-adiabatic systems. *Mol. Phys.*, 106:2077–2091, 2008.

[87] G. W. Richings, I. Polyak, K. E. Spinlove, G. A. Worth, I. Burghardt, and B. Lasorne. Quantum dynamics simulations using Gaussian

wavepackets: the vMCG method. *Int. Rev. Phys. Chem.*, 34:269–308, 2015.

[88] D. Mendive-Tapia, B. Lasorne, G. A. Worth, M. A. Robb, and M. J. Bearpark. Towards converging non-adiabatic direct dynamics calculations using frozen-width variational Gaussian product basis functions. *J. Chem. Phys.*, 548:22A548–10, 2012.

[89] G. A. Worth, M. A. Robb, and I. Burghardt. A novel algorithm for non-adiabatic direct dynamics using variational gaussian wavepackets. *Faraday Discuss.*, 127:307–323, 2004.

[90] G. A. Worth and M. A. Robb. Applying direct molecular dynamics to non-adiabatic systems. *Adv. Chem. Phys.*, 124:355–432, 2002.

[91] U. Manthe. A multilayer multiconfigurational time-dependent Hartree approach for quantum dynamics on general potential energy surfaces. *J. Chem. Phys.*, 128:164116, 2008.

[92] G. A. Worth, K. Giri, G. W. Richings, M. H. Beck, A. Jäckle, and H.-D. Meyer. Quantics package, version 1.1, 2015.

[93] A. Raab, G. A. Worth, H.-D. Meyer, and L. S. Cederbaum. Molecular dynamics of pyrazine after excitation to the S_2 electronic state using a realistic 24-mode model Hamiltonian. *J. Chem. Phys.*, 110:936–946, 1999.

[94] G. A. Worth, M. H. Beck, A. Jäckle, and H.-D. Meyer. The MCTDH package, version 10.2. Technical report, University of Heidelberg, Heidelberg, Germany, 2012.

[95] C. Lanczos. An iterative method for the solution of the eigenvalue problem of linear differential and integral operators. *J.Res. Natl. Bur. Stand.*, 45:255, 1950.

[96] T. J. Park and J. C. Light. Unitary quantum time evolution by iterative Lanczos reduction. *J. Chem. Phys*, 85:5870, 1986.

[97] H. Tal-Ezer and R. Kosloff. An accurate and efficient scheme for propagating the time dependent Schrödinger equation. *J. Chem. Phys*, 81:3967–3971, 1984.

[98] C. Leforestier, O. Roncero, R. Bisseling, C. Cerjan, M. D. Feit, R. Friesner, A. Guldberg, A. Hammerich, R. Kosloff, G. Jolicard, et al. A comparison of different propagation schemes for the time-dependent Schrödinger equation. *J. Comput. Phys.*, 89:490–491, 1990.

[99] O. Kühn. Multidimensional hydrogen bond dynamics in salicylaldimine: Coherent nuclear wave packet motion versus intramolecular vibrational energy redistribution. *J. Phys. Chem. A*, 103:8458–8466, 2003.

[100] M. Petković and O. Kühn. Ultrafast wave packet dynamics of an intramolecular hydrogen transfer system: from vibrational motion to reaction control. *Chem. Phys.*, 304:91–102, 2004.

[101] I. Polyak, C. S. M. Allan, and G. A. Worth. A complete description of tunnelling using direct quantum dynamics simulation: Salicylaldimine proton transfer. *J. Chem. Phys.*, 143:84121, 2015.

[102] M. K. Abdel-Latif and O. Kühn. Infrared laser driven double proton transfer. An optimal control theory study. *Chem. Phys.*, 368(1-2):76–82, 2010.

[103] M. K. Abdel-Latif and O. Kühn. Laser control of double proton transfer in porphycenes: towards an ultrafast switch for photonic molecular wires. *Theor. Chem. Acc.*, 128(3):307–316, 2011.

[104] Y. Litman, J. O. Richardson, T. Kumagai, and M. Rossi. Elucidating the nuclear quantum dynamics of intramolecular double hydrogen transfer in porphycene. *J. Am. Chem. Soc.*, 141(6):2526–2534, 2019.